Mathematical modelling of the regulation of immune responses in viral and bacterial diseases

Von der Fakultät für Lebenswissenschaften

der Technischen Universität Carolo-Wilhelmina

zu Braunschweig

zur Erlangung des Grades eines

Doktors der Naturwissenschaften

(Dr. rer. nat.)

genehmigte

D i s s e r t a t i o n

von Sebastian Christoph Valentin Binder
aus Ulm

1. Referent: Prof. Dr. Michael Meyer-Hermann
2. Referent: Prof. Dr. Dieter Jahn
eingereicht am: 28.08.2014
mündliche Prüfung (Disputation) am: 08.12.2014

Druckjahr 2015

Vorveröffentlichungen der Dissertation

Teilergebnisse aus dieser Arbeit wurden mit Genehmigung der Fakultät für Lebenswissenschaften, vertreten durch den Mentor der Arbeit, in folgenden Beiträgen vorab veröffentlicht:

Publikationen

- Binder, S. C., Telschow, A., & Meyer-Hermann, M. (2012). Population Dynamics of Borrelia burgdorferi in Lyme Disease. Frontiers in Microbiology, 3, 104. doi:10.3389/fmicb.2012.00104
- Hernandez-Vargas, E. A., Wilk, E., Canini, L., Toapanta, F. R., Binder, S. C., Uvarovskii, A., Ross, T. M., Guzmán, C. A., Perelson, A. S., Meyer-Hermann, M. (2014). Effects of Aging on Influenza Virus Infection Dynamics. Journal of Virology, 88(8), 4123–4131. doi:10.1128/JVI.03644-13
- Binder, S. C., Hernandez-Vargas, E. A., & Meyer-Hermann, M. (2014). Reducing complexity: an iterative strategy for parameter determination in biological networks. Comput. Phys. Commun., under review.

Tagungsbeiträge

- Binder, S.C., Telschow, A., & Meyer-Hermann, M. A mathematical model of the population dynamics of Borrelia burgdorferi in Lyme disease (Poster). 13th International Conference on Lyme Borreliosis and Other Tick Borne Diseases, Boston (2013).
- Binder, S.C., Pongratz, G., Ebensen, T., Guzmán, C. A., Hernandez-Vargas, E. A., Straub, R.H. & Meyer-Hermann, M. A dynamic model of the cytokine response to influenza infections, Systems Biology of Infection Symposium, Ascona (2013).

Summary

The role of the first days of an infection is crucial for the immune protection from many bacterial and viral diseases. Already in the first hours after infection, molecules with antiviral and antibacterial properties are secreted, and the recruitment of the first immune cells to the infection site starts. Although these early immune responses often determine the disease severity and can prevent the establishment of an infection, their dynamics and the interplay between different components of immunity are often poorly understood.

In this study, dynamic mathematical modelling approaches were explored in order to elucidate quantitative relationships between different parts of the host immmunity and the pathogen. To this end, models for a bacterial disease and a viral disease were developed that describe the within-host dynamics of the pathogen and the induction of immune responses, as well as the interplay between different parts of the immune system.

Lyme disease is a widespread tick-borne infection caused by *Borrelia burgdorferi* and can lead to severe symptoms in humans. It induces strong and effective immune responses in mammals, but it still yields a remarkably high infectivity. Several hypotheses exist how the bacterium survives the early immune response and establishes an infection, but no conclusive evidence for the impact of different potential immune evasion strategies is known. Mathematical models for bacterial movement during dissemination of the bacteria, phagocytosis and molecular adaptation of the bacteria were investigated in order to gain insight into escape from the host immunity by *B. burgdorferi*. Several hypotheses that might explain this phenomenon were investigated *in silico*. The model has been analysed with respect to these questions in basic science; however, it provides the basis for evaluation with respect to options in prevention and therapy of Lyme disease.

As a viral disease, influenza was analysed in this study. Influenza poses a significant threat to public health due to seasonal epidemics that lead to mortality and cause significant economic loss, but also due to its risk for causing global pandemics. In this study, a model for the immune reaction to influenza in lung tissue was developed based on experimental influenza infection in mice. The focus in this model were the dynamics of different immune strategies and their interplay. A dynamic quantitative model describing the dynamics of cytokines as the major component in immune signalling and their interplay was developed. Due to difficulties in parts of the modelling process, the existing methodology was extended by a novel method for the estimation of model parameters and the method was validated. The cytokine model is useful not only in modelling viral infections, but as a modelling framework for a variety of different problems, since cytokines are involved in the immune response to all infectious diseases and in autoimmune diseases.

Zusammenfassung

Die ersten Tage einer Infektion spielen eine entscheidende Rolle für den Schutz durch das Immunsystem vor diversen bakteriellen und viralen Erkrankungen. Bereits in den ersten Stunden nach einer Infektion werden Moleküle mit antiviralen und antibakteriellen Eigenschaften abgegeben und erste Immunzellen werden an den Infektionsherd rekrutiert. Obwohl diese frühe Immunantwort oft entscheidend für die Schwere einer Erkrankung ist und sogar eine Erkrankung ganz verhindern kann, ist ihre Dynamik und das Wechselspiel zwischen verschiedenen Bestandteilen des Immunsystems oft nicht im Detail verstanden.

In dieser Studie wurden mathematische Modellierungsansätze untersucht, um quantitative Zusammenhänge zwischen verschiedenen Teilen der Wirtsimmunität und dem Pathogen zu verstehen. Dazu wurden Modelle für eine bakterielle und eine virale Erkrankung entwickelt, die die Dynamik der Pathogene im Wirt und die Induktion einer Immunantwort sowie die Wechselwirkungen zwischen verschiedenen Bestandteilen des Immunsystems beschreiben.

Lyme Borreliose ist eine weitverbreitete, von Zecken übertragene Krankheit, die von *Borrelia burgdorferi* ausgelöst wird und schwere Symptome im Menschen verursacht. Sie führt zu einer ausgeprägten und effektiven Immunantwort in Säugetieren, aber ist dennoch sehr ansteckend. Es gibt verschiedene Hypothesen, wie das Bakterium die frühe Immunantwort überlebt und eine Infektion erreicht, aber es existiert kein schlüssiger Beweis für den Einfluss verschiedener möglicher Immunevasionsstrategien. Um die Immunevasion besser zu verstehen, wurden mathematische Modelle für bakterielle Fortbewegung während der Ausbreitung der Bakterien, für Phagozytose und molekulare Anpassungen der Bakterien untersucht. Verschiedene Hypothesen wurden *in silico* getestet. Das Modell wurde in Bezug auf Fragestellungen aus der Grundlagenforschung untersucht; es stellt aber eine Basis dar, auf der eine Untersuchung in Bezug auf Fragen der Therapie und Prävention von Lyme Borreliose möglich ist.

Als virale Erkrankung wurde Influenza untersucht. Influenza stellt durch saisonale Epidemien, die zu erheblicher Mortalität und wirtschaftlichen Einbußen führen, aber auch durch die ständige Gefahr einer globalen Pandemie eine erhebliche Bedrohung für die öffentliche Gesundheit dar. In dieser Studie wurde ein Modell für die Immunreaktion gegen Influenza im Lungengewebe entwickelt. Es basiert auf Infektionsexperimenten mit Influenza in Mäusen. Im Fokus ist in diesem Modell die Dynamik der verschiedenen Immunstrategien und ihr Wechselspiel. Es wurde ein quantitatives Modell entwickelt, dass die Dynamik von Zytokinen, einem wichtigen Bestandteil in Immunsignalwegen, und ihre Interaktionen beschreibt. Aufgrund von Problemstellungen in Teilen des Modellierungsprozesses konnte die bestehende Methodik durch eine neue Methode zur Abschätzung von Modellparametern erweitert und die Methode validiert werden. Das entwickelte Zytokinmodell ist nicht nur für die Modellierung viraler Erkrankungen hilfreich, sondern überdies als Modellierungskonzept für eine Reihe verschiedener Probleme, da Zytokine Bestandteil der Immunreaktion in allen Infektionskrankheiten und auch in Autoimmunerkrankungen sind.

Contents

1

Introduction

Biology and the life sciences have undergone major changes in the last century. These changes are related to a slow, gradual change in the nature of research in the field from a merely descriptive to an analytical science that culminates today with the advent of new technologies in molecular biology, bioimaging and related fields.

This slow but constant change has been accompanied by the emergence of a new interdisciplinary field that became necessary in order to understand biological systems in quantitative manner. Early roots of this new field can be traced back to the early 20th century when for example the Hardy-Weinberg principle [73, 228] describing the quantitative relationship of mendelian traits between parents and their offspring was discovered as one of the early mathematical laws used to describe the behaviour of biological systems. The need of a theoretical area in biology had already been recognised by scientists at this time, e.g. by the plant physiologist and philosopher Johannes Reinke, who was the first to use the term "Theoretical Biology" in a book title [176]. This newly emerging field has found successful application in various areas in the biological and medical sciences since then. Ecology and evolutionary biology as well as biophysics have a long tradition in mathematically describing fundamental laws of biological systems [57, 73, 81, 146, 226, 228]. However, while much of early research in theoretical biology has been focused on these areas, it spread to other areas soon. In the second half of the 20th century, mathematical models were applied in areas as diverse as cancer research [4], neuroscience [189], biochemistry [183] or epidemiology [2], to name only a few prominent examples out of a large number of specialized research areas supported by mathematical modelling efforts [144–146].

Today, biology in general and theoretical biology in particular faces new challenges arising from an explosion of quantitative, high-quality time-resolved data. While these data provide invaluable information about biological systems such as metabolic pathways in cells or signalling networks, their overall behaviour is often beyond intuitive understanding and properties of these complex systems such as bistability or modulation and integration of signals of different origin are critical to the functionality of these systems [75].

1.1 Mathematical Models of Viral and Bacterial Diseases

Modelling of disease transmission and spread within populations has a long tradition [99] and is widely accepted as a central method in epidemiology [2, 66] and is broadly used to aid in policy decisions about public health issues, e.g. vaccination guidelines [61].

Compared to the history of models of disease transmission, models of the within-host dynamics have appeared rather late. However, models of some bacterial and many viral systems have been developed and provided important insight. The main focus in modelling of within-host kinetics in the recent past has clearly been on viral infection [reviewed in 26]. Early models of viral kinetics were concerned mainly with HIV [161]. These models were basic ordinary differential equation (ODE) models and consist mainly of three quantities: virions, target cells and infected cells. Virions infect target cells that in turn shed virus. Models of the same type have since been applied to other viral infections such as Hepatitis [34]. Influenza in particular has gained much attention from theoretical biology in the past decade [13]. Models of influenza infection often include simple models that do not describe any immune response, but still describe measured viral titers surprisingly well [7]. Other models of influenza include immune responses in varying amount of detail [79, 132, 160]. Many of the viral kinetics models are related to the idea of modelling target cell infection and virus production by infected cells.

In comparison to the published studies on viral kinetics, models of bacterial disease are scarce. There are some studies that focus on the interactions between phagocytic cells and bacteria and try to derive general principles [109, 125, 166]. Some other models have been published that describe specific diseases [192, 195], but many bacterial diseases have never been studied by theoretical scientists.

Mathematical modelling as a tool to explore and understand biological systems is used in many different areas nowadays. In this doctoral thesis, mathematical models are employed to gain a deeper understanding of the within-host dynamics of infectious agents and their interactions with the host immune system. In chapter 3, a bacterial disease is investigated with respect to determinants of its survival inside a mammalian host. Chapter 4 focuses on a viral disease with an emphasis on the different branches of the immune system that critically influence the viral dynamics within the host. In both cases, simple growth models of the pathogens are complemented with a basic description of central components of the early immune response and their influence on the development of pathogen loads inside a host over the course of an infectious disease.

1.2 The Early Immune Response in Viral and Bacterial Diseases

The goal in the following chapters is to elucidate the role of different parts of the innate and early adaptive immune response against two infectious diseases. In both cases, the pathogen induces strong inflammatory responses that can contribute to the pathogens as well.

The first system that will be studied is a tick-borne bacterial infection that has been discovered only a few decades ago [25, 205]. The causative agent, *B. burgdorferi*, is highly infective [191] and survives inside infected mice despite a pronounced inflammatory reaction by the host, exploiting mechanisms that are not fully understood. It causes the most common vector-borne disease in the United States and Europe [6]. The bacterium has various distinguishing properties that commonly lead to systemic infections and can result in severe late symptoms and irreversible tissue damage in humans [202].

The second system is experimental infection with influenza virus in mice. Influenza is of significant importance due to its risk for global pandemics, but even more due to seasonal influenza which is a continuous cause of mortality and economic loss [152]. Although many models on the within-host dynamics exist, the majority of them has focused on the viral kinetics, and interactions between different branches are usually ignored.

In both systems, the aim is to develop a mathematical model that

1. Describes the pathogen dynamics and local immune reactions in the respective tissue,
2. Includes a model of the early immune response with an emphasis on innate immunity and its activation by the pathogens, and
3. Gives insight into the impact of particular immune strategies for the disease and possible evasion by the pathogen.

In addition to these common goals, slightly different aspects of the immune response are investigated in the two models. In the case of *B. burgdorferi*, the phagocytic cells have a central role in protection and clearance of the bacteria [137] and the model for the immune response focuses on phagocytes. Furthermore, potential immune evasion mechanism of the bacterium are analysed.

In the case of influenza, the focus is on the regulation of the immune response and the interaction of different immune branches by means of cytokine secretion. Cytokine dynamics in the lung tissue form the base of the model and immune effects are modelled as antiviral cytokine effects. The advantage of this description is twofold: first, it complements the existing modelling work on influenza by a description of the neglected signalling component and second, a dynamic description of the cytokine response is a versatile tool that can be used in many different contexts like other infectious diseases or autoimmune diseases.

2

Methods

2.1 Choice of the modelling strategy

Dynamic mathematical models can be grouped into different classes of models according to their properties. Specifically, these classes differ in whether they describe the system in a stochastic or deterministic manner, whether or not they provide spatial information, and whether they describe individual agents and their internal state or an average of agents on a population level. The choice of the most appropriate class of model depends very much on the system under study and the question motivating the modelling work. The amount of detail that the model describes determines the mathematical tools available to analyse them. In general, the analytical power of available tools decreases with the amount of complexity of the model type while the computational effort increases. Biological systems are often vast networks of different components with highly non-linear interactions at multiple scales. As such, modelling these systems presents a tradeoff between describing a model that is biologically realistic and provides enough detail to answer the biological question of interest on the one hand and a model that is statistically sound and computationally feasible on the other hand.

ODEs are a very well studied class of models. They have been used extensively in theoretical biology [2, 144] and were among the first mathematical models describing biological systems [226]. Ordinary differential equations neglect spatial effects and internal state of the system, implicitly assuming a well-mixed system of agents with homogenous behaviour and without consideration of stochastic effects. While this is a vast simplification of real-world biological systems, it is one of the most popular types of models in mathematical biology due to the powerful mathematical tools available for their analysis. For simple ODE models, analytical solutions may even be found, although this is commonly not feasible with the non-linear models typically encountered in theoretical biology. Furthermore, numerical simulations of ODE models require little computational effort. This allows to use methods for numerical exploration, model calibration and statistical analysis that would be impractical to use with more complex models types since they rely on numerous repeated evaluations of model simulations.

In models of within-host pathogen dynamics in infectious diseases, ODEs are often a natural choice. Commonly, the focus of such studies is on the population dynamics of the infectious agent in the whole

body or in certain compartments. The pathogen is typically present in large numbers and stochastic effects are therefore often of secondary importance. Hence, they clearly are the predominant approach in mathematical modelling of viral [7, 13, 20, 72, 79, 132, 151, 161, 162] and bacterial [125, 166, 178, 195] infections.

Since the focus in this doctoral thesis is on the within-host dynamics of pathogen populations and their interactions with the host's immune system, ODEs are used in all models presented here. However, it should be noted that the use of ODEs makes implicit assumptions about the system and has its limitations, e.g. neglect of spatial effects, that will be discussed in models where this might be a concern.

2.2 Numerical simulations of ordinary differential equation models

In the case of linear ODEs (i.e. one that can be expressed as a linear combination of the derivatives), finding exact solutions is often possible and very useful. However, in the case of non-linear ODEs which are frequently encountered in mathematical modelling of biological systems, this is impossible in most cases. Instead, the solution is numerically approximated, which is sufficient for many practical applications. Typically, this means solving an initial value problem of the form

$$\frac{dy}{dt} = f(t, y(t)), \qquad y(t_0) = y_0, \tag{2.1}$$

where y_0 is the initial condition, i.e. the value of the variable y at the first time point, t_0. A variety of algorithms for this problem are available that approximate solutions by starting at the initial condition and then evaluating the next point of the solution by taking a small finite timestep from the previous point. The algorithms vary in their degree of accuracy, performance and suitability for particular systems. One of the most common types of algorithms for the solution of non-stiff ODEs is called Runge-Kutta methods. The Dormand-Prince algorithm belongs to this family of algorithms. Its main advantage is that it allows to adjust the size of the timestep according to the accuracy of the solution by providing an error estimate.

If not stated otherwise, a Dormand-Prince algorithm of the order 8(5,3) is used in implementations either in R, Python or C (see appendix B for used libraries).

2.3 Parameter estimation

The term "inverse problem" describes a class of mathematical problems in modelling. If the prediction of the behaviour of a system given a model of the system and known values of its parameters could be seen as a "forward modelling problem", an inverse modelling problem is the opposite: given measurements

of the behaviour of a system, the goal is to draw conclusions about the parameters that determine the system. An example is the measurement of bacterial concentrations in a suspension. In this example, the prediction of a bacterial concentration after a certain period of growth under controlled circumstances according to a known model for bacterial growth with known parameters would constitute a forward problem. Conversely, the identification of a model parameter, e.g. the growth rate of the bacteria, from actual measurements of bacterial concentrations would be considered an inverse problem.

In mathematical models of biological systems, parameters are often difficult, expensive or outright impossible to measure. Some model parameters may not even have a directly measurable biological equivalent, e.g. in the case of phenomenological descriptions of parts of a system. Hence, identifying model parameters from the observed behaviour of a system is a central problem in the field and often referred to as parameter estimation. Since this process is critical for the development of the presented mathematical models and an extension of the existing methodology is part of this dissertation, an overview of commonly used methods and a more detailed description of the algorithms employed here is given in the following paragraphs.

Parameter estimation problems pose challenges on multiple levels. The procedure involves comparing model output with a given set of parameters to the observed data and choosing the parameter set that minimises the error of the model. This raises the question how the model error should be measured, i.e. how the level of agreement between model and data can be measured. The most commonly used method is to minimise the sum of squared errors (SSE) defined as

$$SSE = \sum_{i=1}^{n} \left(y_i - y(x_i; \Theta)\right)^2, \tag{2.2}$$

where n is the number of data points, x_i are values of the independent variable and $y(x; \Theta)$ is the model output as a function of the independent variable x and a vector of parameters Θ.

If the error of all measurements was normally distributed and equal for all data points, minimising SSE would correspond to maximising the likelihood of the parameter values given the observed data [174]. However, the error is usually not equal in all data points. Given measurements with an independent and normally distributed error and standard deviations σ_i for all datapoints y_i, the likelihood of the parameter values is maximised by minimising the quantity χ^2 [170; p. 778 ff]:

$$\chi^2 = \sum_{i=1}^{n} \left(\frac{y_i - y(x_i; \Theta)}{\sigma_i} \right)^2. \tag{2.3}$$

Minimisation of this function is known as χ^2*-fitting* or *weighted least-squares fitting*. Different variants for weighting and rescaling exist, but objective functions based on the least squares criterion are widely used due to their computational efficiency, ease of implementation and the relation to the maximum likelihood, although the latter only holds if the assumption of normally distributed errors is true.

2.3.1 Local and global optimisation methods

The parameter space to be searched for optimal values is often large and high dimensional in parameter estimation problems for modelling of biological systems. Thus, exhaustive search, i.e. scanning the whole range of parameters is usually not a practical alternative and sophisticated algorithms for the minimisation of the cost function have to be applied. A large number of numerical optimisation algorithms are available, and some of the most common ones will be discussed in the next paragraphs.

Cost functions for non-linear parameter estimation problems will often have multiple local minima. Hence, parameter estimation methods can be classified according to whether they converge the nearest local minimum or attempt to find a global one. Algorithms of the former type include gradient descent methods such as the Gauss-Newton [174] method and variants thereof that are highly efficient in the case of continuous objective functions. Some direct search algorithms such as the popular Nelder-Mead algorithm [150] do not require the calculation of derivatives and are thus useful in the case of highly non-linear or non-continuous functions, but belong to the class of local optimisers as well. While these methods are computationally efficient and useful in many cases, their disadvantage is that they may fail to converge to a global optimum and converge to a local minimum in the case of larger, non-convex problems [130].

In contrast, global optimisation methods attempt to find a global optimum. While there are deterministic approaches that converge to a global optimum [53], they are not always applicable and have requirements with respect to the objective function and the system dynamics that cannot always be met [134]. As an alternative, many stochastic optimisation algorithms are available that do not have any requirements such as differentiability of the cost function and rely only on the model output. Hence, they are suitable for many models and often easy to implement. Global convergence of stochastic optimisers cannot be guaranteed; however, for practical applications, there is often no alternative tool available and proof of global optimality may be of secondary importance.

2.3.2 Stochastic Global Optimisation

Simulated annealing A vast number of stochastic global optimisers are available. An algorithm that has gained high popularity in different fields is called simulated annealing [101]. The core of the algorithm is an analogy to thermodynamic processes during cooling and crystal formation, where slow and controlled cooling leads to the formation of pure crystals. At high temperatures, the molecules of a material, e.g. a metal, can move freely. As temperature decreases, they become less mobile and settle in an arrangement that minimises the free energy. Simulated annealing lends itself well to combinatorial problems such as the traveling salesman problem due to its nature, but is easily adapted to continuous optimisation as well [170; p. 549 ff]. In this algorithm, solutions are allowed to go in a direction that

increases the value of the cost function. However, the probability of taking a worse solution decreases with decreasing temperature, i.e. with increasing number of steps in the algorithm.

Evolutionary Computation Another important class of stochastic optimisers are methods derived from evolutionary computation. These algorithms, sometimes called biologically inspired algorithm, are based on the idea of fitness selection in evolution. All evolutionary computation is based on subsequent generations of candidate solutions that are selected for the contribution to the next generation based on their "fitness" which is determined by a cost function.

Genetic algorithms are one type of evolutionary computation algorithm that has been widely used for parameter estimation in biological models [135]. In genetic algorithms, a population of candidate solutions is initialised at random. The individuals of a population are often represented as bitstrings. Subsequent generations of this population are created by iteratively selecting candidates with a probability that corresponds to their fitness. The selected candidates are allowed to contribute to the next generation by "reproduction", a process that involves mutations (e.g. flipping of a random bit) and a crossover operation that recombines parts of two candidate solutions are defined [91].

Another type are evolutionary strategies [16]. Similar to genetic algorithms, they iterate over offspring generations of an randomly initialised population. However, in contrast to genetic algorithms, the parents for the offspring generation are usually selected randomly without consideration of the fitness value. Offspring is generated using mutation, e.g adding a normally distributed random value, and recombination. The recombination step can be either dominant or intermediate, where the dominant strategy chooses parameters from one of the parents and the intermediate strategy which takes an average of the parent values. The next generation is then generated by selecting only the best individuals.

Other Stochastic Global Optimisation methods Many other stochastic global optimisers have been invented and applied successfully to some problems [63]. This includes multistart methods that attempt to find the global optimum by evaluating local optima in different neighbourhoods, ant colony optimisation [48] which searches for global solutions based on indirect communication between simple agents similar to the pheromone communication seen in foraging ants. The field of stochastic global optimisation is vast, and the best strategy is likely domain specific. In the models presented here, an algorithm called Differential Evolution is used extensively. This algorithm has produced high quality solutions, albeit at the cost of a limited computational efficiency, in large non-convex optimisation problems [134] and has been successfully applied for ODE models of within-host pathogen dynamics [79].

2.3.3 The Differential Evolution (DE) algorithm

Originally developed by Storn and Price [208], Differential Evolution (DE) is a global stochastic optimiser that is based on generating populations of candidate solutions and is related to evolutionary computation algorithms. The algorithm iteratively creates offspring generations by recombination and mutation according to a specific strategy. Although many extensions and variations of the algorithm exist [e.g. 21, 80, 117, 171], the general procedure can be outlined by simple steps similar to the original proposal (Algorithm 1).

Initialise Generation of candidate vectors $G_0 = \{x_1, x_2, \ldots, x_{N_P}\}$ at random;
for $k \leftarrow 0$ **to** k_{max} **do**
  pick best candidate from G_k;
  if *termination criterion* **then**
    break;
  end
  for $i \leftarrow 1$ **to** N_P **do**
    // parents must be different from each other and from x_i
    select parents p_1, p_2, p_3 from G_k;
    // Mutation operation:
    $v_i = p_1 + F \cdot (p_2 - p_3)$;
    pick random index $r \in \{1, \ldots, n\}$ // n:number of parameters
    // Crossover operation:
    for $j \leftarrow 1$ **to** n **do**
      pick a random uniform number s;
      if $j = r$ *or* $s < CR$ **then**
        // Take parameter from mutant
        $u_j = v_i j$;
      else
        // Take parameter from old vector
        $u_j = x_i j$;
      end
    end
    // Selection operation (evaluate cost function f):
    if $f(u_j) < f(x_j)$ **then**
      replace x_i by u_i for G_{k+1};
    else
      retain x_i for G_{k+1};
    end
  end
end
return best candidate;

Algorithm 1: Steps in the Differential Evolution algorithm. Each generation consists of N_P parameter vectors of n parameters. A trial vector is created by mutation, crossover and selection operations. If the trial vector yields lower values of the cost function, it replaces the vector of the previous generation; otherwise, the old vector is retained for the next generation The algorithm terminates when either a termination criterion such as a particular value of the cost function is met or the maximal number of steps is reached.

The initial population of candidate solutions is created by randomly selecting parameter values according to a uniform distribution from predefined boundaries. The creation of offspring generations consists of the three main operations: mutation, crossover and selection. In the classical strategy, the mutation operation consists of selecting three parent vectors p_1, p_2 and p_3 that have to be distinct from each other and from the base vector x_i. Then, the mutation operation creating a mutant vector v_i is defined as

$$v_i = p_1 + F \cdot (p_2 - p_3), \tag{2.4}$$

where $F \geq 0$ is the mutation weight, an algorithm parameter that can be arbitrarily chosen. While there is no upper limit to F, useful values are typically not greater than 1.

This step is followed by the crossover step which creates a trial vector u by combining values from the mutant v_i and the base vector x_i. For each of the n parameters, the value is taken from the mutant vector v_i with a probability CR. CR is the second important parameter, the *crossover probability* and can take values between 0 and 1. In addition, at least one parameter (picked at random) is taken from the mutant to ensure that the trial vector and the base vector are different. In the selection operation, either the base vector or the trial vector is retained for the next generation according to the highest fitness. This strategy is known as *DE/rand/1/bin* in the terminology proposed by [171]: the base vector is chosen at random (*rand*), *1* difference of vectors is added and the number of parameters the mutant contributes to the trial vector follows a binomial distribution *bin*.

In addition to the parameters F and CR, the population size N_P, the maximal number of generations, k_{max} and the other termination criteria are central for the behaviour of the algorithm. Price et al. [171] recommend setting the population size N_P to at least ten times the dimensionality of the problem, whereas optimal settings for F and CR largely depend on the problem. Useful termination criteria include reaching a predefined value of the cost function and failure to produce significant improvements over a certain number of generations.

There are many variations to the algorithm in terms of selection and mutation and many different strategies have been proposed. For practical purposes, the classical DE/rand/1/bin strategy works well for many problems [171]. A useful alternative is the DE/local-to-best/1/bin strategy which is similar to the classical strategy, but replaces the mutation function (Equation 2.4) by

$$v_i = x_i + F \cdot (x_{best} - x_i) + F \cdot (p_1 - p_2), \tag{2.5}$$

where x_{best} is the vector that yields the lowest value for the cost function in the parent generation. This strategy has shown good success during the development of the models described in the following

chapters and has thus been defined as a default strategy in the implementation of the DE algorithm described in the appendix.

Another deviation to the original algorithm proposed by Storn and Price [208] was implemented by enforcing parameter bounds. In their original work, no handling of parameter bounds was described. In the DE implementation that was developed in the context of the models presented in the next chapters, bounds are enforced by simple reinitialisation: when a parameter exceeds the predefined bounds, it is selected from the allowed interval at random.

3

The immune response in early Lyme disease

Lyme disease is still the most common arthropod-borne disease in the northern hemisphere despite the extensive research and significant improvements in prevention and therapy in more than thirty years since its discovery [179]. It was originally described by Steere et al. [205] who noticed a significant accumulation of severe cases of juvenile arthritis, preceded by a characteristic skin rash, in a distinct geographical area and consequently suggested an infectious origin by a pathogen likely transmitted by arthropod bites.

Several years after the discovery, a previously unknown bacterium that belongs to the spirochaetes, a phylum of bacteria with a distinctive spiral-shaped, elongated morphology, was recovered from the suspected arthropod vector of the disease, a tick of the genus *Ixodes* [25]. Today, this bacterium is known as *B. burgdorferi* sensu stricto (s.s.) and is, together with other species of the same genus, accepted as the cause of Lyme disease. Since this discovery, the number of reported cases has increased dramatically [202]. This is most likely in parts due to increased awareness and improved diagnostic methods, but the geographical distribution of the disease is increasing as well[179], possibly linked to the changing geographical distribution of its vector [67].

In addition to the high prevalence, the severe clinical symptoms, including arthritis, cardiological and neurological complications, have sparked increasing interest in the disease. These symptom can persist as the disease becomes chronic [147]. Moreover, symptoms fail to resolve after successful antibiotic treatment in approximately 10% of patients [202] and there is evidence suggesting an autoimmune component in this phenomenon [204].

Borreliosis and its causative agent have a number of unique features that will be discussed in the next paragraphs. One conundrum is the contradiction between the seemingly effective early innate immune response and the high infectivity of *B. burgdorferi* (an ID_{50} as low as $1.8 \cdot 10^2$ has been described for mice, [153]). Phagocytic cells rapidly infiltrate infected tissue rapidly [10] and kill *B. burgdorferi* effectively *in vitro* [138]. This raises the question how *B. burgdorferi* survives the early immune response, in particular considering the fact that active downregulation of the early immune response seems unlikely [136, 139]. The mathematical models in this chapter were developed with the aim to test the plausibility of

several hypotheses that might explain this phenomenon *in silico*. Bacterial load at the infection site in the skin of infected mice serves as the data basis for the analysis of the early immune response.

3.1 Background

3.1.1 Biology of Lyme disease spirochaetes

The genus *Borrelia* belongs to the Spirochaetes. Spirochaetes are a bacterial phylum with a characteristic morphology (Figure 3.1). Most of the species in this group are free-living, non-pathogenic bacteria, but it includes four genera that infect mammals and cause a number of infectious diseases. Besides *Borrelia*, the genera *Leptospira*, *Treponema* and *Brachyspira* can cause diseases like Leptospirosis (*Leptospira interrogans*) and Syphilis (*Treponema pallidum*). The human pathogens of the genus *Borrelia* can be grouped according to their clinical symptoms. A rather large group of bacteria causes varieties of tick-borne relapsing fever [49]. The second group, which is the focus of the following models, causes Lyme disease and is commonly referred to as *B. burgdorferi* sensu lato (s.l.). The species complex consists of 18 or more species [200]. *B. burgdorferi* sensu stricto (s.s.) is the species that was originally described by Burgdorfer et al. [25] and is predominant in Lyme disease cases in North America. In contrast, *B. burgdorferi* s.s. is present in Europe, but the prevalence of two other human pathogenic species, *Borrelia garinii* and *Borrelia afzelii*, is higher [179]. A fourth pathogenic species, *Borrelia spielmanii*, is found in Europe as well, albeit less frequently. *Borrelia bavariensis* has been identified as a distinct species in 2009 after being treated as a serotype of *B. afzelii* before [127]. For the other species in the *B. burgdorferi* s.l. complex, pathogenicity is either not or only rarely shown [86]. If not explicitly stated otherwise, the term *B. burgdorferi* refers to *B. burgdorferi* s.s. hereafter, since much of the discussed research used *B. burgdorferi* s.s. and results are not in all cases shown across the whole *B. burgdorferi* s.l. complex.

Spirochaetes share a common, unique morphology that is easy to distinguish and sets them apart from other phyla. Many spirochaetes such as the *Leptospiraceae*, commonly used as a model organism for spirochaete motility [e.g. 32], have a helically coiled, corkscrew-like structure [65, 172] The other characteristic morphology observed in spirochaetes is a planar wave (see Figure 3.1(a) that is common to *Borrelia burgdorferi* [31, 65] and *Treponema pallidum* [94].

The flagella in *B. burgdorferi* differ from those of model organisms of bacterial motility such as *E. coli* in their position and function. While most flagella are externally located and rotate freely on the outside of the bacterium, they are situated in the periplasmic space between the cytoplasmic membrane and the outer sheath in *B. burgdorferi* and other spirochaetes [30]. Hence, these flagella are commonly referred to as "endoflagella" or "periplasmic flagella". Beyond their complex function for bacterial motility discussed below, the periplasmic flagella also determine the flat wave shape in *B. burgdorferi*. In the absence of functional flagella, *B. burgdorferi* assumes the shape of a straight rod and loses its

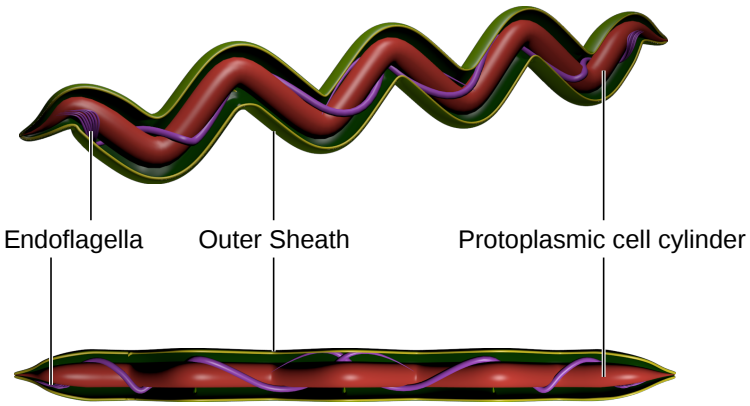

(a) Schematic representation of the planar wave morphology of *B. burgdorferi* in longitudinal view from two perspectives.

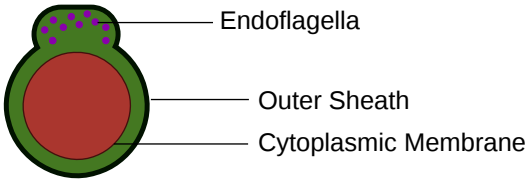

(b) Crosssection of *B. burgdorferi* (schematic). The flagella form a ribbon between outer sheath and cytoplasmic membrane.

Figure 3.1: Morphology and motility apparatus of *B. burgdorferi*. The overall morphology resembles a planar wave that is determined by the periplasmic flagella situated in the periplasmic space between the outer sheath and the cell cylinder. The ends of the flagella are attached to the cell cylinder. The flagella form a ribbon that is helically coiled around the cell cylinder and causes a bulge in the outer sheath that is visible in microscopical images.

ability to move [141]. This surprising skeletal function has been explained by a theoretical model taking into account biophysical properties of the cell cylinder and the periplasmic flagella [46]. A schematic representation of the morphology of *B. burgdorferi* and the position of the periplasmic flagella is depicted in Figure 3.1.

Given the particular shape and motility apparatus and the fact that *B. burgdorferi* has been shown to move at high velocities of up to $627\,\mu\mathrm{m\,min}^{-1}$ in dense tissue *in vivo* [110], the nature of *B. burgdorferi* locomotion is puzzling and has been subject to a number of studies [30; and references therein]. Charon and Goldstein [31] proposed a model which suggests that the flagella on both ends counterrotate. The result of this rotation is a backwards propagating wave similar to the undulating movement of worms and with a simultaneous rotation of the spirochaete around the cell axis.

In contrast to most bacterial genomes, the $\approx$ 1Mb chromosome of *B. burgdorferi* is linear. Its genome contains several plasmids, some of which are linear and others circular [59]. Genes involved in metabolic pathways are mostly located on the chromosome, while the majority of outer surface proteins

are encoded in plasmid genes [28]. While most of the plasmids do not seem to be essential for *in vitro* growth [28], they may well be required for infectivity and transmission of the bacteria *in vivo* [234].

Interestingly, the genetic variability within one species is high for some genes encoding immunogenic products like outer surface protein C (OspC) [6], which may have an impact on protective immunity against these proteins. Furthermore, there is a lipoprotein located on the outer surface of *B. burgdorferi* that undergoes constant antigenic variation [241]. This protein is encoded on the *vls* locus which consists of 15 silent cassettes that recombine with the encoding region, *vlsE* [240]. There is evidence showing that this antigenic variation is required for bacterial persistence in mammalian hosts [8, 111, 157], but only in the presence of an adaptive immune response [111]. This and the fact that antigenic variation is only observed during mammalian infection strongly suggests that VlsE is involved in an immune evasion mechanism.

The natural reservoir of *B. burgdorferi* are mainly wild rodents. Typically, ticks become infected during the blood meal in the larval stage and transmit the bacteria during nymphal feeding [216]. Vertical transmission between ticks seems to be uncommon [148]. Hence, the bacterial population can only remain stable by transmission between reservoir hosts by ticks. Consequently, *B. burgdorferi* has to survive for months in two very different host environments, and its gene expression has to change drastically according to its host stage. A well-studied example is the reciprocal regulation of *outer surface protein C* (*ospC*) and *outer surface protein A* (*ospA*) [40]. Both genes encode surface exposed lipoproteins, but *ospA* expression is specific to the tick stage in the bacterial life cycle, whereas *ospC* is induced first during transmission from the tick to a vertebrate host. This transition can be triggered by environmental factors [235] and possibly host immune reactions[83]. The processes controlling differential gene expression are not yet understood in all details. However, two central regulatory systems have been identified. The first pathway is initiated by activation of histidin kinase 1 (Hk1) and results in the production of cyclic di-GMP (c-di-GMP) through activation of the Hk1-response regulatory protein 1 (Rrp1), while the second system is controlled by the alternative RNA polymerase σ-factor RpoS (RpoS) [173]. RpoS production is controlled by another σ-factor, the alternative RNA polymerase σ-factor RpoN (RpoN) [87], and at least two other proteins (phosphorylated Hk1-response regulatory protein 2 (Rrp2) [236] and BosR [90]). The RpoS system has been shown to control the expression of known host-stage specific genes such as *ospC* and *decorin binding protein A* (*dbpA*) [87].

3.1.2 *B. burgdorferi* in the mammalian host

The infection in the mammalian host begins with the entry of the bacteria through the skin lesion created by a feeding tick. When the tick starts to feed, bacteria migrate from the tick's midgut into its salivary glands and are transmitted within the saliva that the tick secretes into the feeding pit [165]. Upon entry into the mammalian host, the infection remains localised for several days before the bacteria

begin to disseminate [12]; during this time, excision of the infected skin region can prevent disseminated infection [191]. During this stage, many of the changes in gene expression take place that are necessary to adapt to the host environment. The production of OspC is of particular importance during this stage [68], although its role is not fully elucidated.

The complement system is among the first defence mechanisms that *B. burgdorferi* encounters in its mammalian host. In particular, the opsonising function of the complement system has been shown to have a significant impact on the control of bacterial loads in mice [112], whereas defects in parts of the complement system involved in complement-mediated lysis of bacterial cells had no effects [19].

B. burgdorferi is recognised and induces immune responses in many different cell types. Central to its recognition in most cells is toll-like receptor (TLR)-signalling. TLR2 and the adapter molecule MyD88 in particular are critical for the induction of early immune responses [229], and TLR2-deficient mice show severe defects in induction of proinflammatory signals and production of *B. burgdorferi*-specific antibody [1].

Phagocytic cells such as macrophages and neutrophils are among the first effective immune responses against *B. burgdorferi* as well. Their ability to engulf and efficiently digest *B. burgdorferi* is well documented *in vitro* [137, 138] and is likely to be present in the *in vivo* situation as well [229]. In addition to phagocytosis of the bacteria, a main role of phagocytic cells in the early immune reaction is the secretion of pro-inflammatory signals that reinforces the innate immune response [36]. Interestingly, *B. burgdorferi* induces anti-inflammatory signalling by interleukin 10 (IL-10) production in phagocytes as well [113]. This anti-inflammatory signalling seems to play a role in the severity of the disease. Mice deficient in IL-10 show significantly reduced severity of symptoms such as arthritis. This increase in severity is not linked to an increase in spirochaete burden; to the contrary, the same mice showed a 10-fold lower bacterial load in tissues [23]. These results highlight the dual role of inflammatory signalling in the pathogenesis of Lyme disease: on the one hand, it has a protective role by controlling the infection, but an excessive immune response contributes to tissue damage and disease symptoms on the other hand.

After the initial delay of two days, *B. burgdorferi* begin to disseminate [12]. However, dissemination seems to start slow, since excision of the infection site within the next days still prevented a systemic infection in a majority of experimentally infected mice [191]. For the penetration of tissues during dissemination of the spirochaetes, they move through the extracellular matrix. This process is assisted by the recruitment of several host factors and activation of matrix metalloproteinases in the host [173]. In this stage, the bacteria penetrate endothelial barriers and migrate into the bloodstream which could lead to hematogenous dissemination of bacteria and is associated with symptoms of the systemic disease [233]. However, the relative importance of the hematogenous route as opposed to other routes such as the lymphatic route or even direct migration to other tissues is not clear. Given the high motility of the spirochaetes discussed before, such other ways of dissemination can not be excluded and might

be supported by the fact that while almost all patients with detectable bacteria in the blood display symptoms, by far not all patients with systemic symptoms also show spirochaetemia [233].

The humoral immune response is crucial for control and protective immunity in mice [229]. IgM antibody appears first approximately one week post infection and increases in concentration until reaching a plateau approximately two weeks post infection. At the same time, *B. burgdorferi* specific IgG appears in high concentration and continues to increase through day 30 [12]. Especially IgM is important for the early control of *B. burgdorferi* infections in mice. A specific IgM response is T cell independent and mediated by the encounter of blood-borne *B. burgdorferi* by marginal zone B cells, a subset of B cells localised in the marginal zone of the spleen that provides a fast specific antibody response [14]. IgG is required for neither control of the infection nor protective immunity [229]. However, it can have protective effects in mice [55]. Interestingly, antibody production is largely independent of TLR signalling [1].

During the disseminated stage of the infection, persistence of the bacteria requires a number of adaptions of *B. burgdorferi*. It has been shown to actively downregulate outer surface protein A (OspA) in response to the specific immune reaction in its host [83] and also OspC, which is only required during the early stage in the mammalian infection and may present a target for specific antibodies later [115, 215]. The changes in the expression of surface antigens include the increased expression of the highly variable VlsE. While the exact function of VlsE is not known, its expression and variation via antigenic shift has been shown to be required for long-term bacterial persistence [8].

3.1.3 Clinical symptoms of Lyme disease

Humans are only incidental hosts in the life cycle of *B. burgdorferi*. While the infection in its natural reservoir host, mainly rodents and birds, typically does not lead to disease symptoms [216], it causes mild to severe symptoms in the majority of infected human patients. The symptoms can be divided into different disease stages that start with the early localized infection and end with late symptoms that can occur years after infection.

The first visible symptom in humans typically consists of a circle shaped skin rash that develops around the site of the tick bite and spreads and moves with time. The development and severity of this skin rash depends on the species causing the infection and it is not necessarily present in all patients. In the case of *B. burgdorferi* s.s., the skin rash, called erythema migrans, is often associated with strong inflammation and dissemination of the spirochaetes, which is less pronounced in the predominant strains in Europe, *B. afzelii* and *B. garinii* [202]. In general, all Lyme disease spirochaetes can cause all disease symptoms, but the incidence of some symptoms in infected patients may differ. In the following, the symptoms described are typical of *B. burgdorferi* s.s.. Hence, the ratio of patients displaying a particular symptom applies to *B. burgdorferi* s.s. infection, although the other species cause similar symptoms.

After the early infection stage, bacteria disseminate and cause symptoms in many different tissues. Common symptoms include CNS complications (15% of patients), cardiac involvement (5% of patients) and an inflammation in the synovial tissue in the joints known as Lyme arthritis (60% of patients) [202].

Although not the most common symptom, much of the discussion and public attention concerns neurological symptoms of acute and late Lyme disease. Manifestations of neurological involvement include cases of encephalopathy and peripheral neuropathy that have been attributed to late Lyme disease [71]. Contrary to an ongoing discussion (mainly among patient interest groups and in the lay press) [54], no other symptoms like fatigue or other less than clearly defined symptoms could be linked to Lyme disease [71].

Cardiac complications are rare; typically, they consist of myocarditis with symptoms of arrhythmia and, in some cases, cardiomyopathy [199].

By far the most common symptom of infection with *B. burgdorferi* s.s. is the development of Lyme arthritis. Patients with Lyme arthritis experience recurring attacks of synovial inflammation, mainly in large joints like the knee, that resolve spontaneously without treatment in the course of months to years in a majority of patients [203]. A minority of patients has persistent symptoms; in approximately 10% of patients, these symptoms persist even after antibiotic treatment, a condition termed antibiotic-refractory Lyme arthritis [202]. The root cause for this condition is not known as of today; however, the overrepresentation of certain HLA alleles that are linked to rheumatoid arthritis in patients with antibiotic-refractory Lyme arthritis has led to the hypothesis of an autoimmune component [204].

Treatment of Lyme disease consists mainly of antibiotic therapy with dosage and duration depending on the disease stage and the symptoms involved. Typically, antibiotics applied orally over the course of 2-3 weeks is effective [232] in resolving objective symptoms of Borreliosis. Longer antibiotic treatment has shown no benefit for resolution of subjective persistent symptoms in placebo controlled trials [104]. In terms of prevention, a vaccine targeting OspA has been developed and found to be effective [206]; however, the manufacturer has retracted it shortly after release.

3.1.4 Mouse Models For Borreliosis

Many species that are common as animal models in the laboratory are natural reservoir hosts for *B. burgdorferi*. This poses a problem for the development of suitable animal models, since e.g. wild type mice do not display typical symptoms of Lyme disease [216]. However, some inbred mouse strains show typical disease symptoms such as Lyme arthritis [11]. Although other species such as dogs [3] and Rhesus monkeys [163] show a greater similarity, mouse models are used most frequently for practical reasons.

Perhaps the most commonly used mouse strain for experimental Lyme arthritis today are C3H/HeJ mice. Although other strains such as BALB/c or C57BL/6 mice develop mild arthritis symptoms as

observed microscopically as well, symptoms are more pronounced and include symptoms such as joint swelling more frequently in C3H/HeJ mice. Moreover, the incidence of cardiac symptoms is most frequent in the C3H/HeJ strain [11] and they can be persistently infected [10]. However, it should be noted that mice do not develop the full spectrum of disease symptoms and that other species are more suitable for the study of these symptoms [85].

3.2 Modelling strategy and data basis

All models are based on data measured by Pahl et al. [156]. In their study, mice were intradermally infected with *B. burgdorferi* by subcutaenous injection of the spirochaete burden was quantified over a course of 55 days in BALB/c and C3H/HeJ mice to account for differences in disease susceptibility. Quantification of bacterial load was performed by quantitative polymerase chain reaction (PCR) (qPCR) in different tissues. Since C3H/HeJ mice are a standard animal model for Lyme arthritis in humans whereas BALB/c mice show little to no symptoms [12], the data from C3H/HeJ mice were chosen for modelling. However, although the total bacterial load is different, qualitative features of the observed dynamics are consistent between both mouse strains [156].

The dynamics of the bacterial load at the infection site are remarkable. Figure 3.2 provides an overview of the bacterial load at the infection site, i.e. the skin site where bacteria were injected over 55 days. Interestingly, the bacterial population starts to decrease within the first $24\,\mathrm{h}$ post infection (p.i.) and stabilises at very low levels for several days. During the next $48\,\mathrm{h}$, bacteria can be detected, but in very low numbers. Despite this strong early decrease, *B. burgdorferi* survives this initial challenge and the population grows to a concentration that exceeds the initial load $1\,\mathrm{h}$ p.i. by a factor of 10.

In order to propose plausible reasons for the observed recovery of the bacterial population at the infection site, mathematical models were developed for three different hypotheses:

1. Bacterial migration might help to escape from the immune system to another tissue. Bacteria begin to disseminate at day 2 – 3 p.i. [12]. The bacterial population recovers only after this dissemination has started. Hence, it is hypothesised that spirochaetes escape by migrating to other tissues where they can replicate and migrate back to the infection site (Model 1).

2. Phagocytic cells might not be able to process enough bacteria (Model 2).

3. Bacteria might recognise the host immune reaction and adapt accordingly (Model 3).

Since C3H mice start to develop detectable antibody titers around 7 days p.i. [12], the decrease in bacterial load at time points $>$ 8 days p.i. are likely to result from the adaptive immune response. This notion is further supported by the fact that this decline after the first week of infection is not seen in immunodeficient SCID mice which lack an effective adaptive immune response [83]. However, other

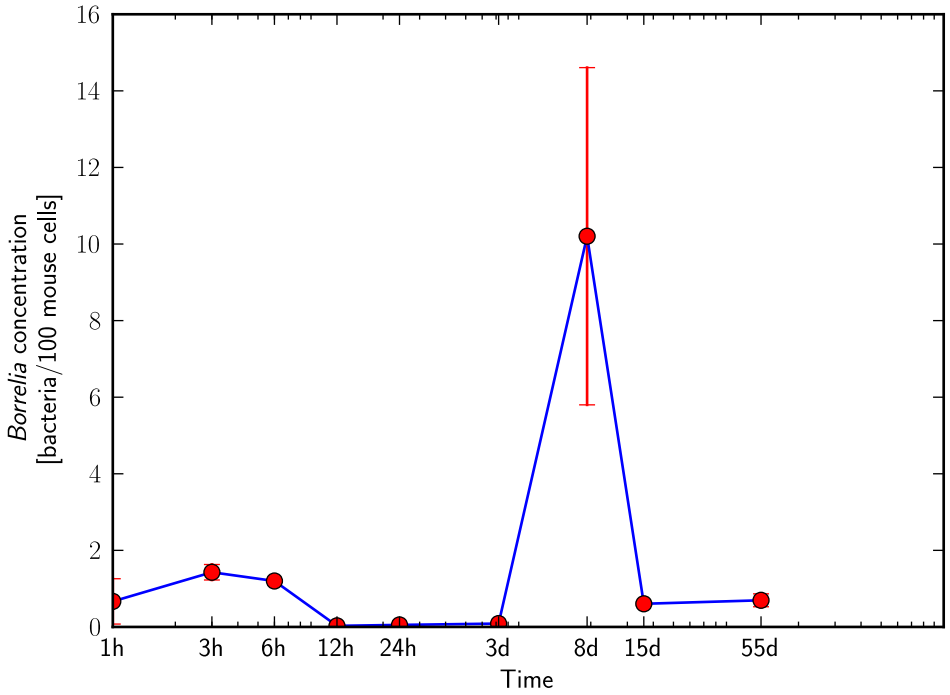

Figure 3.2: Measurement of bacterial load at the infection site in mice infected with *B. burgdorferi*. Displayed are means and standard error of the mean.

factors such as quorum sensing cannot be excluded. In the following modelling work, the late decline is assumed to correspond to antibody production. A full model for the adaptive immune response is beyond the scope of our modelling work, since the initial purpose was mainly to elucidate possible reasons for the bacterial recovery between day 3 and 8 p.i.. Hence, the primary aim is to explain the first 8 days p.i.. The adaptive immune response is introduced in Model 3 by using measured antibody concentrations and simple antibody binding kinetics. All three hypotheses are implemented as deterministic models using ODEs. Parameters were set from empirical findings where possible. In many cases, no empirical data on necessary model parameters was available. In order to estimate these parameters, a fitting procedure using data on the bacterial load at the infection site from the study by Pahl et al. [156] was employed. Fitting involved minimisation of the root of the mean squared residuals in logarithmic space (RMS):

$$RMS = \sqrt{\frac{1}{n}\sum_{i=1}^{n}(\log y_i - \log \hat{y}_i)^2}, \tag{3.1}$$

where n is the number of datapoints, y_i denotes a single measured datapoint and $\hat{y}_i$ the corresponding model output. Parameter sets with parameters used in the simulations can be found in Appendix A.

3.3 A Three-compartment Model Including Bacterial Migration (Model 1)

Hematogenous dissemination, i.e. migration of bacteria within the host by entry into the bloodstream, is commonly viewed as a major factor in the disseminated infection stage in Lyme disease, although the topic is still under debate [155, 209, 233]. Although there is evidence suggesting a role of migration through tissues [e.g. by intravital imaging, 110], its role and relative importance is unclear. In contrast, hematogenous dissemination shows a clear association with disease symptoms [233]. In Model 1 [published in 18], hematogenous dissemination is assumed to be the major route of dissemination.

To model bacterial migration, a structure with three compartments was chosen. The first compartment represents the infection site, the blood is viewed as another component and the third compartment represents a measurement site at the contralateral hindfoot [see 156]. In each of these tissues, bacterial migration is described by a logistic growth model,

$$\beta B_i \left(1 - \frac{B_i}{K}\right), \tag{3.2}$$

where B_i represents the bacterial load per 10^6 mouse cells, β is the bacterial growth rate and K is the carrying capacity, i.e. the maximal concentration that the bacteria can reach. The growth rate, β, can be estimated from *in vitro* studies at approximately $0.06\,\mathrm{h}^{-1}$ [9]. K is difficult to derive for the *in vivo* situation. A rough estimate, however, can be achieved by taking the highest value observed in the *in vivo* data by Pahl et al. [156] as a lower limit and the carrying capacity seen in *in vitro* studies as an upper limit.

For the transmission of bacteria between the tissues, dissemination through the bloodstream is considered exclusively. The model structure resulting from this assumption is depicted in Figure 3.3. Between each of the distal tissue sites and the bloodstream, migration rates from the bloodstream to the tissue, denoted by ν, and from the tissue into the bloodstream, μ, are considered. Since direct measurements of these rates are difficult, the corresponding parameters have to be estimated.

Phagocytic cells are a critical component in the first line of defence against *B. burgdorferi* in mammalian hosts [139]. In this model, a constant phagocytosis rate, ρ, is assumed. This implies the assumption that phagocytosis is not limited by the capacity of uptake and digestion of bacteria by the phagocytic cells; the impact of such limitations is explored in Model 2.

Taking into account bacterial growth, migration between tissues and blood and phagocytosis, bacterial dynamics in the three compartments can be expressed as

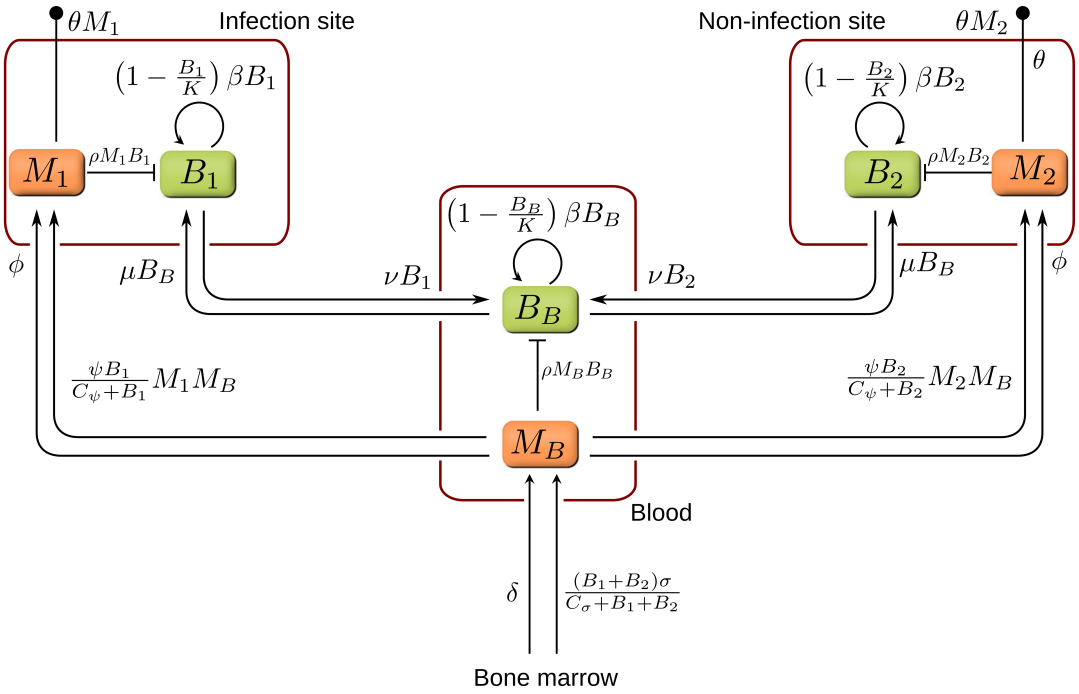

Figure 3.3: Three-compartment model (Model 1) for *B. burgdorferi* population dynamics: model structure. The three compartments are represented by the large rectangles. B represents *B. burgdorferi* and M phagocytic cells in the respective compartments.β: *B. burgdorferi* growth rate; K: carrying capacity; ρ: phagocytosis rate; θ: phagocyte death rate; C_σ, C_ϕ: bacterial load at half-maximal phagocyte recruitment; ϕ, δ: background phagocyte recruitment; σ, ψ: phagocyte recruitment rate (infection response); μ, ν: migration rates from tissue to blood and blood to tissue. Reproduced and modified after [18].

$$\frac{dB_1}{dt} = \left(1-\frac{B_1}{K}\right)\beta B_1 - \nu_1 B_1 + \mu_1 B_B - \rho M_1 B_1, \tag{3.3}$$

$$\frac{dB_2}{dt} = \left(1-\frac{B_2}{K}\right)\beta B_2 - \nu_2 B_2 + \mu_2 B_B - \rho M_2 B_2, \tag{3.4}$$

$$\frac{dB_B}{dt} = \left(1-\frac{B_B}{K}\right)\beta B_B + \nu_1 B_1 + \nu_2 B_2 - (\mu_1+\mu_2) B_B - \rho M_B B_B, \tag{3.5}$$

where B_1 denotes the *B. burgdorferi* population at the infection site, B_2 the population at the secondary site and B_B denotes bacteria in the blood.

In this and the two following models, no distinction is made between different types of phagocytic cells. A population of resident phagocytic cells is assumed to be maintained by constant production and migration to the bloodstream. In addition to this constant supply of phagocytic cells, an infection dependent production and recruitment to the tissues is assumed. Release of phagocytic cells into the bloodstream in response to the infection is given by a saturable function that depends on the bacterial load:

$$\frac{(B_1 + B_2)\,\sigma}{C_\sigma + B_1 + B_2}, \tag{3.6}$$

where σ determines the maximal induction of phagocyte production by *B. burgdorferi* infection and C_σ denotes the bacterial load that yields a half-maximal induction of phagocyte production.

Recruitment of phagocytic cells to the tissue is described in a similar fashion but depends on the concentration of phagocytic cells in the tissue, as those produce inflammatory signals that attract more phagocytes. The recruitment of phagocytic cells into the tissue is expressed by

$$\frac{\psi B_i}{C_\psi + B_i} M_i M_B, \tag{3.7}$$

with ψ denoting the maximal recruitment rate, C_ψ the half-maximal concentration similar to Equation 3.6, and B_i and M_i the bacterial and phagocyte concentrations in the respective tissues.

Taking into account these considerations and assuming a constant death rate for phagocytes (θ), a constant release of phagocytes into the blood (ϕ) and a constant recruitment into the tissue (ψ) that are independent of the infection response, the phagocyte dynamics can be described by the differential equations

$$\frac{dM_1}{dt} = \phi M_B + \frac{\psi B_1}{C_\psi + B_1} M_1 M_B - \theta M_1, \tag{3.8}$$

$$\frac{dM_2}{dt} = \phi M_B + \frac{\psi B_2}{C_\psi + B_2} M_2 M_B - \theta M_2, \tag{3.9}$$

$$\frac{dM_B}{dt} = \delta + \frac{(B_1 + B_2)\,\sigma}{C_\sigma + B_1 + B_2} - \left(2\phi + \frac{\psi B_1}{C_\psi + B_1} M_1 + \frac{\psi B_2}{C_\psi + B_2} M_2 + \theta\right) M_B. \tag{3.10}$$

An overview of the full model is provided in Figure 3.3.

3.3.1 Model simulations

Parameters were set according to experimental observations where such data were available; unknown parameters were estimated using the DE algorithm as described in 3.2. Model simulations with these parameters reveal that bacterial migration can result in a recovery of the bacterial population. Figure 3.4 shows the development of bacteria and phagocytes in the three compartments modelled here.

The model can qualitatively reproduce the bacterial recovery observed in the data (Figure 3.4(a). The initial immune response significantly decreases the bacterial load at day 1 p.i. and is overwhelmed between day 5 and day 8. However, the initial decline is not fully reproduced. Furthermore, these simulations involve strong assumptions about the biological situation and parameters involved.

First, the estimated parameters for the bacterial migration show highly unbalanced migration rates. The migration rate from the infection site into the blood is more than 30 fold higher than the migration

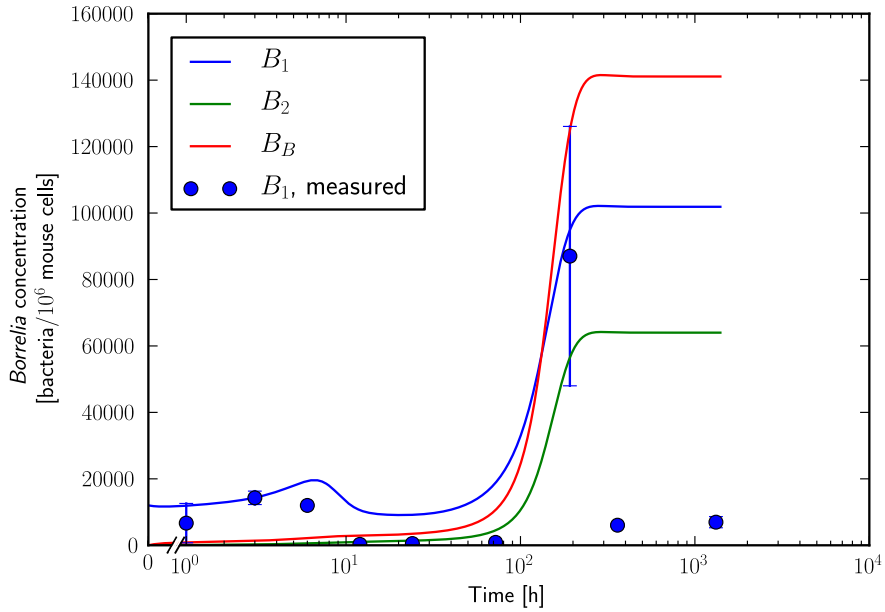

(a) Bacterial dynamics in the three compartments under consideration. The blue points show the measured bacterial load at the infection site. The corresponding model simulation is show in the blue curve.

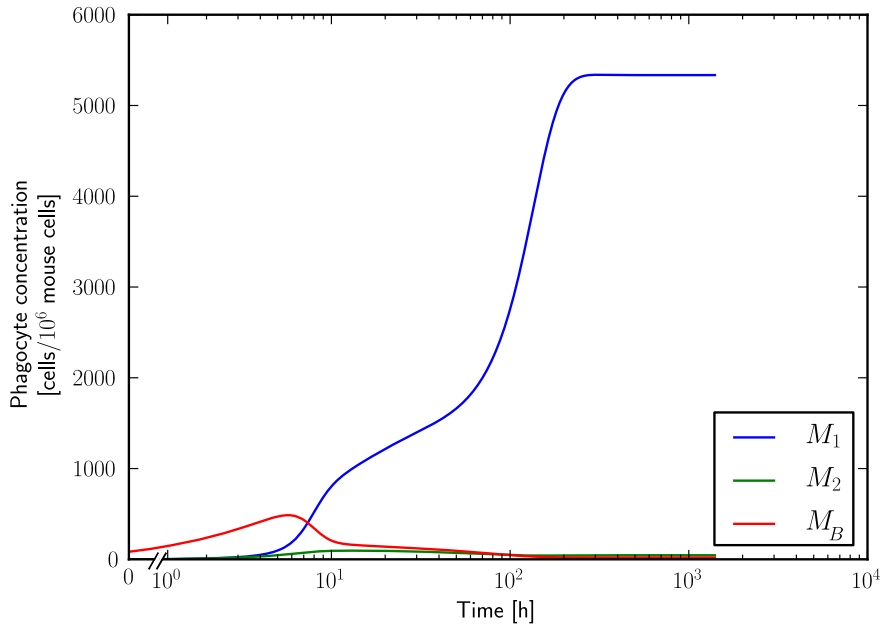

(b) Phagocyte dynamics in the three compartments under consideration.

Figure 3.4: Simulation results of Model 1. Dynamics of phagocytes in three compartments are shown: B_1, M_1 (blue): infection site, B_2, M_2 (green): non-infection site, B_B, M_B (red): blood

rate from the blood into the tissue. For the non-infection site, the situation is reversed: the estimated migration rate from the blood into the tissue is more than 30 fold higher than the migration rate from the tissue into the blood. This means that the movement of the bacteria would have to be directed. While such a mechanism is conceivable, experimental data to support this assumption are missing.

Second, the bacterial load in the blood is consistently very high compared to the tissue. While spirochaetemia is commonly observed in both mice and humans, the high spirochetal burden predicted by simulations of Model 1 seems unlikely. In experimental studies in C3H/HeJ mice, spirochaetes could not be cultured from the blood of infected animals before day 10 p.i. [12, 83], and even at late times, cultures were not consistently positive. This suggests that the bacterial concentration in blood is rather low and that the predicted high blood concentrations are not realistic.

A limitation of this model is its neglect of spatial effects at the infection site through the use of ODE. The model describes transmission and migration within the host on an abstract level, dividing the system into compartments. Hence, for example, movement within the dermis at the infection site cannot be described, as it is within the same compartment. However, as Radolf et al. [173] note, *B. burgdorferi* is a highly motile organism that can move more rapidly than immune cells within dense tissue such as the skin. While the impact of this effect is not known, it has been suggested that motility might aid the bacteria in the evasion of phagocytosis [110, 173]. Such effects are not mapped in the described model and require more explicit modelling of spatial effects.

3.4 A Single Compartment Model With Limited Phagocytic Capacity (Model 2)

The second hypothesis to be tested *in silico* was a limitation in the phagocytosis capacity. A volume that can be phagocytosed is limited naturally by the size of phagocytes. If bacteria take time to digest, phagocytic cells might operate at the limit of their uptake capacity, going into a saturated state in which they cannot take up more bacteria until a part of the engulfed ones is digested. In this model, only a single compartment is described, ignoring migration processes. Similar to the previous model, bacteria are assumed to grow according to a logistic growth model. Phagocytosis is modelled as a simple mass action term. Phagocytic cells, however, are subdivided into to populations: one population is active and can phagocytose more bacteria (M_a), the other one is inactive and does nothing but digest bacteria (M_i). Hence, bacterial dynamics can be expressed as

$$\frac{dB}{dt} = \left(1 - \frac{B}{K}\right)\beta B - \rho B M_a, \tag{3.11}$$

where the parameters β and K characterise the logistic growth function and ρ denotes the phagocytosis rate.

The phagocyte recruitment and death are modelled similar to the previous model. A constant influx ϕ is complemented by an infection dependent recruitment function that is saturable in B:

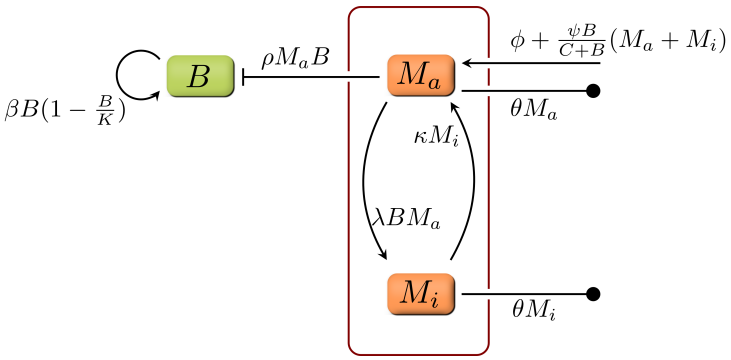

Figure 3.5: Structure of Model 2, describing bacterial and phagocyte dynamics in a single compartment with a limitation in the phagocytic capacity. B: Bacterial population, M_a: active phagocytes, M_i: saturated inactive phagocytes. Rates: ϕ,ψ: infection independent and -dependent phagocyte recruitment; λ,κ: transition from active to inactive state and vice versa; θ: phagocyte death rate; β,K: bacterial growth parameters; ρ: phagocytosis rate.

$$\frac{\psi B}{C+B}\left(M_a + M_i\right), \tag{3.12}$$

where ψ is the maximal infection dependent recruitment rate and C is the spirochaete concentration where phagocyte recruitment reaches its half-maximal value.

In the absence of detailed information about the kinetics of phagocyte uptake and the maximal uptake capacity, the transition to the saturated state was described simply by a mass action term, $\lambda B M_a$. The clearance of engulfed bacteria is described by a rate κ at which saturated phagocytes return to the active state. This leads to the following description of phagocyte dynamics:

$$\frac{dM_a}{d_t} = \phi + \frac{\psi B}{C+B}\left(M_a + M_i\right) - \lambda B M_a + \kappa M_i - \theta M_a, \tag{3.13}$$

$$\frac{dM_i}{d_t} = \lambda B M_a - \kappa M_i - \theta M_i. \tag{3.14}$$

Figure 3.5 shows an overview of the whole model structure.

3.4.1 Model simulations

Figure 3.6 shows numerical simulations of Model 2 with a parameter set determined by experimental data and fitted parameters (see appendix A for details). The model provides an explanation for the late recovery of the bacterial population after the initial decline. However, the dynamics do not fit well with the experimental results.

Furthermore, the clearance half-time of engulfed bacteria is approximately $20\,\mathrm{min}$ [138], which makes the observed phagocyte dynamics unlikely: although the rate κ cannot be directly compared to

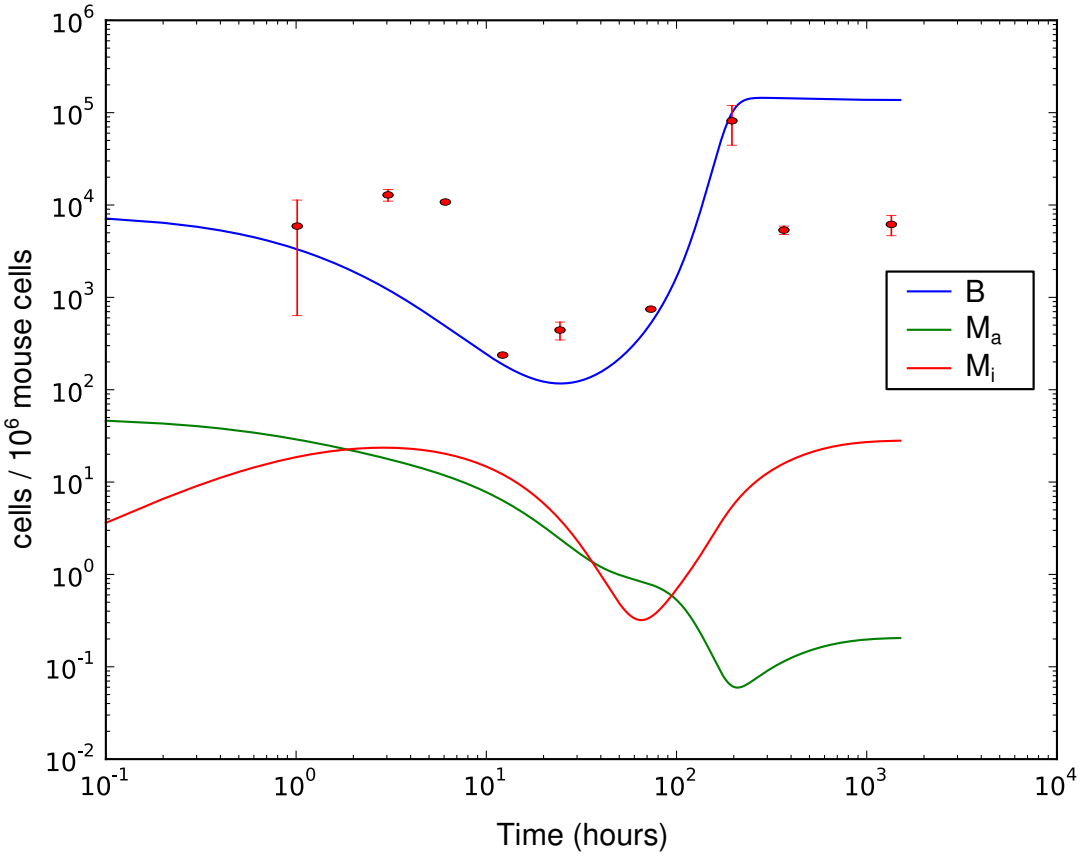

Figure 3.6: Bacterial and phagocyte concentrations in simulations of Model 2. While bacterial recovery after an initial decline is seen, the dynamics differ from experimental results.

the clearance rate from *in vitro* studies, the phagocytes remain in the inactive state for several days (Figure 3.6). More detailed information about the kinetics of *B. burgdorferi* phagocytosis by phagocytes would allow a more accurate model of the transition between active and inactive states of the phagocytes. However, results from this model suggest that this mechanism is unlikely to provide a full explanation for the observed bacterial dynamics.

3.5 Modelling Bacterial Adaptations To Its Host Environment (Model 3)

In view of the diverse adaptations that *B. burgdorferi* shows in its mammalian hosts, modelling all bacteria as a single homogenous population might not be appropriate. As discussed in 3.1.1, *B. burgdorferi* undergoes a variety of changes in its gene expression after entry into its vertebrate host, especially with respect to the expression of outer surface proteins [reviewed in 221]. Perhaps the best known example is the reciprocal regulation of OspA and OspC that depends on different environmental parameters [235] and the presence of certain host immune responses [83].

Considering that typical changes in gene expression patterns can take several days to occur in the skin of infected mice [82], the bacteria may well be in a suboptimal state that is not yet fully adapted to the new environment. However, the role of these adaptations during the early localised infection is not known. In Model 3, it is hypothesised that adaptations to the new host environment are responsible for the peculiar pattern during the early infection stage in the mouse skin. According to this view, bacteria are in an initial, not fully adapted state that makes them vulnerable to the hosts immune defence. However, they adapt to the new environment and change to a less vulnerable state.

Similar to Model 2, the infection site is the only compartment included in this model. Bacterial growth is modelled as logistic growth (Equation 3.2). However, the bacteria are now subdivided into two populations representing the vulnerable (B_t) and the adapted (B_m) state. Since the extent to which the bacteria are protected from the immune response is not known, the bacteria are assumed to be completely resistant against phagocytosis by the host.

Since the host environment is constantly present as a stimulus driving the bacteria to the resistant state B_m, a reversion to the vulnerable state seems unlikely. Hence, the transition from the vulnerable to the resistant state is modelled as an irreversible reaction. Combining bacterial growth in both populations and this transition, the bacterial dynamics can be expressed as

$$\frac{dB_t}{dt} = \left(1 - \frac{B_t + B_m}{K}\right)\beta B_t - \alpha B_t - \rho M, \tag{3.15}$$

$$\frac{dB_m}{dt} = \left(1 - \frac{B_t + B_m}{K}\right)\beta B_m + \alpha B_t, \tag{3.16}$$

where B_t is the population of vulnerable bacteria, B_m the adapted bacteria and α the transition rate between them. As in the previous models, β and K denote the growth rate and carrying capacity determining bacterial growth and ρ denotes the phagocytosis rate.

The dynamics of the phagocytic cells are modelled similarly to Model 2. However, since no evidence for a critical role of a limitation of the phagocytic capacity could be shown, such a limitation is not included in this model. This considerably simplifies the description of the phagocyte dynamics to

$$\frac{dM}{dt} = \phi + \frac{\psi B_{tot}}{C + B_{tot}} * M - \theta M. \tag{3.17}$$

In Equation 3.17, a constant infection independent recruitment is denoted by the rate ϕ. As in the previous models, attraction of more phagocytes in response to the infection (Equation 3.7) is included and θ denotes the death of phagocytic cells. B_{tot} refers to the sum of all bacterial populations, implying that bacterial cells are not invisible for the immune system, but resist phagocytosis. This is consistent with the fact that *B. burgdorferi* induces a strong inflammatory reaction at the infected site.

In the absence of phagocytosis of the resistant bacteria (B_m), this population cannot be controlled in the model. However, at the later measurements, a decline of the bacterial load is observed. An obvious

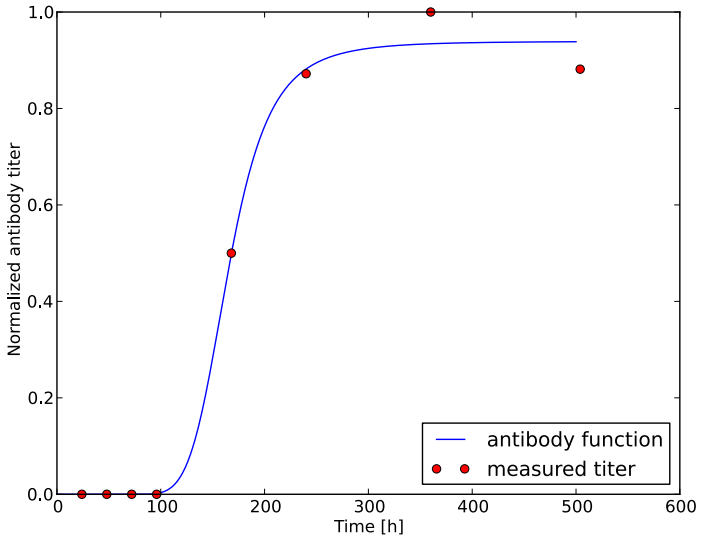

Figure 3.7: Measured antibody titers [12] and approximation by a smooth function given in 3.18.

explanation of this phenomenon is the onset of a humoral immune response that begins approximately one week p.i.. The transition from innate to adaptive immune responses is a complex process, and its description is beyond the scope of this model. Hence, measured titers of *B. burgdorferi* specific antibody are included as external input to the model. In order to approximate the measured data by a smooth function, the following piecewise definition was used:

$$I(t) = \begin{cases} 0 & t \leq \Delta t_{ig}, \\ \frac{(t-\Delta t_{ig})^n}{t_{1/2}^n + (t-\Delta t_{ig})^n} & t > \Delta t_{ig}. \end{cases} \tag{3.18}$$

In this description, Δt_{ig} denotes the delay until the onset of antibody production and $t_{1/2}$ is the time until the antibody concentration reaches half of its maximum. Figure 3.7 shows this function with the parameters that minimise the deviation from experimentally measured [12] antibody titers. Since only relative antibody concentrations are known, the antibody concentration is given in arbitrary units in the model.

The opsonisation of bacteria by antibody is modelled as reversible binding of antibody to bacteria:

$$\frac{dB_m}{dt} = -\mu I(t) B_m + \nu B_m^*, \tag{3.19}$$

$$\frac{dB_m^*}{dt} = \mu\ I(t)\ B_m - \nu B_m^* - \rho B_m^* M. \tag{3.20}$$

Hence, the total bacterial population is now subdivided into three parts: bacteria in the vulnerable state, resistant bacteria and opsonised bacteria. In the model, opsonised bacteria do not grow and the

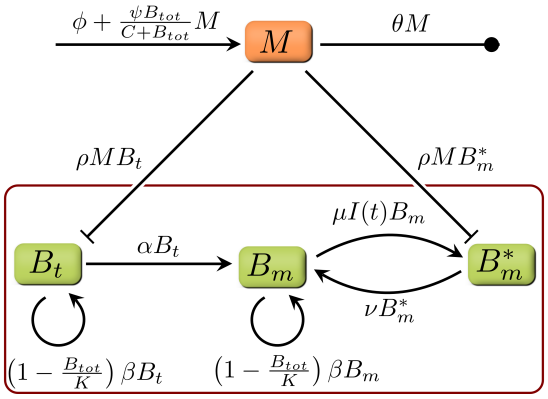

Figure 3.8: Model for population dynamics of *B. burgdorferi* with bacterial adaptations and antibody response. B_t represents bacteria in an initial vulnerable state after host entry, B_m are bacteria that have adapted to the new host environment and cannot be killed by phagocytes, B_m^* are bacteria opsonised by specific antibody and M represents phagocytic cells. I represents the antibody concentration. Parameters: ϕ: background phagocyte recruitment; ψ: phagocyte recruitment (infection response); θ: phagocyte death rate; β, K: growth rate and carrying capacity of bacteria; ρ: phagocytosis rate; α: transition rate to resistant state; μ,ν: antibody binding and dissociation rates.

bound antibody marks them for digestion by phagocytic cells. Combining Equations 3.20 and 3.16, the bacterial dynamics can be expressed as

$$\frac{dB_t}{dt} = \left(1 - \frac{B_t + B_m}{K}\right) \beta B_t - \alpha B_t - \rho M, \tag{3.21}$$

$$\frac{dB_m}{dt} = \left(1 - \frac{B_t + B_m}{K}\right) \beta B_m + \alpha B_t - \mu\, I(t)\, B_m + \nu B_m^*, \tag{3.22}$$

$$\frac{dB_m^*}{dt} = \mu\, I(t)\, B_m - \nu B_m^* - \rho B_m^* M. \tag{3.23}$$

3.5.1 Model simulations

Unknown model parameters were estimated using the DE algorithm. Numerical simulations of the model with these parameters show that it can reproduce the experimentally observed recovery of the bacterial population without considering a limitation in the phagocytic capacity or bacterial migration. Figure 3.9 shows simulations with the parameters listed in A.1.3: in Figure 3.9(a), a comparison between model output and experimental results is shown. An overview of the full model structure is depicted in Figure 3.8.

In the model, most bacteria have already adapted to the resistant state approximately $24\,\mathrm{h}$ p.i. (3.9(b). This results from the combined effect of the active transition to the resistant state and the phagocytosis of *B. burgdorferi* in the vulnerable state. Additionally, with decreased numbers of vulnerable bacteria, the resistant population can grow faster due to less competition for limited resources.

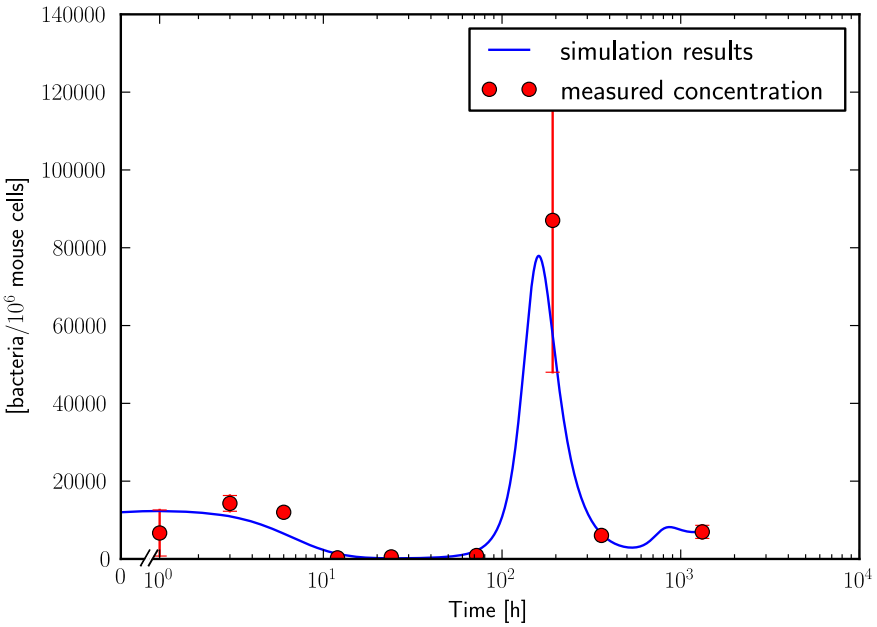

(a) Model simulation in comparison to experimental results by Pahl et al. [156]. The simulation (solid line) shows the sum of all three bacterial populations B_t, B_m and B_m^*.

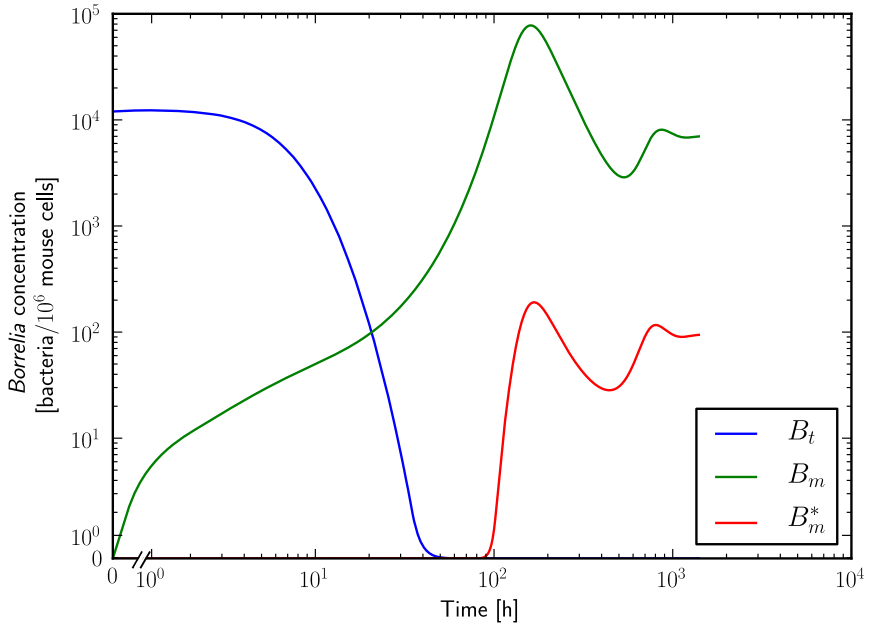

(b) Model simulation of all three bacterial populations. B_t shows bacteria in the initial, vulnerable state, B_m adapted bacteria and B_m^* opsonised bacteria.

Figure 3.9: Simulation results of Model 3: Bacterial dynamics.

These effects lead to an almost complete transition of the whole local bacterial population to the resistant state by $48\,\mathrm{h}$ which is consistent with experimental results where many typical changes in gene expression in the bacterial population are complete by day 2 p.i. [82].

Numerous adaptations of *B. burgdorferi* to environmental stimuli are well documented [40, 68, 83, 157, 173, 221, 241]. Interestingly, among other stimuli such as temperature and pH, *B. burgdorferi* has also been shown to react to the presence of certain parts of the host immune response. An example is the paradigmatic reciprocal regulation of OspA and OspC, where Hodzic et al. [83] could show that in immunodeficient C3H-*scid* mice, *B. burgdorferi* frequently expresses OspA. In comparison, immunocompetent C3H mice did not express OspA, highlighting an influence of the host's immune response and suggesting a role of OspA downregulation in immune evasion. Thus, the inclusion of an adaptation mechanism in the model seems appropriate, although the exact molecular details are not known and not described in the model.

The assumption of complete resistance against phagocytosis as the only immune mechanism at the early infection stage is a significant simplification of the *in vivo* situation. *B. burgdorferi* is recognised by different parts of the immune system that have a complex interplay and appear in sequence [229]. Further investigation of the early immune response and the immune evasion mechanisms of *B. burgdorferi* might elucidate the contribution of different immune evasion mechanisms and allow for more detailed models of the bacterial adaptations; so far, the current model suggests that bacterial adaptations are likely to play a role in the establishment of an early infection.

In the model, the late decrease in bacterial load is related to the onset of the antibody reaction. Since antibodies start to be produced around one week p.i., they are likely to be involved in this late control. The assumption is that antibody opsonisation inactivates the bacteria (no growth) and, more importantly, marks them for phagocytosis. This is in line with the experimental observation that opsonisation with specific antibody significantly increases the efficiency of phagocytic cells against *B. burgdorferi*.

The fitted antibody binding parameters, μ and ν, should be interpreted with caution, since the antibody binding kinetics neglect some details and antibody titers are measured in the serum and not in the tissue. Moreover, since no absolute concentrations are known, antibody concentrations have to be expressed in arbitrary units, which makes a comparison to known antibody binding kinetics difficult. The ratio $\frac{\mu}{\nu}$ can be seen as antibody affinity. This antibody affinity determines the bacterial load at day 55. However, $\frac{\nu}{\mu}$ can be altered by a factor of 100 without qualitatively changing the behaviour of the system in simulations (Figure 3.10). Hence, the model behaviour is considered to be qualitatively robust with respect to the antibody affinity.

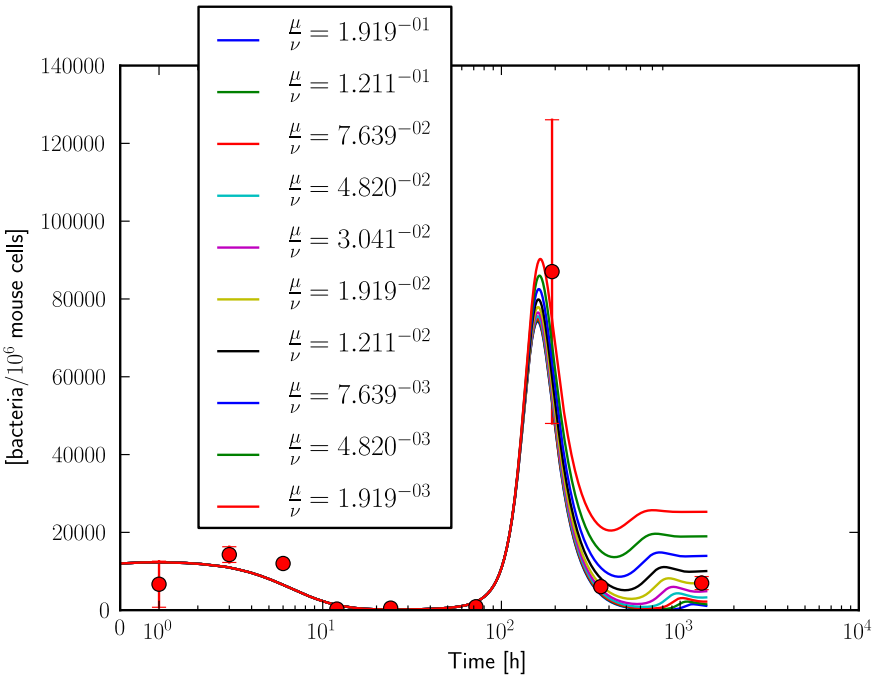

Figure 3.10: Bacterial dynamics with varying values for $\frac{\mu}{\nu}$. The bacterial load shown here is the sum of all three bacterial populations B_t, B_m and B_m^* All other model parameters were kept constant.

3.6 Model Comparison and Discussion

While all three models under consideration might provide an explanation for the observed recovery of the bacterial population after an initial decline, only Model 3 explains the bacterial dynamics under biologically realistic assumptions. Model 1 predicts unrealistically high bacterial loads in the blood, while Model 2 does not fit the observed dynamics well and predicts a low clearance rate of phagocytosed bacteria, which is inconsistent with experimental observations.

Although Model 1 suggests that hematogenous dissemination of the bacteria is not likely as an immune evasion mechanism during the first infection stage, bacterial motility cannot be excluded in general. In particular, the rapid movement of *B. burgdorferi* through dense tissues might aid the spirochaete to escape from the comparatively slow phagocytes. However, this question is difficult to answer by using an ODE approach and tackling this problem raises new questions such as whether or not bacterial movement is biased towards a signal or away from the infection site, how bacterial chemotaxis works with the unique motility system and how phagocytes are attracted towards the bacteria. The evaluation of intravital imaging data from *B. burgdorferi* inside murine skin [110] might aid in developing spatially resolved models for answering these questions.

Model 3 provides a reasonable explanation for the observed behaviour at the infection site. It has been hypothesised that the delay before bacterial dissemination starts is due to “reprogramming” of

the bacterial gene expression [229], which fits well with the idea of bacterial adaptation in Model 3. Altogether, the results from simulations of Model 3 warrant further investigation. Future work on the model could be focused in two major directions: including a more detailed description of the adaptation process and evaluating the long-term persistence of bacteria.

A more detailed model of the adaptation process can help to elucidate questions about the impact and function of certain host-specific adaptations. E.g., the role of OspC is under debate: to date, it is not clear whether its main function is to aid in dissemination within the tick or survival within the infection site of the host [173]. In this context, the influence of tick saliva that contains a multitude of immunomodulatory substances [229] is of interest. In the majority of infection experiments, needle inoculation has been used to infect the subjects. This is due to better control of timing and dose of infection, but the obvious disadvantage of this procedure is a loss of information about the natural infection route. There are, however, studies analysing infections transmitted by ticks that study bacterial dynamics and gene expression during the first days of the infection [82].

Analysing long-term persistence of *B. burgdorferi* involves modelling of antibody targets and bacterial evasion of antibody responses. Some interactions like antigenic variation in VlsE are known to be required for persistence of the spirochaetes. Another example is OspC: the protein has been shown to induce a specific antibody response and bacteria are selected against expression of OspC after its strict requirement during early infection [173].

The model highlights the importance of bacterial adaptations, especially in the early phase when the infection is established. Analysing the role of these adaptations as well as bacterial adaptations that occur during persistent infections can aid in selecting promising targets for vaccination and make suggestions for therapy optimisations. Extension in this direction should be the next step in future developments of the presented model.

4

Immune Response and Regulation in Influenza Infections

In the previous chapter, the dynamics of the early stage of a bacterial infection and interactions with the immune system have been presented. However, only one component of the immune system, phagocytic cells, was described. While this is appropriate for a model describing this particular bacterial infection due to the central role of the phagocytes in the immune reaction at that stage, a more detailed description of different immune strategies is required for other infections. In this chapter, a novel strategy for a more detailed description of the immune reaction is studied with the example of a viral infection.

With 20% of the children and 5% of adults worldwide developing new cases of influenza [152], influenza is a global threat to public health. Although the disease is mild in most cases, influenza poses a signifcant threat to certain patients [29, 58, 214]. Furthermore, the virus undergoes frequent antigenic variations, causing a constant risk for a global pandemic. The social and economic impact of influenza has sparked significant interest in models on the within-host viral dynamics [13].

There are two main goals in this chapter. The first objective is to elucidate the impact of different immune strategies in the early infection phase. The second goal is to establish a framework for the description of the immune responses and their interactions by modelling the dynamics of cytokine concentrations.

Cytokines are signalling molecules that play a central role in the regulation of the immune system. A large number of cytokines with various biological functions has been discovered in the last decades [45], and they are an important factor in the defence against immune reactions. Due to their central role in the regulation of immune reactions, understanding cytokines and their interactions helps to disentangle the activity of different branches of the immune system and their complex interactions. Furthermore, a model describing cytokine interactions has broad potential applications that range from the application in other infections to autoimmune diseases and other inflammatory conditions.

4.1 Background

4.1.1 Biology of Influenza Viruses

Influenza belongs to the family of *Orthomyxoviridae*. The family consists of the influenza A, B and C virus, of which the influenza A and B genera are pathogenic for humans. Influenza A virus is further classified according to two important transmembrane glycoproteins, Haemagglutinin (HA) and Neuraminidase (NA). Subtypes of influenza A virus are named by referring to the subtypes of these proteins; e.g., the subtype H1N1 is an influenza A virus with subtype 1 of HA and subtype 1 of NA. Out of the 15 HA and 9 NA subtypes that have been discovered, only the HA subtypes H1, H2 and H3 and the NA subtypes N1 and N2 are commonly found in human infections [152].

Influenza virus infections most commonly affect the upper respiratory tract, where the virus replicates within epithelial cells, but can also infect other cells like macrophages [96]. HA mediates the entry of the virus into the host cell by binding to sialic acid receptors [193]. Upon attachment of the virus, it enters the host cell via endocytosis. Endocytosis is mainly clathrin-mediated, but multiple pathways are exploited in parallel [181]. The endocytosed virus is then trafficked to endosomes, where a low pH triggers viral fusion with the vesicle and viral ribonucleoproteins are released into the cytoplasm [107, 193]. The ribonucleoprotein complex containing the single-stranded RNA of the virus then enters the nucleus, where the viral genome is replicated and transcribed. Viral messenger RNA (mRNA) is then exported into the cytoplasm, where new viral proteins are translated and imported into the nucleus. In the nucleus, they can encapsulate viral RNA and form new RNPs that are exported from the nucleus and transported to the plasma membrane. When the concentration of viral proteins on the plasma membrane is high enough, new virions are assembled and released from the cell with the help of NA [89].

4.1.2 The Immune Reaction to Influenza

Innate immune reactions

The importance of innate immune reactions has been discussed in the context of a bacterial infection in the previous chapter, but the rapidly acting first line of defence is central in the immune response to viral infections as well. One of the first immune responses to influenza infections is triggered by the detection of single-stranded RNA (ssRNA) by retinoic acid-inducible gene I (RIG-I) [164] and TLR-7 [122]. TLR-7 is mainly important for the recognition of viral ssRNA in plasmacytoid dendritic cells (pDCs) [43, 122], whereas RIG-I is central in many other cell types like epithelial cells or conventional dendritic cells (cDCs) [98, 106]. In addition to RIG-I and TLR-7, NOD-like receptors (NLRs) are involved in the recognition of the virus by infected cells [159].

The intracellular recognition by these pathogen recognition receptors (PRRs) induces the production of several proinflammatory cytokines and the type I interferons interferon α (IFN-α) and interferon β (IFN-β) [122, 164]. The expression of type 1 interferons is one of the first immune responses to influenza infections and is typically visible only hours after the infection and has direct antiviral effects by inducing the production of a whole set of antiviral products. Genes that are induced by type I interferons are commonly referred to as interferon-stimulated genes (ISGs) and comprise hundreds of genes, among them the Mx proteins that significantly limit viral infection of target cells [77, 198]. However, the virus produces the NS1 protein that inhibits the type 1 interferon response by interfering with the RIG-I system [70, 227], which highlights the important role of type 1 interferon in the antiviral immune response.

Multiple cell types are involved in innate immunity against influenza. Neutrophils and macrophages both contribute significantly to viral clearance by the removal of apoptotic infected cells [74, 140]. Macrophages detect virus in phagocytosed cells via TLR-3 receptors, which induces the production of pro-inflammatory cytokines like tumour necrosis factor (TNF) and type 1 interferon; pDCs endocytose influenza virus and react by production of a similar set of cytokines [93]. cDCs are mainly important for their role as antigen presenting cells that interact with $CD8^+$ and $CD4^+$ T cells [106], promoting the activation of specific immune responses. Another cell type that plays an important role in influenza immunity are natural killer cells (NKs) [62], a cell type that recognises opsonised infected cells and mediates apoptosis.

Adaptive immune responses

While the innate immune system forms the first line of defence and is critical in the early phase when the infection is established, the adaptive immunity has a central function in clearance of the virus and protective immunity [93].

Among humoral immune responses, HA is well established as an antibody target that protects from influenza infections [60, 64, 126]. HA is highly immunogenic and induces IgA and IgG responses. HA reactive IgA is central in the mucosal immunity induced by influenza infections, and the serum IgG antibody provides highly efficient, long term immunity and protects from lung infection [92, 177]. HA, however, is highly variable [27], which poses a problem especially for vaccination [39]. Other antibody targets include NA and Matrix preotein 2 [106].

Cytotoxic $CD8^+$ T cells (CTLs), a T cell subtype that can lyse infected cells, are a crucial component of the cellular immune reaction to influenza virus. Mice with defective CTLs show severe deficiencies in viral clearance [15], and CTLs protect mice without antibodies and functional B cells from influenza [51]. In contrast to HA and NA, the proteins targetet by CTL display a low amount of variation between different influenza subtypes, and consequently, the immune protection provided by CTL depends less on the subtype [149, 223].

4.1.3 Cytokines in Influenza Infections

The interactions of cytokines and the reactions they cause in immune effectors are highly complex. In addition to their important role in the immune system in general, they are of particular significance in influenza infections. Cytokines are crucial in control, but also pathogenesis of the infection, as they mediate not only immune responses critical for control of the viral infection, but also symptoms of the disesease [24]. They may also be involved in the increased vulnerability of influenza infected patients to secondary bacterial infections that are associated with high mortality, especially with increasing age [128]. The model of the immune response to influenza presented in this chapter focuses on the cytokine response in order to predict the interactions between different parts of the immune system. In the next paragraphs, several cytokines are briefly introduced that are considered important during influenza infections.

Type I Interferons IFN-α and IFN-β are an important part of the innate immune system. Their direct antiviral activity as the first part of the innate immune reaction has already been discussed in Section 4.1.2. In addition, they also contribute to the expression of chemokines that attract macrophages and type 1 T helper cells (T_h1 cells) to the infection site [96]. In NK, type 1 interferon stimulates cytotoxicity [116] and induces interferon γ (IFN-γ) expression [123]. Another effect of this cytokine is an increase in antigen presentation that in turn promotes the activation of CTLs [201].

Interferon γ IFN-γ is the central cytokine of the T_h1 cell subset. It is produced by T_h1 cell, CTL, and NK and has effects on a variety of cells. Similar to type I interferon, it upregulates antigen presentation by upregulating various parts of the antigen presentation pathways [reviewed in 187]. In addition to some overlap in functionality between type I interferons and IFN-γ with respect to direct antiviral effects, IFN-γ activates and stimulates the proliferation NK [230], which are also an important source of IFN-γ [184]. Furthermore, it activates macrophages and increases production TNF [225] and inhibits the production of interleukin 4 (IL-4) [158]. IL-4 is an important type 2 T helper cell (T_h2 cell) cytokine; thus, inhibition of IL-4 promotes T_h1 cell differentiation [158].

Tumour necrosis factor TNF is a pro-inflammatory cytokine that is produced by macrophages, lymphocytes, NK and endothelial cells during influenza infection and has shown strong antiviral effects [190]. It induces the production of a large number of other cytokines such as IFN-γ or interleukin 6 (IL-6)(see also Table 4.2.2) and contributes to the recruitment of phagocytes, CTL and NK [194].

Interleukin 1β interleukin 1β (IL-1β) is a pro-inflammatory cytokine that shows widely overlapping functions with TNF [96]. Similar to TNF, it contributes significantly to viral clearance, but also to the lung pathology induced by the infection [186]. It was found to recruit neutrophils, participate in the activation of $CD4^+$ T cells and enhance IgM production [186].

Interleukins 12 and 18 interleukin 12 (IL-12) and interleukin 18 (IL-18) are inflammatory cytokines produced by macrophages. The main effect of both cytokines is an activation of IFN-γ expression in NK and T cells [154]. Interestingly, only IL-18 promotes CTL function [42].

Interleukin 2 While not specifically important for the regulation of the immune response to influenza, interleukin 2 (IL-2) is mentioned here because of its central role in lymphocyte proliferation. It has long been known that IL-2 promotes the proliferation of T cells [196]. However, it has an important role in the homeostasis of the immune system as well, and is involved in the maintenance of regulatory T cells (T_{reg}). Additionally, it increases NK cytotoxicity [78].

Interleukin 6 Main sources of IL-6 include antigen presenting cells, B cells and epithelial cells. It is often considered a pro-inflammatory cytokine and its functions in lymphocyte activation, proliferation, and differentiation as well as in activation of macrophages have long been described [102]. However, IL-6 has a multitude of functions and is involved in the regulation of different immune reactions. Notably, it is essential in the transition from the innate to the adaptive immunity [95] and promotes antibody production mediated by induction of interleukin 21 (IL-21) production in $CD4^+$ T cells [44]. A recent study supports the view of IL-6 as an essential component in the initiation of an adequate adaptive immune response and suggests a role in control of tissue inflammation during influenza infection [108].

Interleukin 10 IL-10 is an antiinflammatory protein that can be produced by many immune cells. Its main function is control of inflammatory responses to prevent tissue damage by the inhibition of inflammatory cytokines such as IFN-γ [182]. During influenza infections, mice deficient in IL-10 showed increased influx of T cells into the lungs and increased IFN-γ expression and recovery from the infection was delayed [118].

4.2 Modelling Cytokine interactions

4.2.1 Experimental Data

As cytokines play an important role in the context of influenza infections, a number of studies have measured the cytokine dynamics over the course of influenza infection [e.g. 76, 169, 211, 217]. The available studies differ in which organism the study was performed, how long and how frequently and which cytokines were monitored and how cytokine dynamics were measured. Depending on these parameters, some of these studies are better suited for particular modelling approaches than others. For the development of this model, a transcriptome wide gene expression study by Pommerenke et al. [169] in a mouse model of influenza infection was selected. In this study, C57BL/6J mice were infected with a

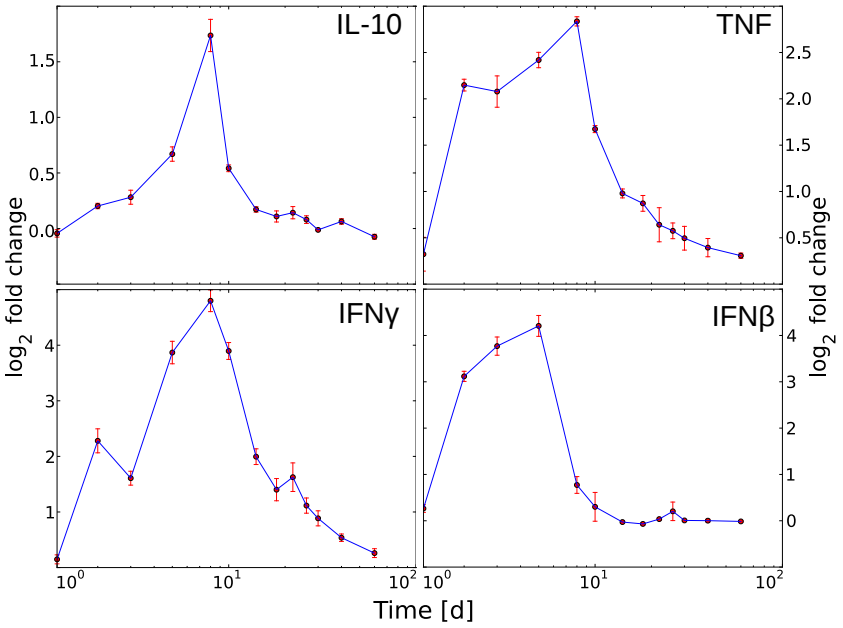

Figure 4.1: Data on cytokine gene expression over the whole 60 days time frame. Dots show the mean value, error bars show standard deviations. Data are extracted from microarray data published by Pommerenke et al. [169].

mouse adapted influenza A H1N1 strain, and gene expression was assessed in microarray experiments over a course of 60 days as described in [169].

This study has two main advantages for the development of a model of the cytokine network: First, the use of a microarray experiment provides measurements for a large number of genes, and model development is thus not limited by the availability of observable variables in the system. Consequently, extensions of the model in unexpected directions does not require new experiments, and all state variables in the networks are observed. Second, the dense measurements in the beginning and the long follow-up until day 60 p.i. offers enough data from all relevant time periods of the infection to model different parts of the immune response. It should be noted, however, that the use of microarray data also imposes limitations on parts of the modelling work; e.g., measured quantities cannot be directly interpreted in terms of cytokine concentrations.

For use of the data in the model, pre-processed data from Pommerenke et al. [169] were used and the corresponding values for cytokine transcript extracted using the R software. Figure 4.1 shows the data on cytokine expression for four of the cytokines in the model.

Viral dynamics were not published in the study. However, viral kinetics from identical experiments were published by the same authors [41] and more pooled measurements from identical experiments were kindly provided by the authors. Viral concentrations were determined in a focus formation assay following the procedure outlined in [41] and concentrations were reported as focus formation units (FFU) per mL lung homogenate. Figure 4.2 shows the measured virus concentrations.

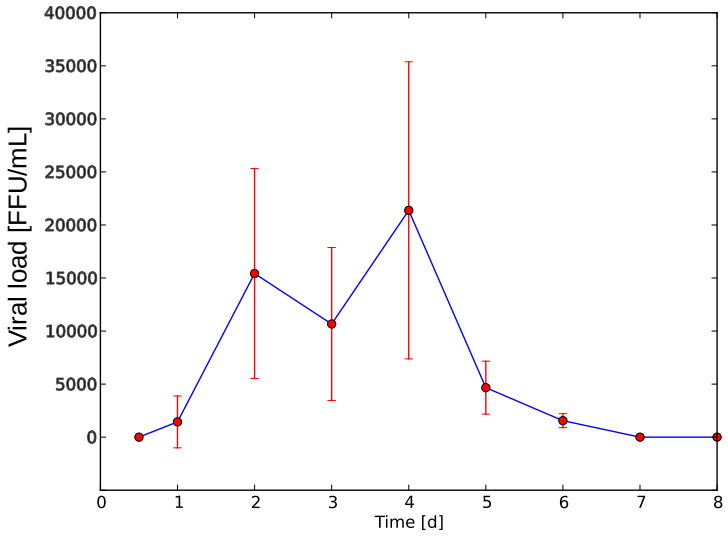

Figure 4.2: Data on virus loads during experimental influenza infection of C57BL/6J mice as described in Dengler et al. [41]. Dots show the mean value, errror bars show standard deviations.

4.2.2 Model Structure

Modelling cytokine interactions is the core of this mathematical description of the immune response to influenza infections. The underlying observation is that the changes in the concentration of a cytokine have effects on the production of other cytokines. The exact nature or source of the change in cytokine production is modelled implicitly in a dose-response function between two cytokines. In essence, the interactions between cytokines are treated as direct effects.

The interactions of cytokines are highly complex and their behaviour often poorly understood. The first objective in the development of a model designed to describe the dynamics of cytokines was to identify a network of cytokine interactions by evaluation of published studies. Figure 4.3 provides an overview of a network of cytokine interactions. Literature references for the cytokine interactions depicted in the network can be found in Table 4.2.2. Cytokines were included in the overview if they are a) relevant and b) non-redundant with respect to their function in the immune response to influenza and its regulation.

In many experimental studies that analysed the relationship between cytokine concentration and the production of cytokines by cells, a dose-response relationship resembling log-sigmoidal functions is observed [e.g. 52, 120, 213]. Log-sigmoidal functions dose-response functions have been succesfully applied in the context of mathematical modelling of cytokine regulation and interactions of the immune and neuroendocrine systems [131]; a similar strategy is chosen for the description of cytokine interactions in this model.

Dose-response relationship were described by log-sigmoidal functions that are characterised by four parameters. An activating or inhibiting interaction between one cytokine with a concentration X_i and

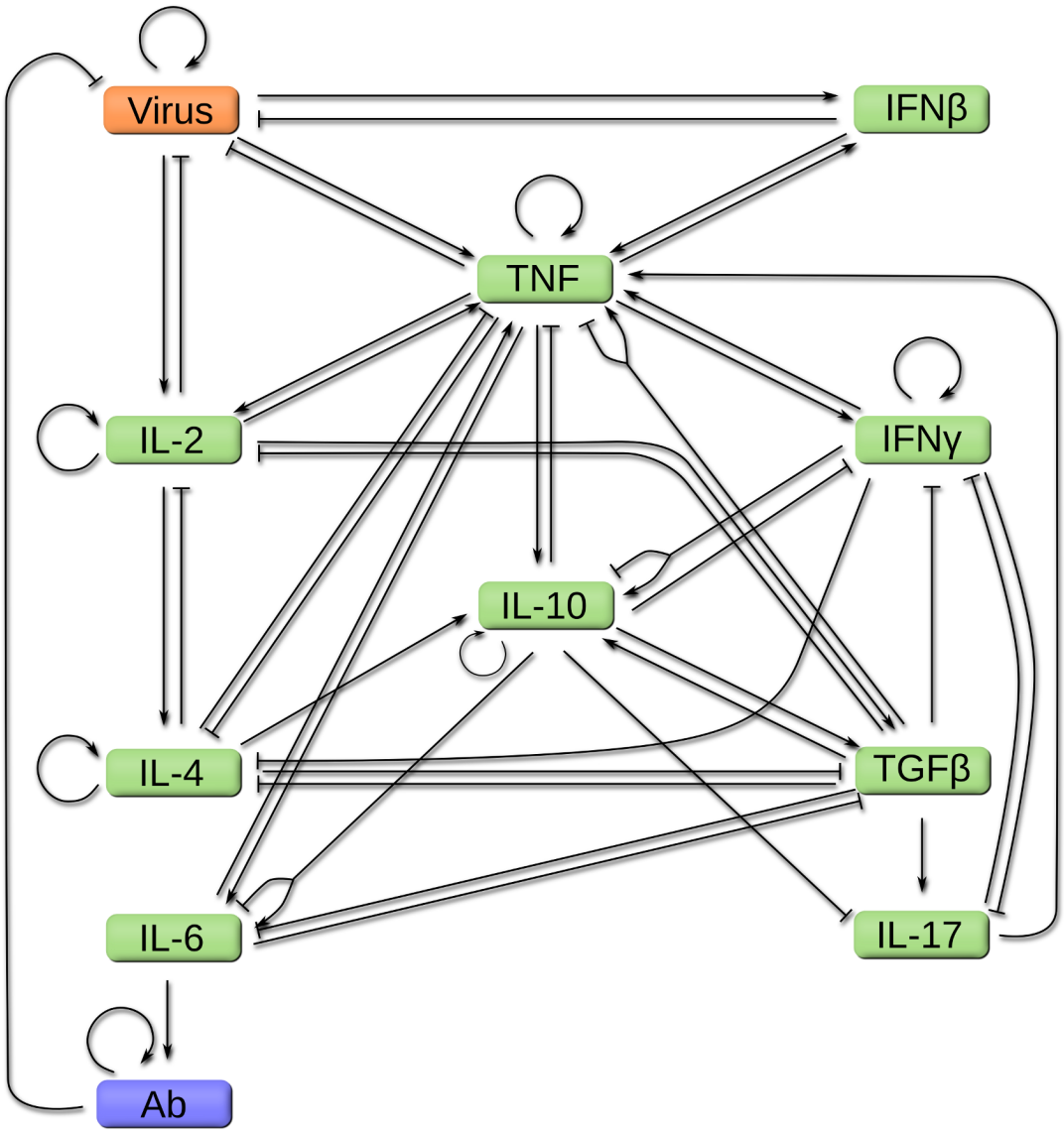

Figure 4.3: Interactions of cytokines involved in the immune reaction to influenza infections. Activating relationships are depicted by arrows, crossbars indicate inhibiting relationships. Relationships with crossbar *and* arrow indicate different mechanisms that mediate activating and inhibiting influences. Ab: Antibody.

	IFNα/β	IFNγ	TNFα	TGFβ	IL-2	IL-4	IL-6	IL-10	IL-17
IFNα/β			[237]						
IFN-γ		[114]	[225]	[222]		[188]	[129]		[207]
TNF	[238]	[187]	[22]		[167]	[143]	[105]	[168]	
TGF-β		[210][84	[210]	[100]	[52]	[84]	[52]	[97]	[103]
IL-2			[175]	[38]	[119]	[69]			
IL-4			[213]	[37]	[239]	[47]	[213]		
IL-6			[95]	[95]					[95]
IL-10		[56]	[5][220]	[33]	[212]		[220]	[185]	[121]
IL-17		[218]	[219]						

Table 4.1: Literature references for the interactions depicted in Figure 4.3 in an interaction matrix. References given in the table cells show the effect of the cytokine in the respective row on the cytokines in the columns. A red background color indicates an inhibiting interaction, green background an activation.

the production of another cytokine with a concentration denoted as X_j can be expressed as a function of X_i:

$$\sigma_{ij}(X_i) = p_{ij} + (q_{ij} - p_{ij}) \cdot \frac{X_i^{n_{ij}}}{K_{ij}^{n_{ij}} + X_i^{n_{ij}}}, \tag{4.1}$$

where p_{AB} is the minimal effect, q_{AB} is the maximal effect, K_{AB} is the concentration of A that yields a half-maximal effect and the Hill coefficient n_{AB} regulates the steepness of the function. The parameters p_{AB} and q_{AB} differ slightly depending on the type of the interaction between the cytokines. If σ_{AB} describes an activating interaction, p_{AB} is the minimal function value and q_{AB} is the maximal value. In case of an inhibiting interaction, $p_{AB} > q_{AB}$ denotes the maximal value of the sigmoidal. Figure 4.4 illustrates the relationship between the four parameters and the function values.

Each cytokine in the model is assumed to have a homeostatic production rate α and a degradation rate γ. The dynamics of a cytokine with a concentration denoted as X_j are expressed as the product of the homeostatic production rate and all activating and inhibiting interactions:

$$\frac{dX_j}{dt} = -\gamma_j X_j + \alpha_j \cdot \prod_{i=1}^{k_j} \sigma_{ij}(X_i), \tag{4.2}$$

where X_i denotes the concentrations of cytokines that regulate cytokine A.

Data on the cytokine dynamics are scaled to a value of 1 under homeostatic conditions (see section 4.2.1). In this model, the sigmoidal functions are defined in a way that their value is exactly one under homeostatic concentrations of the regulating cytokine, i.e. $\sigma_{ij}(1) = 1$ and all sigmoidal functions are 1 under homeostatic conditions.

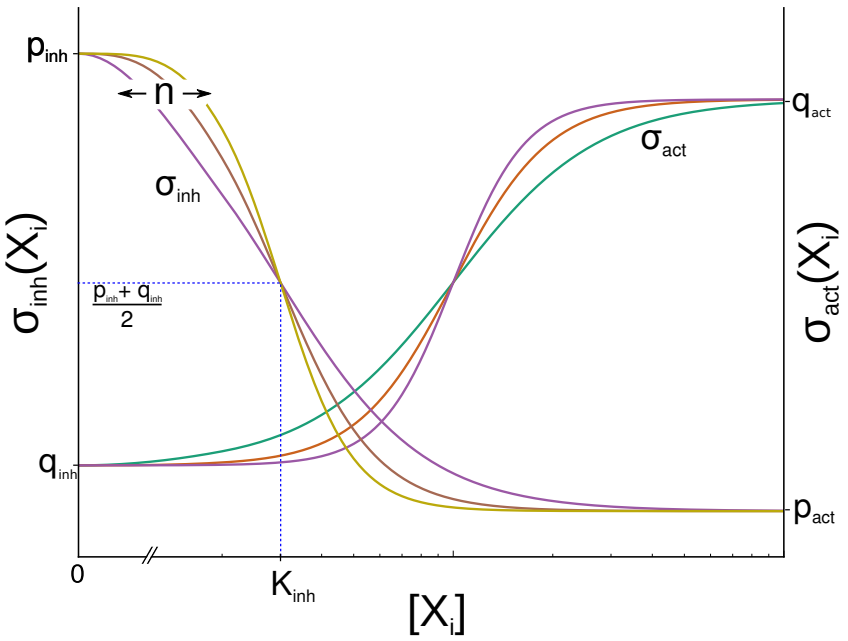

Figure 4.4: Effects of sigmoidal parameters on function values. The parameters p and q regulate the minimal and maximal function values; note the difference between inhibiting (left y-axis) and activating (right y-axis) functions. K is the concentration of A at the half-maximal function value of $\sigma(X_i)$ and n determines the steepness of the function.

4.3 A Novel Strategy for Parameter Estimation

Parameter estimation in systems such as the described cytokine network is challenging due to the number of state variables and associated parameters. While one of the parameters can be fixed by the requirement that $\sigma_{ij}(1) = 1$, the dimensionality of the parameter estimation problem is still very high, decreasing the likelihood of finding a global minimum even with the global stochastic optimisers introduced in chapter 2.

Since experimental observations for the dynamics of all cytokines in the model are available for the whole time course of the infection, a new strategy for parameter estimation has been developed that attempts to optimally exploit the available data for the purpose of parameter fitting [17]. Before application of the method to the fitting problem at hand, the goal was to evaluate the performance of this method. Testing the performance of a parameter estimation method on real data has the disadvantage that the true parameters of the system are generally not known. Thus, the method was tested on a synthetic data set. This data set was generated by building a model with the same structure as the cytokine model, but with arbitrary quantities, randomly chosen interactions and randomly chosen parameters. The model was simulated with the chosen parameters and data points were generated by adding noise to points in the model output [17].

This procedure has two main advantages. The problem of parameter estimation is analysed independently without any uncertainties with respect to model selection, since the model structure is known:

any uncertainties in the parameter estimates are due to the parameter estimation process. More importantly, the quality of the parameter estimates can be assessed not only by the goodness of fit, but also by the distance from the known, true parameters that have been used to generate the synthetic data.

4.3.1 Generation of an Artificial Dataset

Assuming cytokine dynamics given in Equation 4.2, the dynamics of a network that consists only of cytokine interactions can be expressed as

$$\frac{dX}{dt} = f(\Theta, X) = \begin{bmatrix} -\gamma_1 \cdot X_1 + \alpha_1 \cdot \prod_{i=1}^{k_1} \sigma_{i1}(X_i) \\ \vdots, \\ -\gamma_j \cdot X_j + \alpha_j \cdot \prod_{i=1}^{k_j} \sigma_{ij}(X_i) \\ \vdots, \\ -\gamma_l \cdot X_l + \alpha_l \cdot \prod_{i=1}^{k_l} \sigma_{il}(X_i) \end{bmatrix}, \tag{4.3}$$

where Θ is a vector of parameters and σ_{ij} is given in Equation 4.1. According to the requirement for homeostatic conditions, the parameter p_{ij} is calculated by setting $\sigma_{ij}(1) = 1$, which yields

$$p_{ij} = \frac{1 + K_{ij}^{n_{ij}} - q_{ij}}{K_{ij}^{n_{ij}}}. \tag{4.4}$$

Given equations 4.3 and 4.4, it can be concluded that the function is activating for $q > 1, k^n > 0$ and inhibiting for $q < 1, k^n > 0$.

For the creation of an artificial dataset, the first step was the creation of a network of arbitrary interactions. The size of the network was set to 5 state variables $X = X_1, X_2, \ldots, X_5$. To avoid any bias in choosing connections between these nodes in the hypothetical network, connections were randomly assigned. For all pairs of state variables $\binom{X}{2}$, either an activating, an inhibiting or no interaction were chose with equal probabilities. The resulting network is depicted in Figure 4.5.

For data generation, the resulting system was solved numerically with randomly assigned parameters (see appendix A for details) in the time interval $[0, 100]$. For 100 timepoints $1, 2, \ldots, 100$, five data points were generated by adding 10% noise to the model output at the corresponding point. Figure 4.6 depicts the resulting artificial data and the numerical solution of the ODE system given the true parameters.

4.3.2 Fitting Procedure

The core of the procedure is the fitting of single variables by decoupling the equations similar to an idea mentioned in [124]. The parameters for a single differential equation are fitted using all other variables

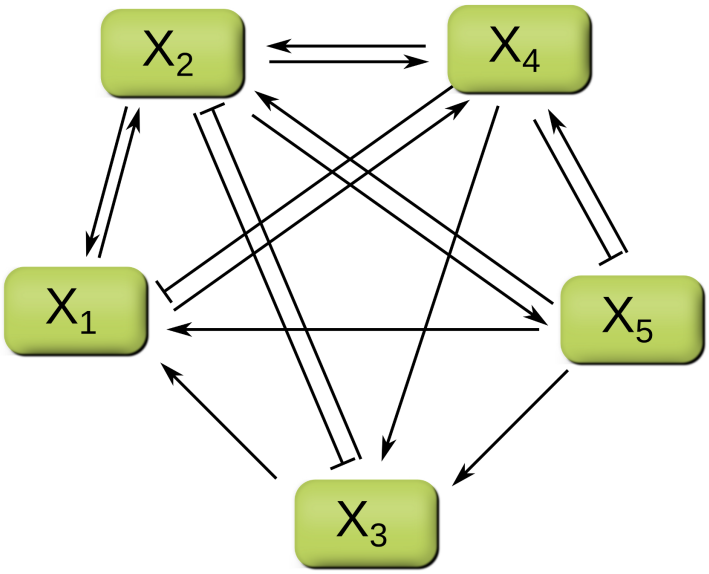

Figure 4.5: Structure of the artificial cytokine network used to generate data. Crossbars indicate inhibiting interactions, arrows indicate activations. Interactions were randomly picked from the three possibilities no interaction, activation or inhibition for all possible pairs in the network. (Modified from [17]).

as given input to the system. This leads to a division of the full fitting problem into a set of smaller subproblems of lower dimensionality. The dynamics of a single equation are then given by

$$\frac{dX_j}{dt} = -\gamma_j X_j \cdot \prod_{i=1}^{k_j} \sigma_{ij} \left(\hat{X}_i(t) \right), \tag{4.5}$$

where $\hat{X}_i(t)$ represents a piecewise linear function interpolating the artificial data for the respective variable.

Parameters were fitted for all single equations in five subsequent steps using this procedure. By simply combining all parameters from each of the single steps, an estimate for the parameters of the whole system of coupled ODEs was achieved. This estimate is the result of a sequence of iterative fitting steps and hence called *iterative* fit hereafter.

In addition to this novel fitting procedure, a final optimisation step was introduced to account for errors in the single fitting steps. For this final optimisation step, the combined parameters from the *iterative* fit were used as an initial guess. The parameters were then re-fitted in a region of 10% variation around the initial guess using the DE algorithm on the whole set of parameters and using all coupled ODEs. The result of this final step is called *iterative+global* in the following.

To evaluate the quality of the results of the novel fitting procedure, they were compared to the results of the classical DE algorithm used on the full set of equations (referred to as *global* in the following). For comparison of the fits, all fitting procedures were repeated 50 times.

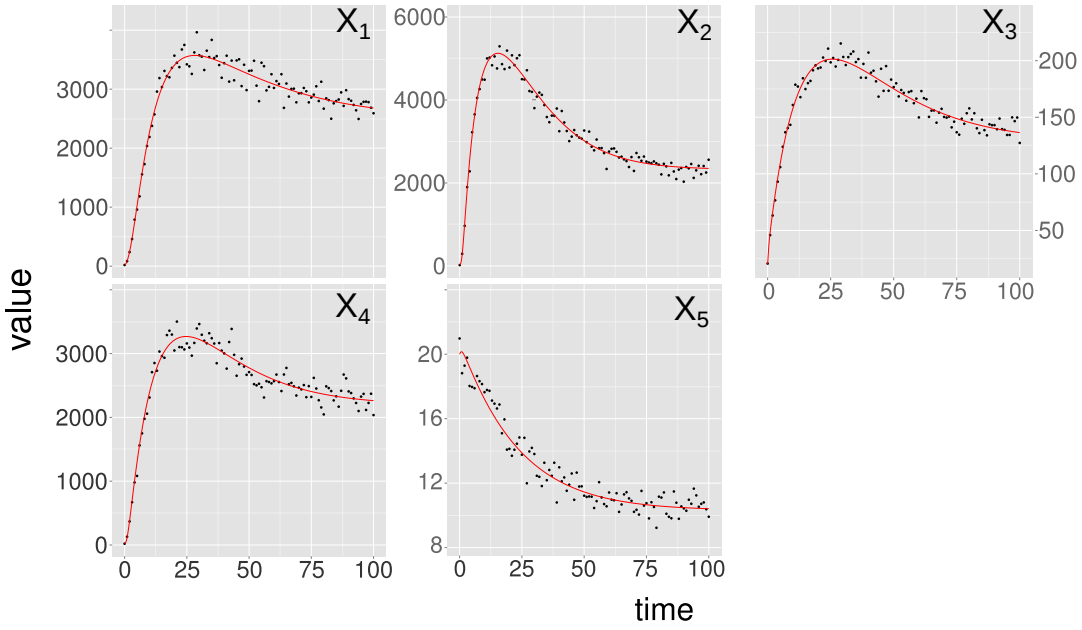

Figure 4.6: Mean values of the artificial data generated by the network depicted in 4.5. Dots represent data, the curve shows the error free value (i.e. model output without noise). Modified from [17].

All fits were produced using the Differential Evolution algorithm [208] using the DEoptim library in R [142; see appendix B] to minimise the RSS defined as

$$RSS = \sum_{j=1}^{l} \sum_{i=1}^{n} \left(\frac{x_{ij} - \bar{x_{ij}}}{s_{ij}} \right)^2, \tag{4.6}$$

where x_{ij} is the mean value of the data for the jth variable at the ith time point, s_{ij} is the standard deviation of the data in that point and $\bar{x_{ij}}$ is the corresponding model output.

For performance reasons, numerical integration of the ODE system was implemented in C++ using a 5th order Dormand prince method (Appendix B). Unless stated otherwise, the DE paramters used were $F = 0.8$ and $CR = 0.5$ with the classical DE/rand/1/bin strategy (see chapter 2) and a population size $N_P = 10D$, where D is the dimensionality of the fitting problem. The algorithm was terminated after 600 generations in case of the *global* strategy and after 100 generations in each of the single fitting steps in the *iterative* fitting strategy. 600 generations for the *global* strategy were chosen to match the sum of all generations in the *iterative+global* strategy, which were 100 generations for each of the five variables and an additional 100 generations for the final optimisation step.

4.3.3 Quality of the fits

All three fitting procedures outlined above were applied to the synthetic data set. First, the quality of the estimates was evaluated with respect to the goodness of fit by comparing the best RSS values

achieved in each of the 50 algorithm runs. Using the *global* strategy, the average RSS was 689.3. In contrast, the best RSS with the *iterative* strategy was 417.95. The final optimisation step achieved a further significant improvement to an average RSS of 266.5 in the *final+global* step.

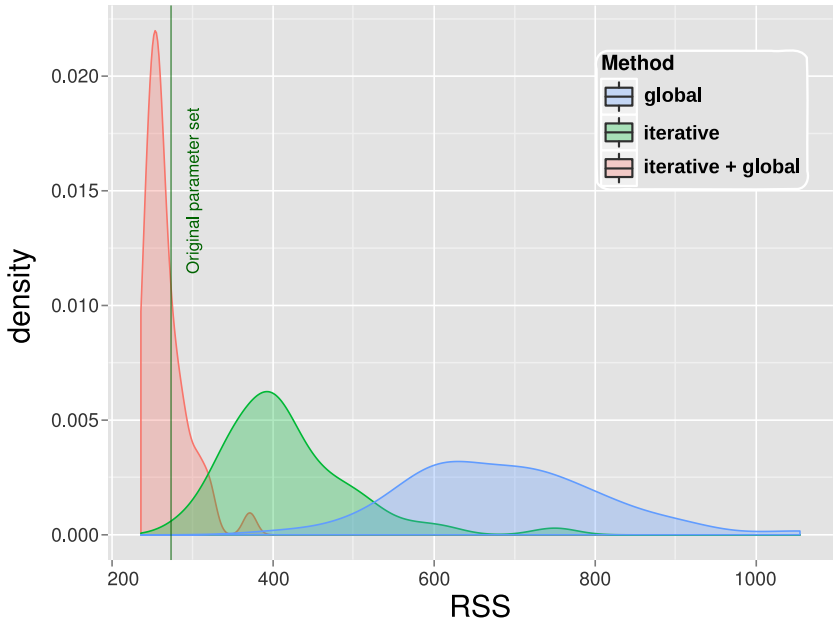

(a) Kernel density estimate of the distribution of the best RSS values.

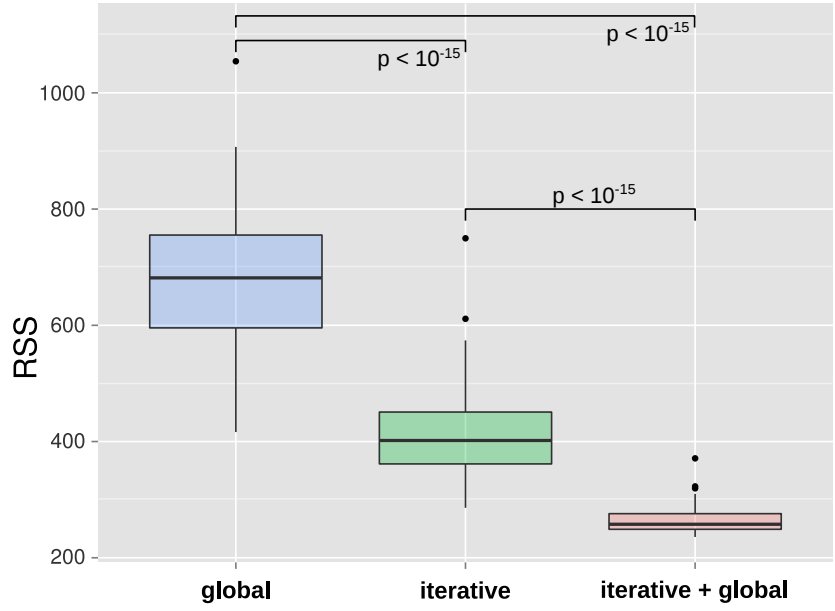

(b) Boxplot of the distribution of the best RSS values.

Figure 4.7: Comparison of the best RSS values in 50 runs of the three procedures *global* (blue), *iterative* (green) and *iterative+global* (red). Statistical significance was tested using the Welch two-sample t-test. (Modified from [17])

Figure 4.7 shows the distribution of the results of all three procedures. The strong improvement of the results in the final optimisation step is surprising. The DE algorithm succeeds optimising all parameters at once if it operates in the vicinity of a good solution, but not if parameters are allowed to vary in a wider range. Interestingly, the average RSS after the *final+global* procedure is below the expected best result: simulating the model with the known parameters yields an RSS of 273.22 (indicated by the green line in Figure 4.7(a)). Obviously, the true parameters are not the best estimate as defined by the cost function. This is a result of the noise in the data and is considered a limitation in fitting noisy data in general rather than a limitation in the parameter estimation procedure. For practical purposes, this means that even if there is a unique global best parameter set found by the optimiser, it does not necessarily reflect the true parameters, a limitation that should be taken into consideration in particular when data are noisy and/or sparse.

4.3.4 Quality of the parameter estimates

While the improved goodness of fit of the *iterative* compared to the *global* strategy is a good indication that the algorithm is better at optimising the cost function than its conventional counterpart, the question remains whether or not the improvement in the RSS values is reflected in the data. Since the true parameters are known, deviations of the estimate can easily be calculated by computing the euclidean distance between the parameter estimates and the true parameters. Figure 4.8 shows the results of the parameter estimates from 50 runs of the algorithm.

The advantage of the *iterative* compared to the *global* strategy is significant with respect to the distance of the estimated parameter vectors to the true parameters. However, the improvement of the final optimisation step in the *iterative+global* strategy seen in the RSS values does not correspond to an improvement in the parameter distances (Fig. 4.8(b)). This is consistent with the observation that the average best RSS value is below the RSS value that simulation with the true parameters yields and suggests that the final optimisation step in the *iterative+global* strategy does not have any benefit over the *iterative* strategy alone.

4.3.5 Computational effort

The main goal here was to establish whether or not the *iterative* parameter estimation strategy yields better results than its conventional counterpart, the DE algorithm applied to the full parameter estimation problem. Hence, termination criteria have been chosen to ensure that the cause for an improvement in fitting performance is not simply achieved by increasing the amount of computation. The algorithm was terminated only by reaching the maximum number of generations. This maximum number of generations was chosen at a maximum of 600 in all generations: the *global* procedure was terminated after 600 generations and in the *iterative* and *iterative+global* procedure, 100 generations per step were

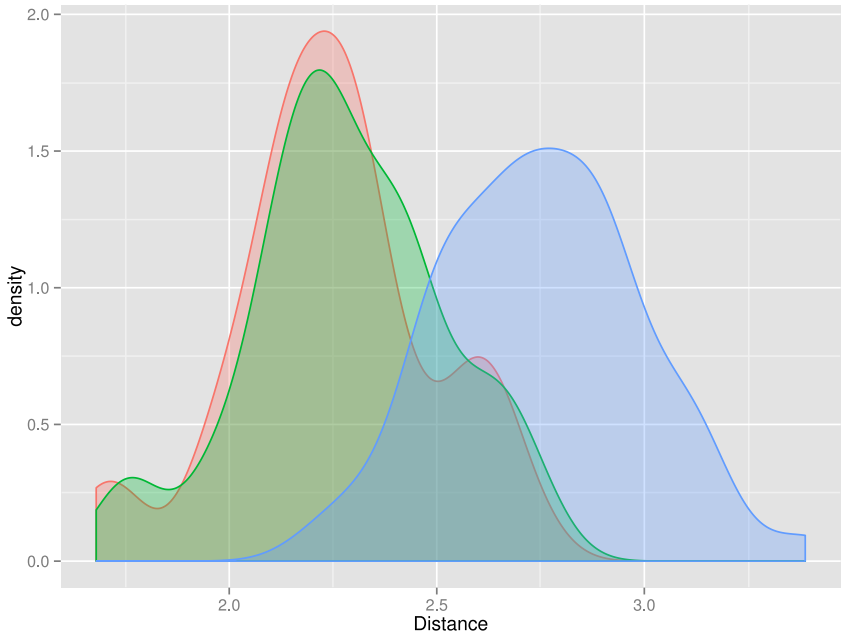

(a) Kernel density estimate of the distribution of parameter vector distances from the true parameters.

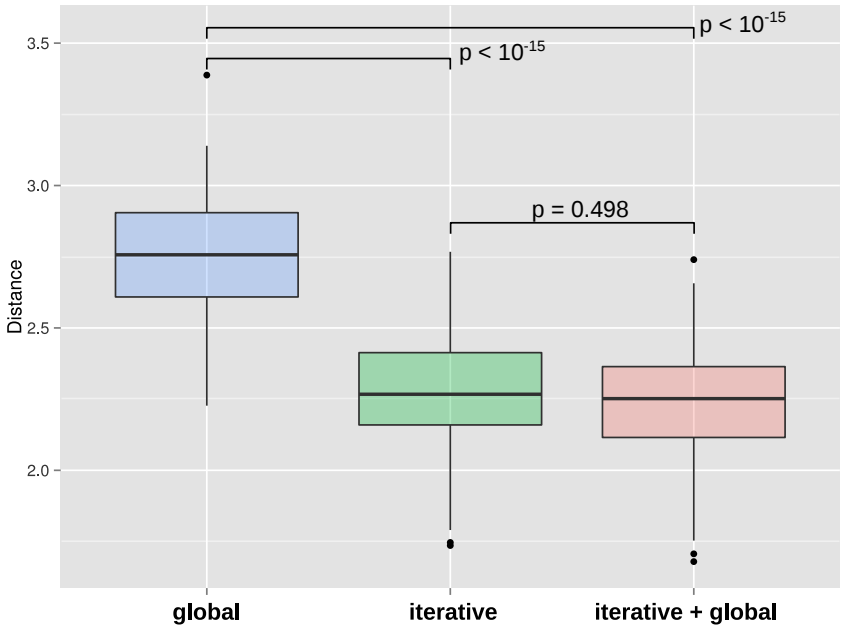

(b) Boxplot of the distribution of parameter vector distances from the true parameters.

Figure 4.8: Comparison of parameter distances in 50 runs of the three procedures *global* (blue), *iterative* (green) and *iterative+global* (red). The figures show euclidean distances between the estimated parameter vectors and theStatistical significance was tested using the Welch two-sample t-test. (Modified from [17])

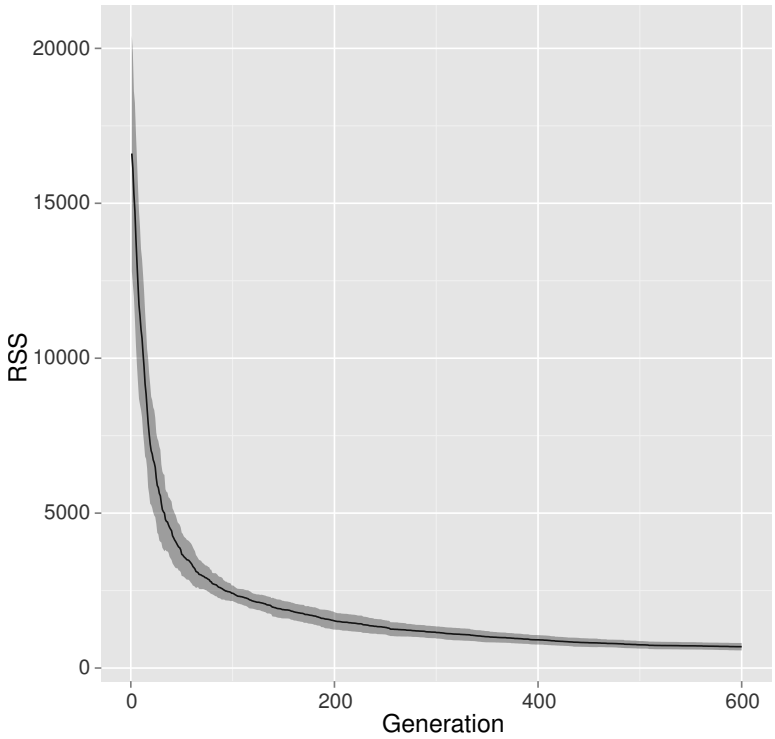

Figure 4.9: Best RSS values during subsequent generations in 50 runs of the *global* optimiser. The curve shows the mean RSS per generation and the shaded area indicates standard deviations. (Modified from [17])

permitted, amounting to 500 generations in total for the *iterative* procedure and 600 generations for *iterative+global*.

These termination criteria are conservative with respect to the computational effort permitted for the novel procedure: the total number of generations is the same, but the dimensionality of the *global* parameter estimation problem is higher. Since the population size in the DE algorithm was set to 10 times the dimensionality of the problem, this means that significantly more different candidate solutions were evaluated in the *global* procedure. While this termination criterion was intentionally chosen here for the establishment of the novel method, for practical purposes, a quality based criterion is advisable. Either reaching a predefined absolute value in the cost function or failure to improve the solution by a given amount over a number of generations are useful criteria for termination.

The results show that even despite a significantly higher amount of computation, the *global* strategy did not reach comparable results to the *iterative* algorithm. However, this does not exclude that the *global* strategy might yield comparable or even better results given enough computation time. To exclude that the DE algorithm terminates prematurely, the lowest RSS value in each generation was recorded during all 50 runs. The results are shown in Figure 4.9. While there is a fast initial decrease in RSS values, there are only small improvements after generation 300-400 and it can be concluded that strong improvements after generation 600 are rather unlikely events.

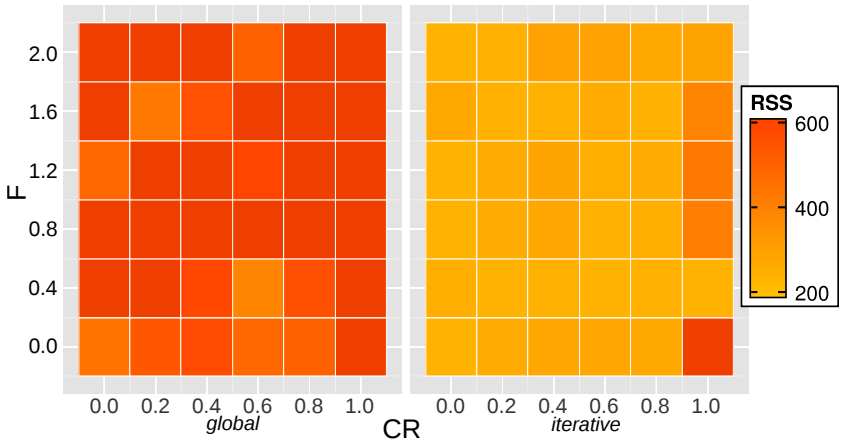

Figure 4.10: RSS values in best fits of *global* and *iterative* optimisation with different combinations of the DE parameters CR and F. The mean RSS of the final results of three runs with each combination is encoded by the color. (Modified from [17])

4.3.6 Evaluation of DE parameters

The DE algorithm itself has parameters that need to be adjusted to a specific problem. The advantage of the *iterative* parameter estimation method has been tested using a parameter set that yields good results for many problems [171]. However, the parameter set could be better suited in case of the lower dimensionality in the *iterative* strategy than in the *global* strategy. To exclude this possibility, a wide variation of parameters was tested. Figure 4.10 shows different combinations of the crossover probality CR and the mutation weight F of the DE algorithm. For each combination, three runs of the algorithm were performed.

The advantage of the *iterative* strategy (Figure 4.10 right) is visible in the whole spectrum of parameter combinations tested. Interestingly, the choice of parameters had no clear impact on the performance of either algorithm, although a value of 1 for CR seems to be disadvantageous. No clear recommendations with respect to the DE parameters can be given based on these tests. The result, however, clearly shows that the advantage of using the *iterative* method is robust to changes in the DE parameters.

In conclusion, the novel parameter estimation method has been tested extensively and has been shown to advantageous compared to the conventional DE strategy. It can be considered to be applicable for the problem of fitting a network of cytokine interactions, as the system used to test the method closely resembles the cytokine interaction network. However, the method may well be applicable to a broader class of problems. The promising results warrant further investigation of the properties of this method, e.g. whether its advantage depends on the connectivity or the number of state variables in a network, how the results are influenced by more or less noise in the data or sparse measurements.

4.4 Reducing the cytokine network

Despite the promising results of the novel parameter estimation strategy, the full cytokine network as shown in Figure 4.3 is a very large system that poses challenges for modelling on multiple levels. Hence, the first objective in creating a functional model for the cytokine response to influenza was a reduction of the model to a subset of the most important cytokines during the first week of a primary challenge in influenza infections.

Reduction of the network was performed by manual assessment of all included quantities and interactions. First, since the primary goal was a description of the immune response in the first week, all cytokines that are mainly involved in humoral response were excluded.

Second, reduction of overlapping functions and non-essential parts of the network was performed. The network shown in Figure 4.3 was already constructed with the purpose of reducing inherent redundancy as far as possible. E.g., IL-1β was omitted although it is known to contribute to the inflammation in infected lungs, since most of its functions for regulation and its antiviral effect are well represented by TNF in the model. Hence, for further reduction, only cytokines were included that are either representative for important antiviral effects or have an essential function for the regulatory part of the network.

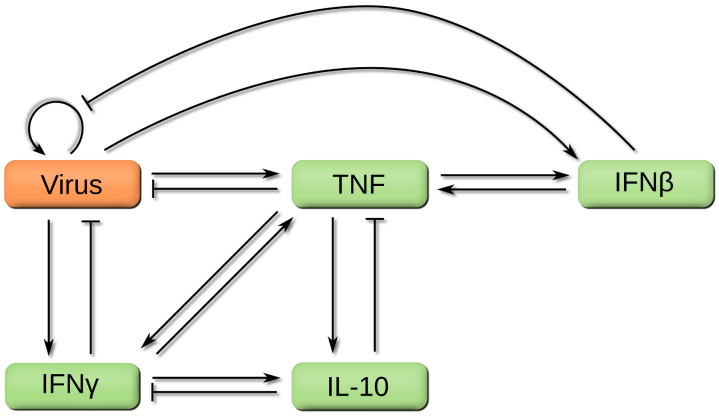

Figure 4.11: The cytokine network after reduction to a minimal set of nodes

Third, interactions between cytokines were copied from the large network. The cytokines included in the reduced model form a subgraph of the larger network. The process of extracting the information about interaction between the nodes was thus straightforward. The resulting network is depicted in Figure 4.11.

IFN-γ was included in the network for representation of the T_h1 cell response and the effects on NK cells; furthermore, it is produced by CTL as well and indicates their activity. Type I interferon is included due to its important direct antiviral effects. TNF is included as the paradigmatic inflammatory cytokine; the central role in the induction of other cytokines can be seen in Figure 4.3 and makes

TNF indispensible for the activation of the network. Its counterpart, IL-10, is included as the only immunosuppressive cytokine in the network that controls the inflammation.

4.4.1 A Model for the Virus Dynamics

Models with varying degrees of detail and complexity have been constructed in order to describe viral replication (see Section 1). Most of these models build upon a basic model formulation that describes infectable target cells, infected cells and virions [161]. While these models have been successful and have been extended to a great amount of detail in some cases [e.g. 72], this kind of description is not suitable for the framework presented here, since it requires a description of two additional quantities. However, a description of the replicating virus is required in order to simulate the effect of the virus on the cytokine network, but also in order to simulate antiviral effects of certain cytokines in the model.

While a description of virus replication without modelling host cell infection and virus shedding by infected cells is necessarily a more abstract model of the viral dynamics, measurements of viral concentration, e.g results of *in vitro* studies [133] suggest that features of viral growth could be approximated by simpler descriptions. A natural assumption is a ressource limited growth model, of which logistic growth is the most basic one:

$$\frac{dV}{dt} = \left(1 - \frac{V}{K}\right) rV, \tag{4.7}$$

where r is the maximal growth rate and K the carrying capacity, i.e. the maximum concentration that the virus can reach.

The next step is then to include antiviral effects of the cytokines. This raises the question of potential impact points in the logistic growth equation. In the case of TNF, it seems natural to assume a direct negative effect on the virus, since it is a strong inducer of inflammatory reactions and phagocytosis and attracts phagocytes.

The two interferon types have overlapping functions. However, the direct induction of an antiviral state in target cells is among core functions of type I interferons, whereas the activation of NK cells is a central function of IFN-γ in influenza [230], and IFN-γ presence is indicative of NK activity [184]. Consequently, IFN-γ was modelled as directly decreasing viral growth. Although IFN-γ and type I interferon share many common features [201], the early induction of an antiviral state in the cells is an important effect of type I interferons [96], and it was decided to model antiviral type I interferon responses as removal of available target cells by inducing a virus resistant state. Removing target cells can be seen as reducing available ressources, effectively reducing the carrying capacity K.

Combining these considerations, the viral dynamics can be given as

$$\frac{dV}{dt} = \left(1 - \frac{(1+\delta_B B)V}{K}\right) rV - (\delta_T T + \delta_G G)V, \tag{4.8}$$

where the rates δ_T and δ_V describe the direct effects of IFN-γ and TNF, and δ_B models the reduction of the carrying capacity K.

4.5 Fitting single equations

As described in Section 4.3, the parameters for all equations can be fitted iteratively by decoupling the equations. In the following fitting steps, data for all other variables were considered as input to the system. For times between measurements, data points were linearly interpolated (see Figure 4.1. In each step, the DE was used for optimisation.

4.5.1 Fitting the single equations

According to the modelling strategy and the interactions depicted in Figure 4.11, the dynamics for IL-10 (I), IFN-β (B), IFN-γ (G) and TNF (T) can be given by the differential equations

$$\frac{dI}{dt} = -\gamma_I \cdot I + \alpha_I \cdot \sigma_{TI}(T) \cdot \sigma_{GI}(G), \tag{4.9}$$
$$\frac{dB}{dt} = -\gamma_B \cdot B + \alpha_B \cdot \sigma_{TB}(T) \cdot \sigma_{VB}(V), \tag{4.10}$$
$$\frac{dG}{dt} = -\gamma_G \cdot G + \alpha_G \cdot \sigma_{IG}(I) \cdot \sigma_{TG}(T) \cdot \sigma_{VG}(V), \tag{4.11}$$
$$\frac{dT}{dt} = -\gamma_T \cdot T + \alpha_T \cdot \sigma_{IT}(I) \cdot \sigma_{BT}(B) \cdot \sigma_{GT}(G) \cdot \sigma_{VT}(V), \tag{4.12}$$

where V denotes the viral load and the rates by α and γ are homeostatic production and degradation rates. The functions denoted by σ are log-sigmoidal functions as defined in Equation 4.1.

Given Equation 4.4, three parameters have to be fitted per sigmoidal function. For the purpose of fitting, all regulating quantities are replaced by linear piecewise functions. Figure 4.12 shows the results of the DE fit for these single steps. As can be seen from the figure, the model error is within the error in most data points. Note that the seeming discontinuities in some of the trajectories are a result of using a linear interpolation function as input.

The last single equation to fit in the iterative procedure is the virus. There are 5 parameters in the equation for the virus. The best fit shows that the dynamics of the viral load can be described by the logistic growth model and the antiviral effects of IFN-β, IFN-γ, and TNF (Figure 4.13.

The function of TNF and IFN-γ as antiviral effects are redundant in the differential equation; however, their dynamics are different. To assess whether both antiviral parameters δ_T and δ_G, could be

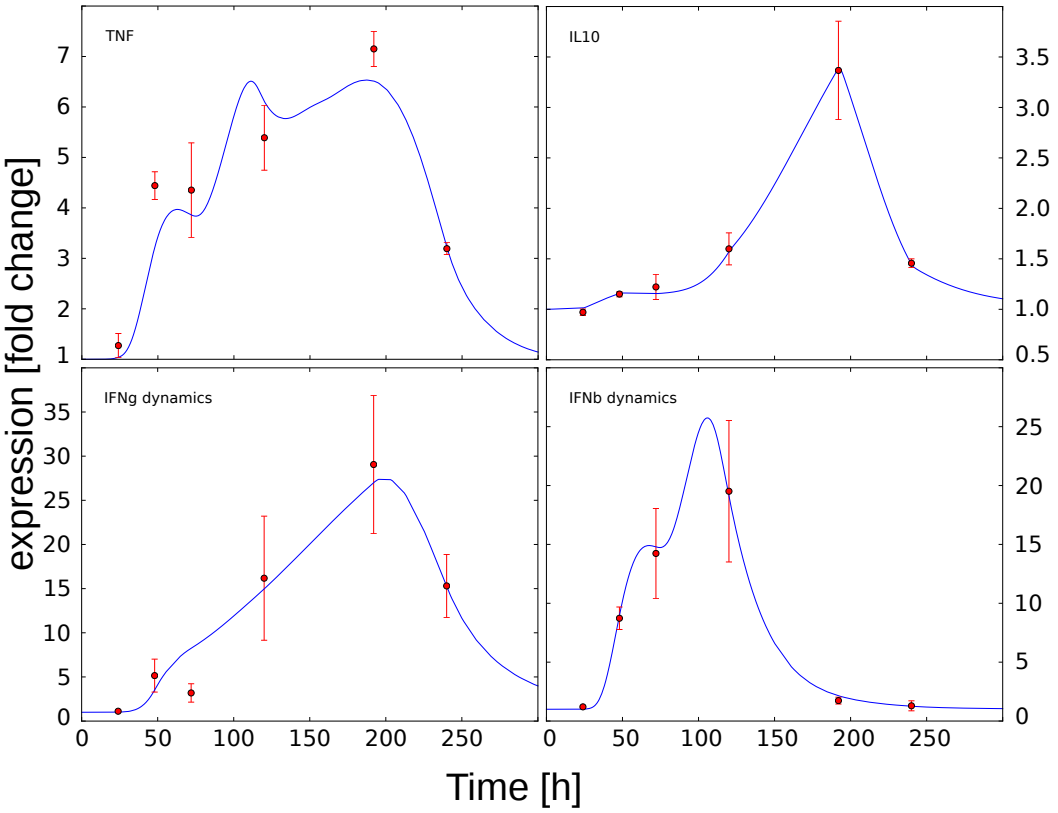

Figure 4.12: Iterative steps for fitting the cytokine interaction parameters. Each of the variables was fitted separately, using values for the other state variables as input.

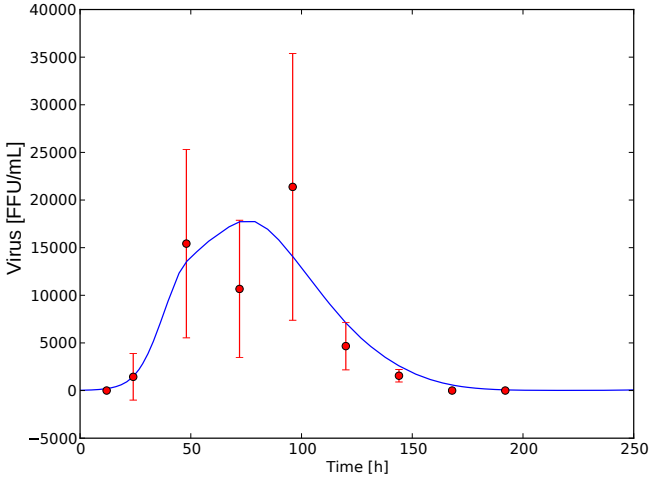

Figure 4.13: Best fit of the viral dynamics in the iterative fitting step. The parameters were fitted for the viral dynamics only, using data for TNF, IFN-β and IFN-γ as input.

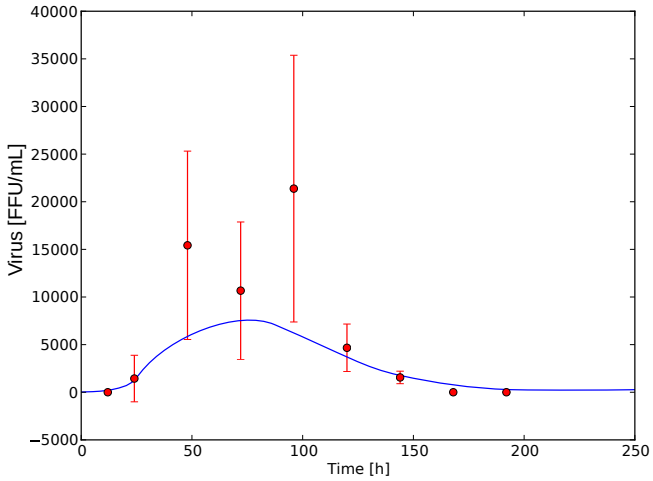

Figure 4.14: Best fit of the alternative viral dynamics model (Equation 4.13 in the iterative fitting step. The parameters were fitted for the viral dynamics only, using data for TNF, IFN-β and IFN-γ as input. Combining the effects visibly affects the quality of the fit.

combined into a antiviral term, the fitting procedure for the virus was repeated with an alternative model for V given by

$$\frac{dV}{dt} = \left(1 - \frac{(1+\delta_B B)V}{K}\right) rV - (T+G)\delta_{TG}V, \tag{4.13}$$

where δ_{TG} is a combined parameter for the antiviral effects of both cytokines. Interestingly, the best fit from this alternative model visibly affected the quality of the fit, suggesting that both separate parameters for both cytokines are beneficial (Figure 4.14).

4.6 Simulations with the full model

Having fitted all parameters on the single equations, the values gained in this process were combined for simulations with the full dynamic system. The combined parameter set can be found in appendix A. Figure 4.15 shows a simulation with the full parameter set.

As expected, the combination of parameters introduced some additional deviation from the plot. This is due to the accumulated error from all steps, since the linear interpolation that was used to fit the parameters of the interaction functions between the cytokines differ from the dynamics that the whole system displays. However, the model still reproduces the measured cytokine dynamics and the viral dynamics with acceptable error.

Interestingly, in TNF and both interferons, there is an early rise in the cytokine levels that is not reproduced by the model. This might either correspond to an unknown event not included in the model or to an early increase in viral load that is masked by the variation in the data.

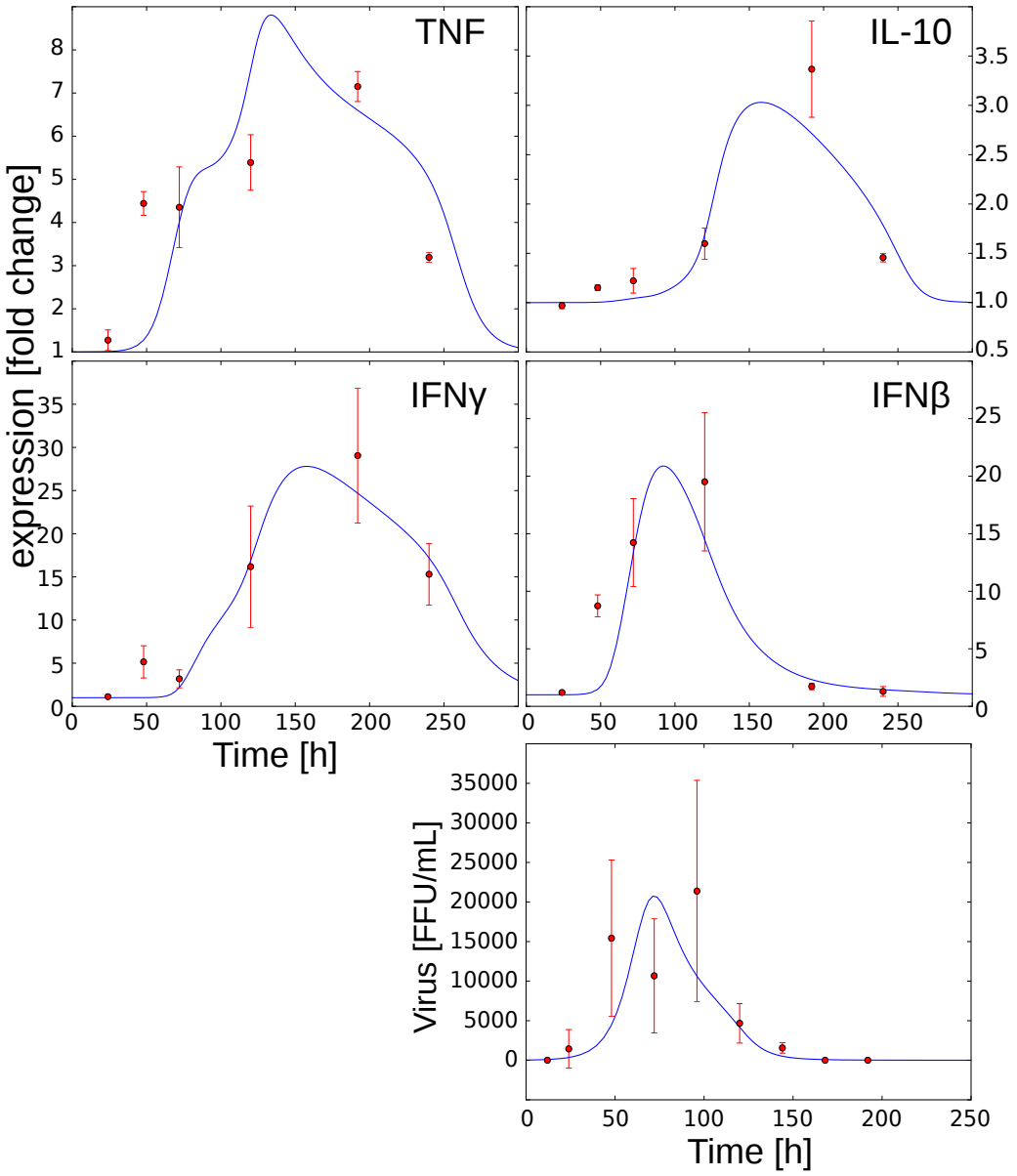

Figure 4.15: Combined parameters estimated in the iterative procedure.

4.7 Conclusion

A cytokine network for the immune response to influenza has been reconstructed from published studies. Further reduction of the model to four essential cytokines has resulted in a subset of cytokines that can reproduce the cytokine dynamics observed in experimental influenza infection in mice.

A novel fitting strategy for the estimation of parameters has been developed in order to allow fitting of the high number of parameters in this system. This strategy has been validated on an artificial dataset with known model structure and parameters and has shown significant advantages compared to conventional fitting algorithms and has been successfully applied to the fitting problem in the reduced cytokine network. The fitting algorithm has been evaluated for a specific problem and with a specific model structure; however, the general principle is likely to hold in other parameter estimation problems as well.

While the cytokine network has been developed in the context of influenza, the framework for describing immune responses developed here is applicable in other infectious or even autoimmune diseases; however, this will most likely require adaptation of the network to other situations, since the reconstruction of the network was performed with the aim of describing the early immune response to influenza, and interactions and cytokines that do not play a significant role in this context were neglected.

5

Discussion

In the previous two chapters, immune responses in the early immune reaction in infected tissues and interactions between host and pathogen were discussed. Mathematical models were developed with the aim to describe the pathogen dynamics inside a tissue and their relationship to host responses in that tissue. The ability of a model to reflect essential parts of the pathogen and the immune system dynamics was assessed by comparison of simulations with experimentally observed pathogen burden.

In the case of *B. burgdorferi*, bacterial concentrations were the only observations for the validation of the model. No data on the number of phagocytic or other immune cells were available. Consequently, the description of the immune response was restricted to the most critical and most basic part of the early immune response. In general, the first days of the infection can be considered the most critical phase during *B. burgdorferi* infection [229]. As seen in Chapter 3, the bacterial load during this critical, localised stage before dissemination is drastically reduced, phagocytic cells are most likely central in the removal of bacteria [173]. While it is not entirely clear to what extent other parts of the immune system such as the complement system [112] are involved, the effectiveness of phagocytes against *B. burgdorferi* has been shown *in vitro* [138] and *in vivo*[139]. Thus, it seems appropriate to restrict the immune system in the model to phagocytic cells.

Out of the three simple hypotheses that were tested *in silico*, only the assumption of bacterial adaptation could explain the bacterial dynamics in the model. This might, in part, be due to a limitation in the modelling technique, since spatial effects are not considered that might well play a role given the highly motile bacterium and comparatively slow phagocytes [173]. Meanwhile, intravital imaging of live *B. burgdorferi* is possible [110], and warrants further investigation of bacterial motility. However, the results from Model 3 that included bacterial adaptations are in agreement with empirical evidence on changes in protein expression and their timing [83] and fit well with the idea that the localised phase before the bacteria begin to disseminate correlates with extensive changes of the bacterial gene expression [229]. The model highlights the critical role of this phase. At the current state, the model only predicts that the adaptation plays an important role. However, modelling specific adaptations like the downregulation of surface proteins can aid in quantifying the impact of particular adaptations, and

possibly, to identify vulnerabilities in the immune evasion system that can be exploited by vaccines or other pharmaceutica.

In the case of influenza infection, the model construction was not limited by the availability of data, but by the amount of complexity that is numerically feasible. The decision for the four cytokines that were finally included in the model was driven by the idea to represent as much critical components of the cytokine network with as few state variables as possible. There are other cytokines that could be included in the network, and some of them were neither in the reduced network with four cytokines nor in the larger one; IL-12/-18 is an example, but also the whole class of chemokines that has been ignored in this model. As such, the construction of the model itself is an iterative process that will most likely result in the inclusion of other cytokines in future applications. For the purpose of this study, a set of cytokines was found that can explain the cytokine and virus dynamics observed in the mouse model – albeit with some notable deviations, in particular for TNF.

The use of microarray data, however, also has disadvantages. First and foremost, it is unclear to what extent RNA expression levels correlate to expressed protein. While the direct comparison of the observed dynamics with studies measuring protein concentrations [217] shows no strong qualitative differences, this is not necessarily the case. Validation of the model with measured protein concentrations is thus an obvious next step.

The development of the cytokine model and its calibration with a dataset can be considered an important step in establishing the idea of modelling immune responses on the cytokine level. The model provides a tool that can be used to test hypotheses *in silico*; e.g, the investigation of critical differences in mice with different host genetic background that show more severe and lethal infections to those with mild symptoms. Similarly, cytokine concentrations measured in human patients can help to identify markers of severe disease and elucidate changes that make e.g. seniors more susceptible to the disease. A further perspective for the use of the model is the extension to other diseases. This includes other infectious diseases. E.g. in Borreliosis, cytokines play an important role for control of the pathogen burden, but also pathogenesis [23, 113, 180].

5.1 Conclusion

Both models developed here provided valuable information about the pathogen and immune dynamics in the early local immune response. The *B. burgdorferi* model was directly used to test hypotheses about potential immune evasion mechanisms of the bacterium, the influenza model has shown that it is possible to describe virus dynamics and antiviral effects based on a small subset of cytokines and their antiviral effects. In addition, the parameter estimation problem in modelling the cytokine model has led to the development of a new strategy that has shown promising results in tests on an artificial dataset and is applicable to a broad class of parameter estimation problems. While both models have

been developed in the context of questions in basic research, they show potential for the development and extension towards medically relevant questions.

Bibliography

[1] Alexopoulou, L., Thomas, V., Schnare, M., Lobet, Y., Anguita, J., Schoen, R. T., Medzhitov, R., Fikrig, E., and Flavell, R. a. (2002). Hyporesponsiveness to vaccination with Borrelia burgdorferi OspA in humans and in TLR1- and TLR2-deficient mice. *Nature Medicine*, 8(8):878–84.

[2] Anderson, R. M. and May, R. M. (1991). *Infectious Diseases of Humans: Dynamics and Control*. Oxford University Press, Oxford.

[3] Appel, M. J., Allan, S., Jacobson, R. H., Lauderdale, T. L., Chang, Y. F., Shin, S. J., Thomford, J. W., Todhunter, R. J., and Summers, B. a. (1993). Experimental Lyme disease in dogs produces arthritis and persistent infection. *The Journal of Infectious Diseases*, 167(3):651–64.

[4] Araujo, R. P. and McElwain, D. L. S. (2004). A history of the study of solid tumour growth: the contribution of mathematical modelling. *Bulletin of Mathematical Biology*, 66(5):1039–91.

[5] Armstrong, L., Jordan, N., and Millar, A. (1996). Interleukin 10 (IL-10) regulation of tumour necrosis factor alpha (TNF-alpha) from human alveolar macrophages and peripheral blood monocytes. *Thorax*, 0:143–149.

[6] Attie, O., Bruno, J. F., Xu, Y., Qiu, D., Luft, B. J., and Qiu, W.-G. (2007). Co-evolution of the outer surface protein C gene (ospC) and intraspecific lineages of Borrelia burgdorferi sensu stricto in the northeastern United States. *Infect Genet Evol*, 7(1):1–12.

[7] Baccam, P., Beauchemin, C., Macken, C. a., Hayden, F. G., and Perelson, A. S. (2006). Kinetics of influenza A virus infection in humans. *Journal of Virology*, 80(15):7590–9.

[8] Bankhead, T. and Chaconas, G. (2007). The role of VlsE antigenic variation in the Lyme disease spirochete: persistence through a mechanism that differs from other pathogens. *Molecular Microbiology*, 65(6):1547–58.

[9] Barbour, A. G. (1983). Isolation and cultivation of Lyme disease spirochetes. *Yale J. Biol. Med.*, 57(4):521–5.

[10] Barthold, S., de Souza, M., Janotka, J., Smith, A., and Persing, D. (1993). Chronic Lyme borreliosis in the laboratory mouse. *The American Journal of Pathology*, 143(3):959–971.

[11] Barthold, S. W., Beck, D. S., Hansen, G. M., Terwilliger, G. a., and Moody, K. D. (1990). Lyme borreliosis in selected strains and ages of laboratory mice. *The Journal of Infectious Diseases*, 162(1):133–8.

[12] Barthold, S. W., Persing, D. H., Armstrong, A. L., and Peeples, R. A. (1991). Kinetics of Borrelia burgdorferi dissemination and evolution of disease after intradermal inoculation of mice. *Am. J. Pathol.*, 139(2):263–73.

[13] Beauchemin, C. a. a. and Handel, A. (2011). A review of mathematical models of influenza A infections within a host or cell culture: lessons learned and challenges ahead. *BMC Public Health*, 11 Suppl 1(Suppl 1):S7.

[14] Belperron, A. a., Dailey, C. M., Booth, C. J., and Bockenstedt, L. K. (2007). Marginal zone B-cell depletion impairs murine host defense against Borrelia burgdorferi infection. *Infection and Immunity*, 75(7):3354–60.

[15] Bender, B. B. S., Croghan, T., Zhang, L., and Small, P. A. (1992). Transgenic mice lacking class I major histocompatibility complex-restricted T cells have delayed viral clearance and increased mortality after influenza virus challenge. *The Journal of Experimental Medicine*, 175(April):1143–1145.

[16] Beyer, H.-G. and Schwefel, H.-P. (2002). Evolution Strategies. *Natural Computing*, 1:3–52.

[17] Binder, S. C., Hernandez-Vargas, E. A., and Meyer-Hermann, M. (2014). Reducing complexity: an iterative strategy for parameter determination in biological networks. *Comput. Phys. Commun.*, (Under review).

[18] Binder, S. C., Telschow, A., and Meyer-Hermann, M. (2012). Population Dynamics of Borrelia burgdorferi in Lyme Disease. *Frontiers in Microbiology*, 3(March):104.

[19] Bockenstedt, L. K., Barthold, S., Deponte, K., Marcantonio, N., and Kantor, F. S. (1993). Borrelia burgdorferi infection and immunity in mice deficient in the fifth component of complement. *Infection and Immunity*, 61(5):2104–7.

[20] Bonhoeffer, S., May, R. M., Shaw, G. M., and Nowak, M. a. (1997). Virus dynamics and drug therapy. *Proceedings of the National Academy of Sciences of the United States of America*, 94(13):6971–6.

[21] Brest, J., Greiner, S., Bošković, B., Mernik, M., and Žumer, V. (2006). Self-adapting control parameters in differential evolution: A comparative study on numerical benchmark problems. *IEEE T. Evolut. Comput.*, 10(6):646–657.

[22] Brinkman, B. M. N., Telliez, J.-B., Schievella, a. R., Lin, L.-L., and Goldfeld, a. E. (1999). Engagement of Tumor Necrosis Factor (TNF) Receptor 1 Leads to ATF-2- and p38 Mitogen-activated Protein Kinase-dependent TNF Gene Expression. *Journal of Biological Chemistry*, 274(43):30882–30886.

[23] Brown, J. P., Zachary, J. F., Teuscher, C., Weis, J. J., and Wooten, R. M. (1999). Dual role of interleukin-10 in murine Lyme disease: regulation of arthritis severity and host defense. *Infection and immunity*, 67(10):5142–50.

[24] Brydon, E. W. a., Morris, S. J., and Sweet, C. (2005). Role of apoptosis and cytokines in influenza virus morbidity. *FEMS Microbiology Reviews*, 29(4):837–50.

[25] Burgdorfer, W., Barbour, a. G., Hayes, S. F., Benach, J. L., Grunwaldt, E., and Davis, J. P. (1982). Lyme disease-a tick-borne spirochetosis? *Science (New York, N.Y.)*, 216(4552):1317–9.

[26] Canini, L. and Perelson, A. (2014). Viral kinetic modeling: state of the art. *J. Pharmacokinet. Pharmacodyn.*

[27] Carrat, F. and Flahault, a. (2007). Influenza vaccine: the challenge of antigenic drift. *Vaccine*, 25(39-40):6852–62.

[28] Casjens, S. R., Eggers, C. H., and Schwartz, I. (2010). Borrelia genomics: chromosome, plasmids, bacteriophages and genetic variation. In *Borrelia: Molecular Biology, Host Interaction and Pathogenesis*, pages 27–54. Caister Academic Press, Norfolk.

[29] CDC (2012). Severe influenza among children and young adults with neurologic and neurodevelopmental conditions - Ohio, 2011. *MMWR. Morbidity and mortality weekly report*, 60(51-52):1729–33.

[30] Charon, N. W., Cockburn, A., Li, C., Liu, J., Miller, K. a., Miller, M. R., Motaleb, M. a., and Wolgemuth, C. W. (2012). The unique paradigm of spirochete motility and chemotaxis. *Annual Review of Microbiology*, 66:349–70.

[31] Charon, N. W. and Goldstein, S. F. (2002). Genetics of motility and chemotaxis of a fascinating group of bacteria: the spirochetes. *Annual Review of Genetics*, 36:47–73.

[32] Charon, N. W., Greenberg, E. P., Koopman, M. B., and Limberger, R. J. (1992). Spirochete chemotaxis, motility, and the structure of the spirochetal periplasmic flagella. *Research in Microbiology*, 143(6):597–603.

[33] Chen, Z.-m., Shaughnessy, M. J. O., Gramaglia, I., Panoskaltsis-mortari, A., Murphy, W. J., Narula, S., Roncarolo, M. G., and Blazar, B. R. (2003). IL-10 and TGF-β induce alloreactive CD4+ CD25–T cells to acquire regulatory cell function. *Transplantation*, 101(12):5076–5083.

[34] Ciupe, S. M., Ribeiro, R. M., Nelson, P. W., and Perelson, A. S. (2007). Modeling the mechanisms of acute hepatitis B virus infection. *Journal of Theoretical Biology*, 247(1):23–35.

[35] Clewley, R. (2012). Hybrid models and biological model reduction with PyDSTool. *PLoS computational biology*, 8(8):e1002628.

[36] Cruz, A. R., Moore, M. W., La Vake, C. J., Eggers, C. H., Salazar, J. C., and Radolf, J. D. (2008). Phagocytosis of Borrelia burgdorferi, the Lyme disease spirochete, potentiates innate immune activation and induces apoptosis in human monocytes. *Infection and Immunity*, 76(1):56–70.

[37] Dardalhon, V., Awasthi, A., Kwon, H., Galileos, G., Gao, W., Sobel, R. a., Mitsdoerffer, M., Strom, T. B., Elyaman, W., Ho, I.-C., Khoury, S., Oukka, M., and Kuchroo, V. K. (2008). IL-4 inhibits TGF-beta-induced Foxp3+ T cells and, together with TGF-beta, generates IL-9+ IL-10+ Foxp3(-) effector T cells. *Nature Immunology*, 9(12):1347–55.

[38] Davidson, T. S., DiPaolo, R. J., Andersson, J., and Shevach, E. M. (2007). Cutting Edge: IL-2 Is Essential for TGF Mediated Induction of Foxp3+ T Regulatory Cells. *The Journal of Immunology*, 178(7):4022–4026.

[39] de Jong, J. C., Beyer, W. E., Palache, a. M., Rimmelzwaan, G. F., and Osterhaus, a. D. (2000). Mismatch between the 1997/1998 influenza vaccine and the major epidemic A(H3N2) virus strain as the cause of an inadequate vaccine-induced antibody response to this strain in the elderly. *Journal of Medical Virology*, 61(1):94–9.

[40] de Silva, A. M. and Fikrig, E. (1997). Arthropod- and Host-specific Gene Expression by Borrelia burgdorferi. *J. Clin. Invest.*, 99(3):377–379.

[41] Dengler, L., Kühn, N., Shin, D.-L., Hatesuer, B., Schughart, K., and Wilk, E. (2014). Cellular Changes in Blood Indicate Severe Respiratory Disease during Influenza Infections in Mice. *PLOS ONE*, 9(7):e103149.

[42] Denton, A. E., Doherty, P. C., Turner, S. J., and La Gruta, N. L. (2007). IL-18, but not IL-12, is required for optimal cytokine production by influenza virus-specific CD8+ T cells. *European Journal of Immunology*, 37(2):368–75.

[43] Diebold, S. S., Kaisho, T., Hemmi, H., Akira, S., and Reis e Sousa, C. (2004). Innate antiviral responses by means of TLR7-mediated recognition of single-stranded RNA. *Science (New York, N.Y.)*, 303(5663):1529–31.

[44] Dienz, O., Eaton, S. M., Bond, J. P., Neveu, W., Moquin, D., Noubade, R., Briso, E. M., Charland, C., Leonard, W. J., Ciliberto, G., Teuscher, C., Haynes, L., and Rincon, M. (2009). The induction of antibody production by IL-6 is indirectly mediated by IL-21 produced by CD4+ T cells. *The Journal of Experimental Medicine*, 206(1):69–78.

[45] Dinarello, C. A. (2007). Historical Review of Cytokines. *European Journal of Immunology*, 37:S34–45.

[46] Dombrowski, C., Kan, W., Motaleb, M. A., Charon, N. W., Goldstein, R. E., and Wolgemuth, C. W. (2009). The elastic basis for the shape of Borrelia burgdorferi. *Biophysical Journal*, 96(11):4409–17.

[47] Dorado, B., Jerez, M. J., Flores, N., Martin-Saavedra, F. M., Duran, C., and Ballester, S. (2002). Autocrine IL-4 Gene Regulation at Late Phases of TCR Activation in Differentiated Th2 Cells. *The Journal of Immunology*, 169(6):3030–3037.

[48] Dorigo, M. and Stützle, T. (2003). Ant Colony Optimization: Overview and Recent Advances. In Gendreau, M. and Ptovin, J.-Y., editors, *Handbook of Metaheuristics*, pages 227–264. Springer, New York, 2nd edition.

[49] Dworkin, M., Schwan, T., Anderson, D. J., and Borchardt, S. (2008). Tick-borne relapsing fever. *Infectious Disease Clinics of North America*, 22(3):9–12.

[50] Eddelbuettel, D. and François, R. (2011). Rcpp: Seamless R and C++ integration. *Journal of Statistical Software*, 40(8).

[51] Epstein, S. L., Lo, C.-y., Misplon, J. A., Jack, R., and Bennink, J. R. (1998). Mechanism of protective immunity against influenza virus infection in mice without antibodies. *The Journal of Immunology*, 160(1):322–327.

[52] Espevik, T., Waage, A., Faxvaag, A., and Shalaby, M. (1990). Regulation of interleukin-2 and interleukin-6 production from T-cells: Involvement of interleukin-1 β and transforming growth factor-β. *Cellular Immunology*, 126(1):47–56.

[53] Esposito, W. and Floudas, C. (2000). Deterministic global optimization in nonlinear optimal control problems. *Journal of Global Optimization*, 17:97–126.

[54] Feder, H. M., Johnson, B. J. B., O'Connell, S., Shapiro, E. D., Steere, A. C., and Wormser, G. P. (2007). A Critical Appraisal of "Chronic Lyme Disease". *New Engl. J. Med.*, 357:1422–30.

[55] Fikrig, E., Bockenstedt, L. K., Barthold, S. W., Chen, M., Tao, H., Ali-Salaam, P., Telford, S. R., and Flavell, R. a. (1994). Sera from patients with chronic Lyme disease protect mice from Lyme borreliosis. *The Journal of Infectious Diseases*, 169(3):568–74.

[56] Fiorentino, D. F., Zlotnik, a., Vieira, P., Mosmann, T. R., Howard, M., Moore, K. W., and O'Garra, a. (1991). IL-10 acts on the antigen-presenting cell to inhibit cytokine production by Th1 cells. *Journal of immunology (Baltimore, Md. : 1950)*, 146(10):3444–51.

[57] Fisher, R. A. (1930). *The genetical theory of natural selection*. Clarendon Press, Oxford.

[58] Fleming, D. M., Pannell, R. S., and Cross, K. W. (2005). Mortality in children from influenza and respiratory syncytial virus. *Journal of Epidemiology and Community Health*, 59(7):586–90.

[59] Fraser, C. M., Casjens, S., Huang, W. M., Sutton, G. G., Clayton, R., Lathigra, R., White, O., Ketchum, K. a., Dodson, R., Hickey, E. K., Gwinn, M., Dougherty, B., Tomb, J. F., Fleischmann, R. D., Richardson, D., Peterson, J., Kerlavage, a. R., Quackenbush, J., Salzberg, S., Hanson, M., van Vugt, R., Palmer, N., Adams, M. D., Gocayne, J., Weidman, J., Utterback, T., Watthey, L., McDonald, L., Artiach, P., Bowman, C., Garland, S., Fuji, C., Cotton, M. D., Horst, K., Roberts, K., Hatch, B., Smith, H. O., and Venter, J. C. (1997). Genomic sequence of a Lyme disease spirochaete, Borrelia burgdorferi. *Nature*, 390(6660):580–6.

[60] Gamblin, S. J. and Skehel, J. J. (2010). Influenza hemagglutinin and neuraminidase membrane glycoproteins. *The Journal of Biological Chemistry*, 285(37):28403–9.

[61] Garnett, G. P., Kim, J. J., French, K., and Goldie, S. J. (2006). Chapter 21: Modelling the impact of HPV vaccines on cervical cancer and screening programmes. *Vaccine*, 24 Suppl 3:S3/178–86.

[62] Gazit, R., Gruda, R., Elboim, M., Arnon, T. I., Katz, G., Achdout, H., Hanna, J., Qimron, U., Landau, G., Greenbaum, E., Zakay-Rones, Z., Porgador, A., and Mandelboim, O. (2006). Lethal influenza infection in the absence of the natural killer cell receptor gene Ncr1. *Nature Immunology*, 7(5):517–23.

[63] Gendreau, M. and Potvin, J.-Y. (2003). *Handbook of metaheuristics*. Springer, New York.

[64] Gerhard, W., Mozdzanowska, K., Furchner, M., Washko, G., and Maiese, K. (1997). Role of the B-cell response in recovery of mice from primary influenza virus infection. *Immunological Reviews*, 159(3):95–103.

[65] Goldstein, S., Buttle, K., and Charon, N. (1996). Structural analysis of the Leptospiraceae and Borrelia burgdorferi by high-voltage electron microscopy. *Journal of Bacteriology*, 178(22).

[66] Grassly, N. C. and Fraser, C. (2008). Mathematical models of infectious disease transmission. *Nature Reviews Microbiology*, 6(6):477–87.

[67] Gray, J. S., Dautel, H., Estrada-Peña, A., Kahl, O., and Lindgren, E. (2009). Effects of climate change on ticks and tick-borne diseases in europe. *Interdisciplinary Perspectives on Infectious Diseases*, 2009:593232.

[68] Grimm, D., Tilly, K., Byram, R., Stewart, P. E., Krum, J. G., Bueschel, D. M., Schwan, T. G., Policastro, P. F., Elias, A. F., and Rosa, P. A. (2004). Outer-surface protein C of the Lyme disease spirochete: a protein induced in ticks for infection of mammals. *P. Natl. Acad. Sci. USA*, 101(9):3142–3147.

[69] Gros, G. L. and Ben-Sasson, S. (1990). Generation of interleukin 4 (IL-4)-producing cells in vivo and in vitro: IL-2 and IL-4 are required for in vitro generation of IL-4-producing cells. *The Journal of Experimental Medicine*, 172(September).

[70] Guo, Z., Chen, L.-m., Zeng, H., Gomez, J. a., Plowden, J., Fujita, T., Katz, J. M., Donis, R. O., and Sambhara, S. (2007). NS1 protein of influenza A virus inhibits the function of intracytoplasmic pathogen sensor, RIG-I. *American Journal of Respiratory Cell and Molecular Biology*, 36(3):263–9.

[71] Halperin, J. J. (2011). Nervous System Involvement. In *Lyme Disease: An Evidence-based Approach*, pages 208–220. CAB International, Oxfordshire.

[72] Hancioglu, B., Swigon, D., and Clermont, G. (2007). A dynamical model of human immune response to influenza A virus infection. *Journal of Theoretical Biology*, 246(1):70–86.

[73] Hardy, G. (1908). Mendelian proportions in a mixed population. *Science*, XXVIII.

[74] Hashimoto, Y., Moki, T., Takizawa, T., Shiratsuchi, a., and Nakanishi, Y. (2007). Evidence for Phagocytosis of Influenza Virus-Infected, Apoptotic Cells by Neutrophils and Macrophages in Mice. *The Journal of Immunology*, 178(4):2448–2457.

[75] Haugh, J. (2008). Mathematical Modelling of Biological Signaling Networks. In *Wiley Encyclopedia of Chemical Biology*, pages 1–9. Wiley.

[76] Hayden, F. G., Fritz, R., Lobo, M. C., Alvord, W., Strober, W., and Straus, S. E. (1998). Local and systemic cytokine responses during experimental human influenza A virus infection. Relation to symptom formation and host defense. *The Journal of Clinical Investigation*, 101(3):643–9.

[77] Hefti, H. P., Frese, M., Landis, H., Di Paolo, C., Aguzzi, A., Haller, O., and Pavlovic, J. (1999). Human MxA protein protects mice lacking a functional alpha/beta interferon system against La crosse virus and other lethal viral infections. *Journal of Virology*, 73(8):6984–6991.

[78] Henney, C., Kuribayashi, K., Kern, D., and Gillis, S. (1981). Interleukin-2 augments natural killer cell activity. *Nature*, 291:335–338.

[79] Hernandez-Vargas, E. A., Wilk, E., Canini, L., Toapanta, F. R., Binder, S. C., Uvarovskii, A., Ross, T. M., Guzmán, C. A., Perelson, A. S., and Meyer-Hermann, M. (2014). Effects of Aging on Influenza Virus Infection Dynamics. *J. Virol.*, 88(8):4123–4131.

[80] Ho, W.-H. and Chan, A. L.-F. (2011). Hybrid Taguchi-Differential Evolution Algorithm for Parameter Estimation of Differential Equation Models with Application to HIV Dynamics. *Math. Probl. Eng.*, 2011:1–14.

[81] Hodgkin, A. and Huxley, A. (1952). A quantitative description of membrane current and its application to conduction and excitation in nerve. *The Journal of Physiology*, pages 500–544.

[82] Hodzic, E., Feng, S., Freet, K., Borjesson, D., and Barthold, S. (2002). Borrelia burgdorferi population kinetics and selected gene expression at the host-vector interface. *Infection and Immunity*, 70(7):3382.

[83] Hodzic, E., Feng, S., Freet, K. J., and Barthold, S. W. (2003). Borrelia burgdorferi Population Dynamics and Prototype Gene Expression during Infection of Immunocompetent and Immunodeficient Mice. *Infection and Immunity*, 71(9):5042–5055.

[84] Holter, W., Kalthoff, F. S., Pickl, W. F., Ebner, C., Majdic, O., Kraft, D., and Knapp, W. (1994). Transforming growth factor-beta inhibits IL-4 and IFN-gamma production by stimulated human T cells. *International Immunology*, 6(3):469–75.

[85] Hovius, J. W. and Wormser, G. P. (2011). Persistence of Borrelia burgdorferi Infection after Antibiotic Treatment: What Can We Learn From Animal Models. In *Lyme Disease: An Evidence-based Approach*, pages 89–99. CAB International, Oxfordshire.

[86] Hubalek, Z. (2009). Epidemiology of Lyme borreliosis. *Curr Probl Dermatol*, 37:31–50.

[87] Hübner, a., Yang, X., Nolen, D. M., Popova, T. G., Cabello, F. C., and Norgard, M. V. (2001). Expression of Borrelia burgdorferi OspC and DbpA is controlled by a RpoN-RpoS regulatory pathway. *Proceedings of the National Academy of Sciences of the United States of America*, 98(22):12724–9.

[88] Hunter, J. (2007). Matplotlib: A 2D graphics environment. *Computing in Science & Engineering*, 9(3):90—-95.

[89] Hutchinson, E. C. and Fodor, E. (2013). Transport of the influenza virus genome from nucleus to nucleus. *Viruses*, 5(10):2424–46.

[90] Hyde, J. a., Shaw, D. K., Smith Iii, R., Trzeciakowski, J. P., and Skare, J. T. (2009). The BosR regulatory protein of Borrelia burgdorferi interfaces with the RpoS regulatory pathway and modulates both the oxidative stress response and pathogenic properties of the Lyme disease spirochete. *Molecular Microbiology*, 74(6):1344–55.

[91] Ingber, L. and Rosen, B. (1992). Genetic algorithms and very fast simulated reannealing: A comparison. *Math. Comput. Model.*, 16(11):87–100.

[92] Ito, R., Ozaki, Y. A., Yoshikawa, T., Hasegawa, H., Sato, Y., Suzuki, Y., Inoue, R., Morishima, T., Kondo, N., Sata, T., Kurata, T., and Tamura, S.-i. (2003). Roles of anti-hemagglutinin IgA and IgG antibodies in different sites of the respiratory tract of vaccinated mice in preventing lethal influenza pneumonia. *Vaccine*, 21(19-20):2362–2371.

[93] Iwasaki, A. and Pillai, P. S. (2014). Innate immunity to influenza virus infection. *Nature Reviews Immunology*, 14(5):315–28.

[94] Izard, J., Renken, C., Hsieh, C.-E., Desrosiers, D. C., Dunham-Ems, S., La Vake, C., Gebhardt, L. L., Limberger, R. J., Cox, D. L., Marko, M., and Radolf, J. D. (2009). Cryo-electron tomography elucidates the molecular architecture of Treponema pallidum, the syphilis spirochete. *Journal of bacteriology*, 191(24):7566–80.

[95] Jones, S. (2005). Directing Transition from Innate to Acquired Immunity: Defining a Role for IL-6. *The Journal of Immunology*, 175(6):3463–3468.

[96] Julkunen, I., Melén, K., Nyqvist, M., Pirhonen, J., Sareneva, T., and Matikainen, S. (2000). Inflammatory responses in influenza A virus infection. *Vaccine*, 19 Suppl 1:S32–7.

[97] Kapitein, B., Tiemessen, M. M., Liu, W. M., van Ieperen-van Dijk, a. G., Hoekstra, M. O., van Hoffen, E., and Knol, E. F. (2007). The interleukin-10 inducing effect of transforming growth factor-beta on human naive CD4+ T cells from cord blood is restricted to the TH1 subset. *Clinical and Experimental Immunology*, 147(2):352–8.

[98] Kato, H., Sato, S., Yoneyama, M., Yamamoto, M., Uematsu, S., Matsui, K., Tsujimura, T., Takeda, K., Fujita, T., Takeuchi, O., and Akira, S. (2005). Cell type-specific involvement of RIG-I in antiviral response. *Immunity*, 23(1):19–28.

[99] Kermack, W. O. and McKendrick, A. G. (1932). Contributions to the Mathematical Theory of Epidemics. II. The Problem of Endemicity. *Proceedings of the Royal Society A: Mathematical, Physical and Engineering Sciences*, 138(834):55–83.

[100] Kim, S., Angel, P., and Lafyatis, R. (1990). Autoinduction of transforming growth factor beta 1 is mediated by the AP-1 complex. *Molecular and Cellular Biology*, 10(4):1492–1497.

[101] Kirkpatrick, S., Gelatt, C., and Vecchi, M. (1983). Optimisation by Simulated Annealing. *Science*, 220(4598):671–680.

[102] Kishimoto, T., Akira, Shizuo, Narazaki, M., and Taga, T. (1995). Interleukin-6 family of cytokines and gp130. *Blood*, 86(4):1243–1254.

[103] Kitani, a. and Xu, L. (2008). Regulatory T cells and the induction of IL-17. *Mucosal Immunology*, 1 Suppl 1(November):S43–6.

[104] Klempner, M. S., Hu, L. T., Evans, J., Schmid, C. H., Johnson, G. M., Trevino, R. P., Norton, D., Levy, L., Wall, D., McCall, J., Kosinski, M., and Weinstein, A. (2001). Two controlled trials of antibiotic treatment in patients with persistent symptoms and a history of Lyme disease. *New England Journal of Medicine*, 345(2):85–92.

[105] Kozawa, O., Suzuki, A., Kaida, T., Tokuda, H., and Uematsu, T. (1997). Tumor Necrosis Factor Autoregulates Interleukin-6 Synthesis via Activation of Protein Kinase C: FUNCTION OF SPHINGOSINE 1-PHOSPHATE AND PHOSPHATIDYLCHOLINE-SPECIFIC PHOSPHOLIPASE C. *Journal of Biological Chemistry*, 272(40):25099–25104.

[106] Kreijtz, J. H. C. M., Fouchier, R. a. M., and Rimmelzwaan, G. F. (2011). Immune responses to influenza virus infection. *Virus Research*, 162(1-2):19–30.

[107] Lakadamyali, M., Rust, M., and Zhuang, X. (2004). Endocytosis of influenza viruses. *Microbes and Infection*, 6(10):929–936.

[108] Lauder, S. N., Jones, E., Smart, K., Bloom, A., Williams, A. S., Hindley, J. P., Ondondo, B., Taylor, P. R., Clement, M., Fielding, C., Godkin, A. J., Jones, S. a., and Gallimore, A. M. (2013). Interleukin-6 limits influenza-induced inflammation and protects against fatal lung pathology. *European Journal of Immunology*, 43(10):2613–25.

[109] Lauffenburger, D. and Kennedy, C. (1983). Localized bacterial infection in a distributed model for tissue inflammation. *Journal of Mathematical Biology*, 16:141–163.

[110] Lavik, J.-P. (2012). *Intravital Microscopy of Borrelia burgdorferi: Delineation of Dissemination Kinetics and Persistence Within Murine Skin*. Dissertation, The University of Toledo.

[111] Lawrenz, M. B., Wooten, R. M., and Norris, S. J. (2004). Effects of vlsE complementation on the infectivity of Borrelia burgdorferi lacking the linear plasmid lp28-1. *Infection and Immunity*, 72(11).

[112] Lawrenz, M. B., Wooten, R. M., Zachary, J. F., Drouin, S. M., Weis, J. J., Wetsel, R. A., and Norris, S. J. (2003). Effect of complement component C3 deficiency on experimental Lyme borreliosis in mice. *Infection and Immunity*, 71(8):4432–4440.

[113] Lazarus, J. J., Kay, M. a., McCarter, A. L., and Wooten, R. M. (2008). Viable Borrelia burgdorferi enhances interleukin-10 production and suppresses activation of murine macrophages. *Infection and Immunity*, 76(3):1153–62.

[114] Li, X., O'Regan, A., and Berman, J. (2003). IFN-γ induction of osteopontin expression in human monocytoid cells. *Journal of Interferon & Cytokine Research*, 265:259–265.

[115] Liang, F. T., Jacobs, M. B., Bowers, L. C., and Philipp, M. T. (2002). An immune evasion mechanism for spirochetal persistence in Lyme borreliosis. *The Journal of Experimental Medicine*, 195(4):415–22.

[116] Liang, S., Wei, H., Sun, R., and Tian, Z. (2003). IFNα regulates NK cell cytotoxicity through STAT1 pathway. *Cytokine*, 23(6):190–199.

[117] Liu, J. and Lampinen, J. (2004). A Fuzzy Adaptive Differential Evolution Algorithm. *Soft Comput.*, 9(6):448–462.

[118] Loebbermann, J., Schnoeller, C., Thornton, H., Durant, L., Sweeney, N. P., Schuijs, M., O'Garra, A., Johansson, C., and Openshaw, P. J. (2012). IL-10 regulates viral lung immunopathology during acute respiratory syncytial virus infection in mice. *PLOS ONE*, 7(2):e32371.

[119] Long, M. and Adler, A. (2006). Cutting edge: Paracrine, but not autocrine, IL-2 signaling is sustained during early antiviral CD4 T cell response. *The Journal of Immunology*, 177(7):4257–4261.

[120] Loomis, W., Namiki, S., Hoyt, D. B., and Junger, W. G. (2001). Hypertonicity rescues T cells from suppression by trauma-induced anti-inflammatory mediators. *American Journal of Cell Physiology*, 281:840–848.

[121] Lubberts, E., Joosten, L. A. B., Chabaud, M., Bersselaar, L. V. D., Oppers, B., Roo, C. J. J. C.-d., Richards, C. D., Miossec, P., and Berg, W. B. V. D. (2000). IL-4 gene therapy for collagen arthritis suppresses synovial IL-17 and osteoprotegerin ligand and prevents bone erosion. *The Journal of Clinical Investigation*, 105(12):1697–1710.

[122] Lund, J. M., Alexopoulou, L., Sato, A., Karow, M., Adams, N. C., Gale, N. W., Iwasaki, A., and Flavell, R. a. (2004). Recognition of single-stranded RNA viruses by Toll-like receptor 7. *Proceedings of the National Academy of Sciences of the United States of America*, 101(15):5598–603.

[123] Mack, E., Kallal, L., Demers, D., and Biron, C. (2011). Type 1 interferon induction of natural killer cell gamma interferon production for defense during lymphocytic choriomeningitis virus infection. *MBio*, 2(4).

[124] Maki, Y., Ueda, T., Okamoto, M., Uematsu, N., Inamura, K., Uchida, K., Takahashi, Y., and Eguchi, Y. (2002). Inference of genetic network using the expression profile time course data of mouse P19 cells. *Genome Inform.*, 13:382–383.

[125] Malka, R., Shochat, E., and Rom-Kedar, V. (2010). Bistability and bacterial infections. *PLoS ONE*, 5(5):e10010.

[126] Mancini, N., Solforosi, L., Clementi, N., De Marco, D., Clementi, M., and Burioni, R. (2011). A potential role for monoclonal antibodies in prophylactic and therapeutic treatment of influenza. *Antiviral Research*, 92(1):15–26.

[127] Margos, G., Vollmer, S. a., Cornet, M., Garnier, M., Fingerle, V., Wilske, B., Bormane, A., Vitorino, L., Collares-Pereira, M., Drancourt, M., and Kurtenbach, K. (2009). A new Borrelia species defined by multilocus sequence analysis of housekeeping genes. *Applied and Environmental Microbiology*, 75(16):5410–6.

[128] McCullers, J. a. (2006). Insights into the interaction between influenza virus and pneumococcus. *Clinical Microbiology Reviews*, 19(3):571–82.

[129] Mcloughlin, R. M., Witowski, J., Robson, R. L., Wilkinson, T. S., Hurst, S. M., Williams, A. S., Williams, J. D., Rose-john, S., Jones, S. A., and Topley, N. (2003). Interplay between IFN-γ and IL-6 signaling governs neutrophil trafficking and apoptosis during acute inflammation. *The Journal of Clinical Investigation*, 112(4).

[130] Mendes, P. (2001). Modeling Large Biological Systems From Functional Genomic Data: Parameter Estimation. In Kitano, H., editor, *Foundations of Systems Biology*, pages 163–188. The MIT Press, Cambridge, Massachusetts.

[131] Meyer-Hermann, M., Figge, M. T., and Straub, R. H. (2009). Mathematical modeling of the circadian rhythm of key neuroendocrine-immune system players in rheumatoid arthritis: a systems biology approach. *Arthritis Rheum.*, 60(9):2585–94.

[132] Miao, H., Hollenbaugh, J. a., Zand, M. S., Holden-Wiltse, J., Mosmann, T. R., Perelson, A. S., Wu, H., and Topham, D. J. (2010). Quantifying the early immune response and adaptive immune response kinetics in mice infected with influenza A virus. *Journal of Virology*, 84(13):6687–98.

[133] Möhler, L., Flockerzi, D., Sann, H., and Reichl, U. (2005). Mathematical model of influenza A virus production in large-scale microcarrier culture. *Biotechnology and Bioengineering*, 90(1):46–58.

[134] Moles, C. G., Banga, J. R., and Keller, K. (2004). Solving nonconvex climate control problems: pitfalls and algorithm performances. *Appl. Soft Comput.*, 5(1):35–44.

[135] Moles, C. G., Mendes, P., and Banga, J. R. (2003). Parameter estimation in biochemical pathways: a comparison of global optimization methods. *Genome Res.*, 13(11):2467–74.

[136] Montgomery, R., Palmarozza, R., and Beck, D. (2000). Functional competence of peritoneal macrophages in murine Lyme borreliosis. *Inflammation*, 24(3):277–288.

[137] Montgomery, R. R., Lusitani, D., de Boisfleury Chevance, A., and Malawista, S. E. (2002). Human phagocytic cells in the early innate immune response to Borrelia burgdorferi. *The Journal of Infectious Diseases*, 185(12):1773–9.

[138] Montgomery, R. R. and Malawista, S. E. (1996). Entry of Borrelia burgdorferi into macrophages is end-on and leads to degradation in lysosomes. *Infection and Immunity*, 64(7):2867–72.

[139] Montgomery, R. R., Wang, X. M., and Malawista, S. E. (2001). Murine Lyme disease: no evidence for active immune down-regulation in resolving or subclinical infection. *Journal of Infectious Diseases*, 183(11):1631–7.

[140] Mori, I., Komatsu, T., Takeuchi, K., Nakakuki, K., Sudo, M., and Kimura, Y. (1995). In vivo induction of apoptosis by influenza virus. *The Journal of General Virology*, 76 (Pt11):2869–73.

[141] Motaleb, M. a., Corum, L., Bono, J. L., Elias, a. F., Rosa, P., Samuels, D. S., and Charon, N. W. (2000). Borrelia burgdorferi periplasmic flagella have both skeletal and motility functions. *Proceedings of the National Academy of Sciences of the United States of America*, 97(20):10899–904.

[142] Mullen, K. M., Ardia, D., Gil, D. L., Windover, D., and Cline, J. (2011). DEoptim: An R package for global optimization by differential evolution. *J. Stat. Softw.*, 40(6).

[143] Murphy, M., Hyun, W., Hunte, B., Levine, a. D., and Epstein, L. B. (1992). A role for tumor necrosis factor-alpha and interferon-gamma in the regulation of interleukin-4-induced human thymocyte proliferation in vitro. Heightened sensitivity in the Down syndrome (trisomy 21) thymus. *Pediatric Research*, 32(3):269–76.

[144] Murray, J. D. (2002). *Mathematical Biology I: An Introduction*. Springer, New York, 3 edition.

[145] Murray, J. D. (2003). *Mathematical Biology II: Spatial Models and Biomedical Applications*. Springer, New York, 3 edition.

[146] Murray, J. D. (2012). Vignettes from the field of mathematical biology: the application of mathematics to biology and medicine. *Interface focus*, 2(4):397–406.

[147] Nau, R., Christen, H.-J., and Eiffert, H. (2009). Lyme disease–current state of knowledge. *Dtsch. Arztebl. Int.*, 106(5):72–81; quiz 82, I.

[148] Nefedova, V. V., Korenberg, E. I., Gorelova, N. B., and Kovalevskii, Y. V. (2004). Studies on the transovarial transmission of Borrelia burgdorferi sensu lato in the taiga tick Ixodes persulcatus. *Folia Parasitologica*, 51(1):67–71.

[149] Neirynck, S., Deroo, T., Saelens, X., Vanlandschoot, P. V., Min Jou, W., and Fiers, W. (1999). A universal influenza A vaccine based on the extracellular domain of the M2 protein. *Nature Medicine*, 5:11571163.

[150] Nelder, J. and Mead, R. (1965). A simplex method for function minimization. *The Computer Journal*.

[151] Neumann, a. U. (1998). Hepatitis C Viral Dynamics in Vivo and the Antiviral Efficacy of Interferon- Therapy. *Science*, 282(5386):103–107.

[152] Nicholson, K. G., Wood, J. M., and Zambon, M. (2003). Influenza. *Lancet*, 362(9397):1733–45.

[153] Norris, S., Howell, J., Garza, S., Ferdows, M., and Barbour, A. (1995). High-and low-infectivity phenotypes of clonal populations of in vitro-cultured Borrelia burgdorferi. *Infection and Immunity*, 63(6).

[154] Okamura, H., Tsutsui, H., Komatsu, T., Yutsudo, M., Hakura, A., Tanimoto, T., Torigoe, K., Okura, T., Nukada, Y., Hattori, K., Aktia, K., Namba, M., Tanabe, F., Konishi, K., Fukuda, S., and Kurimoto, M. (1995). Cloning of a new cytokine that induces IFN-γ production by T cells. *Nature*, 378:88–91.

[155] Oksi, J., Marttila, H., Soini, H., Aho, H., Uksila, J., and Viljanen, M. K. (2001). Early dissemination of Borrelia burgdorferi without generalized symptoms in patients with erythema migrans. *APMIS: Acta Pathologica Microbiologica Scandinavica*, 109(9):581–8.

[156] Pahl, A., Kuehlbrandt, U., Brune, K., Roellinghoff, M., and Gessner, A. (1999). Quantitative detection of Borrelia burgdorferi by Real-Time PCR. *Journal of Clinical Microbiology*, 37(6):1958–63.

[157] Palmer, G. H., Bankhead, T., and Lukehart, S. A. (2009). 'Nothing is permanent but change'-antigenic variation in persistent bacterial pathogens. *Cell. Microbiol.*, 11(12):1697–705.

[158] Paludan, S. R. (1998). Interleukin-4 and interferon-gamma: the quintessence of a mutual antagonistic relationship. *Scandinavian Journal of Immunology*, 48(5):459–68.

[159] Pang, I. K. and Iwasaki, A. (2011). Inflammasomes as mediators of immunity against influenza virus. *Trends in Immunology*, 32(1):34–41.

[160] Pawelek, K. a., Huynh, G. T., Quinlivan, M., Cullinane, A., Rong, L., and Perelson, A. S. (2012). Modeling within-host dynamics of influenza virus infection including immune responses. *PLoS Computational Biology*, 8(6):e1002588.

[161] Perelson, A., Neumann, A., and Markowitz, M. (1996). HIV-1 dynamics in vivo: virion clearance rate, infected cell life-span, and viral generation time. *Science*, 271(5255):1582–6.

[162] Perelson, A. S. and Nelson, P. W. (1999). Mathematical Analysis of HIV-1 Dynamics in Vivo. *SIAM Review*, 41(1):3–44.

[163] Philipp, M. T., Aydintug, M. K., Bohm, R. P., Cogswell, F. B., Dennis, V. a., Lanners, H. N., Lowrie, R. C., Roberts, E. D., Conway, M. D., Karaçorlu, M., Peyman, G. a., Gubler, D. J., Johnson, B. J., Piesman, J., and Gu, Y. (1993). Early and early disseminated phases of Lyme disease in the rhesus monkey: a model for infection in humans. *Infection and Immunity*, 61(7):3047–59.

[164] Pichlmair, A., Schulz, O., Tan, C. P., Näslund, T. I., Liljeström, P., Weber, F., and Reis e Sousa, C. (2006). RIG-I-mediated antiviral responses to single-stranded RNA bearing 5'-phosphates. *Science (New York, N.Y.)*, 314(5801):997–1001.

[165] Piesman, J. (1993). Dynamics of Borrelia burgdorferi transmission by nymphal Ixodes dammini ticks. *The Journal of Infectious Diseases*, 167(5):1082–5.

[166] Pilyugin, S. S. and Antia, R. (2000). Modeling immune responses with handling time. *Bulletin of Mathematical Biology*, 62(5):869–90.

[167] Plaetinck, G., Declercq, W., Tavernier, J., Nabholz, M., and Fiers, W. (1987). Recombinant tumor necrosis factor can induce interleukin 2 receptor expression and cytolytic activity in a rat x mouse T cell hybrid. *European Journal of Immunology*, 17(12):1835–8.

[168] Platzer, C., Meisel, C., Vogt, K., Platzer, M., Volk, H., and Jena, D. (1995). Up-regulation of monocytic IL-10 by tumor necrosis factor-a and cAMP elevating drugs. *International Immunology*, 7(4):517–523.

[169] Pommerenke, C., Wilk, E., Srivastava, B., Schulze, A., Novoselova, N., Geffers, R., and Schughart, K. (2012). Global transcriptome analysis in influenza-infected mouse lungs reveals the kinetics of innate and adaptive host immune responses. *PLOS ONE*, 7(7):e41169.

[170] Press, W. H., Teukolsky, S. A., Vetterling, W. T., and Flannery, B. P. (2007). *Numerical Recipes 3rd Edition: The Art of Scientific Computing*. Cambridge University Press, New York, 3rd editio edition.

[171] Price, K. V., Storn, R. M., and Lampinen, J. A. (2005). *Differential Evolution*. Springer, Berlin.

[172] Raddi, G., Morado, D. R., Yan, J., Haake, D. a., Yang, X. F., and Liu, J. (2012). Three-dimensional structures of pathogenic and saprophytic Leptospira species revealed by cryo-electron tomography. *Journal of Bacteriology*, 194(6):1299–306.

[173] Radolf, J. D., Caimano, M. J., Stevenson, B., and Hu, L. T. (2012). Of ticks, mice and men: understanding the dual-host lifestyle of Lyme disease spirochaetes. *Nature Reviews Microbiology*, 10(2):87–99.

[174] Raol, J., Girija, G., and Singh, J. (2004). *Modelling and Parameter Estimation of Dynamic Systems*. IEEE, London.

[175] Reddy, J., Chastagner, P., Fiette, L., Liu, X., and Theze, J. (2001). IL-2-induced tumor necrosis factor (TNF)-β expression: further analysis in the IL-2 knockout model, and comparison with TNF-α, lymphotoxin-β, TNFR1 and TNFR2 modulation. *International Immunology*, 13(2):135–147.

[176] Reinke, J. (1901). *Einleitung in die theoretische Biologie*. Paetel, Berlin.

[177] Renegar, K. B., Small, P. a., Boykins, L. G., and Wright, P. F. (2004). Role of IgA versus IgG in the Control of Influenza Viral Infection in the Murine Respiratory Tract. *The Journal of Immunology*, 173(3):1978–1986.

[178] Reynolds, A., Rubin, J., Clermont, G., Day, J., Vodovotz, Y., and Bard Ermentrout, G. (2006). A reduced mathematical model of the acute inflammatory response: I. Derivation of model and analysis of anti-inflammation. *Journal of Theoretical Biology*, 242(1):220–36.

[179] Rizzoli, A., Hauffe, H., Carpi, G., Vourc'h, G., Neteler, M., and Rosa, R. (2011). Lyme borreliosis in Europe. *Euro Surveill.*, 16(27):1–8.

[180] Rupprecht, T. A., Koedel, U., Fingerle, V., and Pfister, H.-W. (2008). The pathogenesis of lyme neuroborreliosis: from infection to inflammation. *Mol. Med.*, 14(3-4):205–12.

[181] Rust, M. J., Lakadamyali, M., Zhang, F., and Zhuang, X. (2004). Assembly of endocytic machinery around individual influenza viruses during viral entry. *Nature Structural & Molecular Biology*, 11(6):567–73.

[182] Saraiva, M. and O'Garra, A. (2010). The regulation of IL-10 production by immune cells. *Nature Reviews Immunology*, 10(3):170–81.

[183] Savageau, M. (1969). Biochemical systems analysis: I. Some mathematical properties of the rate law for the component enzymatic reactions. *Journal of Theoretical Biology*, 25:365–369.

[184] Scharton, T. M. and Scott, P. (1993). Natural killer cells are a source of interferon gamma that drives differentiation of CD4+ T cell subsets and induces early resistance to Leishmania major in mice. *The Journal of Experimental Medicine*, 178(2):567–77.

[185] Schmidt-Weber, C. B., Alexander, S. I., Henault, L. E., James, L., and Lichtman, a. H. (1999). IL-4 enhances IL-10 gene expression in murine Th2 cells in the absence of TCR engagement. *Journal of Immunology (Baltimore, Md. : 1950)*, 162(1):238–44.

[186] Schmitz, N., Kurrer, M., Bachmann, M. F., and Kopf, M. (2005). Interleukin-1 is responsible for acute lung immunopathology but increases survival of respiratory influenza virus infection. *Journal of Virology*, 79(10):6441–6448.

[187] Schroder, K., Hertzog, P. J., Ravasi, T., and Hume, D. A. (2004). Interferon-γ: an overview of signals, mechanisms and functions. *Journal of Leukocyte Biology*, 75(February).

[188] Seder, R. a., Paul, W. E., Davis, M. M., and Fazekas de St Groth, B. (1992). The presence of interleukin 4 during in vitro priming determines the lymphokine-producing potential of CD4+ T cells from T cell receptor transgenic mice. *The Journal of Experimental Medicine*, 176(4):1091–8.

[189] Sejnowski, T. J., Koch, C., and Churchland, P. S. (1988). Computational neuroscience. *Science*, 241(4871):1299–1306.

[190] Seo, S. and Webster, R. (2002). Tumor necrosis factor alpha exerts powerful anti-influenza virus effects in lung epithelial cells. *Journal of virology*, 76(3).

[191] Shih, C., Pollack, R., Telford III, S., and Spielman, A. (1992). Delayed dissemination of Lyme disease spirochetes from the site of deposition in the skin of mice. *Journal of Infectious Diseases*, 166(4):827–831.

[192] Shrestha, S., Foxman, B., Dawid, S., Aiello, A. E., Davis, B. M., Berus, J., and Rohani, P. (2013). Time and dose-dependent risk of pneumococcal pneumonia following influenza: a model for within-host interaction between influenza and Streptococcus pneumoniae. *Journal of The Royal Society*, 10.

[193] Skehel, J. and Wiley, D. (2000). Receptor binding and membrane fusion in virus entry: the influenza hemagglutinin. *Annual Review of Biochemistry*, 69:531–69.

[194] Sládková, T. and Kostolanský, F. (2006). The role of cytokines in the immune response to influenza A virus infection. *Acta virologica*, 50(3):151–62.

[195] Smith, A. M., McCullers, J. a., and Adler, F. R. (2011). Mathematical model of a three-stage innate immune response to a pneumococcal lung infection. *Journal of Theoretical Biology*, 276(1):106–16.

[196] Smith, K. (1988). Interleukin-2: inception, impact, and implications. *Science*, 240(4856):1169–1176.

[197] Soetaert, K., Petzoldt, T., and Setzer, W. (2010). Solving differential equations in R: package deSolve. *Journal of Statistical Software*, 33(9).

[198] Staeheli, P., Haller, O., Boll, W., Lindenmann, J., and Weissmann, C. (1986). Mx protein: constitutive expression in 3T3 cells transformed with cloned Mx cDNA confers selective resistance to influenza virus. *Cell*, 44(1):147–58.

[199] Stanek, G., Klein, J., Bittner, R., and Glogar, D. (1990). Isolation of Borrelia burgdorferi from the myocardium of a patient with long-standing cardiomyopathy. *New England Journal of Medicine*.

[200] Stanek, G. and Reiter, M. (2011). The expanding Lyme Borrelia complex–clinical significance of genomic species? *Clinical microbiology and infection : the official publication of the European Society of Clinical Microbiology and Infectious Diseases*, 17(4):487–93.

[201] Stark, G. R., Kerr, I. M., Williams, B. R. G., Silverman, R. H., and Schreiber, R. D. (1998). How cells respond to interferons. *Annual review of Biochemistry*, 67:227–264.

[202] Steere, A. C. (2001). Lyme Disease. *N. Engl. J. Med.*, 345(2):115–125.

[203] Steere, A. C. and Glickstein, L. (2004). Elucidation of Lyme arthritis. *Nat. Rev. Immunol.*, 4(2):143–52.

[204] Steere, A. C., Klitz, W., Drouin, E. E., Falk, B. A., Kwok, W. W., Nepom, G. T., and Baxter-Lowe, L. A. (2006). Antibiotic-refractory Lyme arthritis is associated with HLA-DR molecules that bind a Borrelia burgdorferi peptide. *J. Exp. Med.*, 203(4):961–71.

[205] Steere, A. C., Malawista, S. E., Snydman, D. R., Shope, R. E., Andiman, W. A., Ross, M. R., and Steele, F. M. (1977). An epidemic of oligoarticular arthritis in children and adults in three Connecticut communities. *Arthritis Rheum.*, 20(1):7–17.

[206] Steere, A. C., Sikand, V. K., Meurice, F., Parenti, D., Fikrig, E., Schoen, R. T., Nowakowski, J., Schmid, C. H., Laukamp, S., Buscarino, C., Krause, D. S., and Group, T. L. D. V. S. (1998). Vaccination against Lyme disease with recombinant Borrelia burgdorferi outer-surface lipoprotein A with adjuvant. *The New England Journal of Medicine*, pages 209–215.

[207] Steinman, L. (2007). A brief history of T(H)17, the first major revision in the T(H)1/T(H)2 hypothesis of T cell-mediated tissue damage. *Nature Medicine*, 13(2):139–45.

[208] Storn, R. and Price, K. (1997). Differential evolution–a simple and efficient heuristic for global optimization over continuous spaces. *J. Global Optim.*, pages 341–359.

[209] Straubinger, R. K. (2000). PCR-Based quantification of Borrelia burgdorferi organisms in canine tissues over a 500-Day postinfection period. *Journal of Clinical Microbiology*, 38(6):2191–9.

[210] Sumiyoshi, K., Nakao, A., Setoguchi, Y., Tsuboi, R., Okumura, K., and Ogawa, H. (2003). TGF-beta/Smad signaling inhibits IFN-gamma and TNF-alpha-induced TARC (CCL17) production in HaCaT cells. *Journal of Dermatological Science*, 31(1):53–8.

[211] Szretter, K. J., Gangappa, S., Lu, X., Smith, C., Shieh, W.-J., Zaki, S. R., Sambhara, S., Tumpey, T. M., and Katz, J. M. (2007). Role of host cytokine responses in the pathogenesis of avian H5N1 influenza viruses in mice. *Journal of Virology*, 81(6):2736–44.

[212] Taga, K. and Tosato, G. (1992). IL-10 inhibits human T cell proliferation and IL-2 production. *Journal of immunology (Baltimore, Md. : 1950)*, 148(4):1143–8.

[213] te Velde, a. a., Huijbens, R. J., Heije, K., de Vries, J. E., and Figdor, C. G. (1990). Interleukin-4 (IL-4) inhibits secretion of IL-1 beta, tumor necrosis factor alpha, and IL-6 by human monocytes. *Blood*, 76(7):1392–7.

[214] Thompson, W., Shay, D., Weintraub, E., Brammer, L., Cox, N., Anderson, L. J., and Fukuda, K. (2003). Mortality associated with influenza and respiratory syncytial virus in the United States. *The Journal of the American Medical Association*, 289(2):179–186.

[215] Tilly, K., Krum, J. G., Bestor, A., Jewett, M. W., Grimm, D., Bueschel, D., Byram, R., Dorward, D., Vanraden, M. J., Stewart, P., and Rosa, P. (2006). Borrelia burgdorferi OspC protein required exclusively in a crucial early stage of mammalian infection. *Infection and Immunity*, 74(6):3554–64.

[216] Tilly, K., Rosa, P. A., and Stewart, P. E. (2008). Biology of Infection with Borrelia burgdorferi. *Infect. Dis. Clin. North Am.*, 22(2):217–234.

[217] Toapanta, F. R. and Ross, T. M. (2009). Impaired immune responses in the lungs of aged mice following influenza infection. *Respiratory Research*, 10:112.

[218] Toh, M.-L., Kawashima, M., Zrioual, S., Hot, A., Miossec, P., and Miossec, P. (2009). IL-17 inhibits human Th1 differentiation through IL-12R beta 2 downregulation. *Cytokine*, 48(3):226–30.

[219] Tokuda, H., Kanno, Y., Ishisaki, A., Takenaka, M., Harada, A., and Kozawa, O. (2004). Interleukin (IL)-17 enhances tumor necrosis factor-alpha-stimulated IL-6 synthesis via p38 mitogen-activated protein kinase in osteoblasts. *Journal of Cellular Biochemistry*, 91(5):1053–61.

[220] Trindade, M. C., Lind, M., Nakashima, Y., Sun, D., Goodman, S. B., Schurman, D. J., and Smith, R. L. (2001). Interleukin-10 inhibits polymethylmethacrylate particle induced interleukin-6 and tumor necrosis factor-alpha release by human monocyte/macrophages in vitro. *Biomaterials*, 22(15):2067–73.

[221] Tsao, J. I. (2009). Reviewing molecular adaptations of Lyme borreliosis spirochetes in the context of reproductive fitness in natural transmission cycles. *Veterinary Research*, 40(2):36.

[222] Ulloa, L., Doody, J., and Massagué, J. (1999). Inhibition of transforming growth factor-beta/SMAD signalling by the interferon-gamma/STAT pathway. *Nature*, 397(6721):710–3.

[223] Ulmer, J. B., Fu, T.-m., Deck, R. R., Guan, L., Dewitt, C., Liu, X., Wang, S., Liu, M. A., Donnelly, J. J., Caulfield, M. J., Friedman, A., Witt, C. D. E., Liu, X. U., and Wang, S. U. (1998). Protective CD4+ and CD8+ T cells against influenza virus induced by vaccination with nucleoprotein DNA. *Journal of Virology*, 72(7):5647–5653.

[224] van Furth, R. and Diesselhoff-den Dulk, M. (1970). The kinetics of promonocytes and monocytes in the bone marrow. *J. Exp. Med.*, 132(4):813.

[225] Vila-del Sol, V., Punzon, C., and Fresno, M. (2008). IFN-gamma-Induced TNF-alpha Expression Is Regulated by Interferon Regulatory Factors 1 and 8 in Mouse Macrophages. *The Journal of Immunology*, 181(7):4461–4470.

[226] Volterra, V. (1931). Variations and fluctuations of the number of individuals in animal species living together [Translation by R. Chapman]. In *Animal Ecology*. McGraw-Hill, New York.

[227] Wang, X., Li, M., Zheng, H., Muster, T., Palese, P., Beg, A. A., and Garcia-Sastre, A. (2000). Influenza A virus NS1 protein prevents activation of NF-κB and induction of alpha/beta interferon. *Journal of Virology*, 74(24):11566–11573.

[228] Weinberg, W. (1909). Über Vererbungsgesetze beim Menschen. *Zeitschrift für Induktive Abstammungs- und Vererbungslehre*, 2(1):276–330.

[229] Weis, J. J. and Bockenstedt, L. K. (2010). Host response. In *Borrelia: molecular biology, host interaction and pathogenesis*, pages 413–442. Caister Academic Press, Norfolk.

[230] Weiss, I. D., Wald, O., Wald, H., Beider, K., Abraham, M., Galun, E., Nagler, A., and Peled, A. (2010). IFN-gamma treatment at early stages of influenza virus infection protects mice from death in a NK cell-dependent manner. *Journal of Interferon and Cytokine Research*, 30(6):439–49.

[231] Wickham, H. (2009). *ggplot2: elegant graphics for data analysis*. Springer New York.

[232] Wormser, G. (2006a). Early Lyme disease. *New England Journal of Medicine*, pages 2794–2801.

[233] Wormser, G. P. (2006b). Hematogenous dissemination in early Lyme disease. *Wiener Klinische Wochenschrift*, 118(21-22):634–7.

[234] Xu, Y., Kodner, C., Coleman, L., and Johnson, R. C. (1996). Correlation of plasmids with infectivity of Borrelia burgdorferi sensu stricto type strain B31. *Infection and immunity*, 64(9).

[235] Yang, X., Goldberg, M. S., Popova, T. G., Schoeler, G. B., Wikel, S. K., Hagman, K. E., and Norgard, M. V. (2000). Interdependence of environmental factors influencing reciprocal patterns of gene expression in virulent Borrelia burgdorferi. *Molecular Microbiology*, 37(6):1470–9.

[236] Yang, X. F., Alani, S. M., and Norgard, M. V. (2003). The response regulator Rrp2 is essential for the expression of major membrane lipoproteins in Borrelia burgdorferi. *Proceedings of the National Academy of Sciences of the United States of America*, 100(19):11001–6.

[237] Yarilina, A. and Ivashkiv, L. (2010). Type I interferon: a new player in TNF signaling. *Current Directions in Autoimmunity*, 11:94–104.

[238] Yarilina, A., Park-Min, K.-H., Antoniv, T., Hu, X., and Ivashkiv, L. B. (2008). TNF activates an IRF1-dependent autocrine loop leading to sustained expression of chemokines and STAT1-dependent type I interferon-response genes. *Nature Immunology*, 9(4):378–87.

[239] Zhang, J., Bardos, T., Shao, Q., Tschopp, J., Mikecz, K., Glant, T. T., and Finnegan, a. (2003). IL-4 Potentiates Activated T Cell Apoptosis Via an IL-2-Dependent Mechanism. *The Journal of Immunology*, 170(7):3495–3503.

[240] Zhang, J.-R., Hardham, J. M., Barbour, A. G., and Norris, S. J. (1997). Antigenic variation in Lyme disease borreliae by promiscuous recombination of VMP-like sequence cassettes. *Cell*, 89(2):275–85.

[241] Zhang, J.-R. and Norris, S. J. (1998). Genetic variation of the Borrelia burgdorferi gene vlsE involves cassette-specific, segmental gene conversion. *Infection and Immunity*, 66(8):3698–704.

Acronyms

RMS root of the mean squared residuals in logarithmic space. 21

SSE sum of squared errors. 7

T_h1 cell type 1 T helper cell. 40, 55

T_h2 cell type 2 T helper cell. 40

dbpA *decorin binding protein A*. 16

ospA *outer surface protein A*. 16

ospC *outer surface protein C*. 16

c-di-GMP cyclic di-GMP. 16

cDC conventional dendritic cell. 38, 39

CTL cytotoxic $CD8^+$ T cell. 39–41, 55

DE Differential Evolution. 10, 24, 31, 48, 49, 51, 53, 54, 57

HA Haemagglutinin. 38, 39

Hk1 histidin kinase 1. 16, 84

IFN-α interferon α. 39, 40

IFN-β interferon β. 39, 40, 57–59

IFN-γ interferon γ. 40, 41, 55–59

IL-1β interleukin 1β. 40, 55

IL-10 interleukin 10. 17, 41, 56, 57

IL-12 interleukin 12. 41

IL-18 interleukin 18. 41

IL-2 interleukin 2. 41

IL-21 interleukin 21. 41

IL-4 interleukin 4. 40

IL-6 interleukin 6. 40, 41

ISG interferon-stimulated gene. 39

mRNA messenger RNA. 38

NA Neuraminidase. 38, 39

NK natural killer cell. 39–41, 55, 56

NLR NOD-like receptor. 38

ODE ordinary differential equation. 2, 5, 6, 9, 21, 26, 34, 47–49

OspA outer surface protein A. 18, 19, 28, 33

OspC outer surface protein C. 16–18, 28, 33, 35

p.i. post infection. 20, 21, 24, 26, 30, 31, 33, 42

PCR polymerase chain reaction. 20, 84

pDC plasmacytoid dendritic cell. 38, 39

PRR pathogen recognition receptor. 39

qPCR quantitative PCR. 20

RIG-I retinoic acid-inducible gene I. 38, 39

RpoN alternative RNA polymerase σ-factor RpoN. 16

RpoS alternative RNA polymerase σ-factor RpoS. 16

Rrp1 Hk1-response regulatory protein 1. 16

Rrp2 Hk1-response regulatory protein 2. 16

s.l. sensu lato. 14

s.s. sensu stricto. 13, 14, 18, 19

ssRNA single-stranded RNA. 38

T_{reg} regulatory T cell. 41

TLR toll-like receptor. 17, 18, 38, 39

TNF tumour necrosis factor. 39, 40, 55–59, 64

A

Parameter sets

A.1 The immune response in early Lyme disease

A.1.1 Model 1: A Three-compartment Model including Bacterial Migration

Parameter	Unit	Value	Derived from	Description
β	h^{-1}	0.06	[9]	Bacterial Growth rate
K	cells	$1.5 \cdot 10^6$	[156]	Bacterial carrying capacity
ρ_t	$(\text{cells} \cdot \text{cells})^{-1}$	0.00086	Fitted	Phagocytosis rate
μ_1	h^{-1}	3.47	Fitted	Bacterial migration rate infection site $\rightarrow$ blood
μ_2	h^{-1}	0.112	Fitted	Bacterial migration rate non-infection site $\rightarrow$ blood
ν_1	h^{-1}	0.242	Fitted	Bacterial migration rate blood $\rightarrow$ infection site
ν_2	h^{-1}	7.56	Fitted	Bacterial migration rate blood $\rightarrow$ non-infection site
ϕ	h^{-1}	0.0372	Fitted	Physiological phagocyte recruitment rate
ψ	$(\text{cells}\ \ \mathsf{h})^{-1}$	0.007	Fitted	Infection dependent phagocyte recruitment rate
δ	$\text{cells}\,\mathsf{h}^{-1}$	75.9	Fitted	Physiological phagocyte production rate
σ	$\text{cells}\,\mathsf{h}^{-1}$	507	Fitted	Infection dependent physiological production rate
C_ψ	cells	$9.023 \cdot 10^4$	Fitted	Bacterial concentration at half-maximal phagocyte recruitment
C_σ	cells	$x.786 \cdot 10^4$	Fitted	Bacterial concentration at half-maximal phagocyte production
θ	h^{-1}	0.0076	[224]	Death rate of phagocytic cells

A.1.2 Model 2: A Single Compartment With Limited Phagocytic Capacity

Parameter	Unit	Value	Derived from	Description
β	h^{-1}	0.06	[9]	Bacterial Growth rate
K	cells	$1.5 \cdot 10^6$	[156]	Bacterial carrying capacity
ρ	$(\text{cells h})^{-1}$	$5 \cdot 10^{-5}$	Fitted	Phagocytosis rate
ϕ	$\text{cells}\,\mathsf{h}^{-1}$	10^{-3}	Fitted	Physiological phagocyte migration to the tissue
ψ	h^{-1}	10^{-5}	Fitted	Infection dependent phagocyte recruitment rate
C	cells	5000	Fitted	Bacterial concentration at half-maximal phagocyte recruitment
λ	$(textcells)^{-1}$	10^{-3}	Fitted	rate of phagocyte transition active $\rightarrow$ inactive state
κ	h^{-1}	2.1	Fitted	rate of phagocyte transition inactive $\rightarrow$ active state

A.1.3 Model 3: Modelling Bacterial Adaptations

Parameter	Unit	Value	Derived from	Description
β	h^{-1}	0.06	[9]	Bacterial Growth rate
K	cells	$1.5 \cdot 10^6$	[156]	Bacterial carrying capacity
α	h^{-1}	0.000439	Fitted	Bacterial adaptation rate
ρ	$(\text{cells h})^{-1}$	0.007	Fitted	Phagocytosis rate
Δt	h	72	[12]	Delay until onset of antibody production
$t_{1/2}$	h	93.454	[12]	Time to half-maximal antibody concentration
n	–	4.66	[12]	Hill coefficient of antibody function
μ	h^{-1}	0.0726	Fitted	Antibody binding rate (note that antibody concentration is given in arbitrary units)
ν	h^{-1}	1.153	Fitted	Antibody dissociation rate
ϕ	$\text{cells}\,\mathsf{h}^{-1}$	0.0647	Fitted	Physiological phagocyte migration to the tissue
ψ	h^{-1}	0.0007	Fitted	Infection dependent phagocyte recruitment rate
C	cells	601.3	Fitted	Bacterial concentration at half-maximal phagocyte recruitment
θ	h^{-1}	0.0076	[224]	Death rate of phagocytic cells

A.2 Immune response and Regulation in Influenza Infections

Parameter	Unit	Value	Derived from	Description
K_{TB}		4.664	Fitted	Half-maximal concentration for sigmoidal
K_{TI}		5.702	Fitted	Half-maximal concentration for sigmoidal
K_{TG}		6.663	Fitted	Half-maximal concentration for sigmoidal
K_{BT}		18.61	Fitted	Half-maximal concentration for sigmoidal
K_{IT}		2.929	Fitted	Half-maximal concentration for sigmoidal
K_{IB}		3.363	Fitted	Half-maximal concentration for sigmoidal
K_{IG}		2.253	Fitted	Half-maximal concentration for sigmoidal
K_{GT}		16.84	Fitted	Half-maximal concentration for sigmoidal
K_{GI}		23.24	Fitted	Half-maximal concentration for sigmoidal
K_{VT}		$1.991 \cdot 10^4$	Fitted	Half-maximal concentration for sigmoidal
K_{VB}		$1.519 \cdot 10^4$	Fitted	Half-maximal concentration for sigmoidal
K_{VG}		$1.772 \cdot 10^4$	Fitted	Half-maximal concentration for sigmoidal
δ_T	h^{-1}	0.02134	Fitted	Antiviral effect of
δ_B		3.222	Fitted	Antiviral effect of
δ_G	h^{-1}	0.001544	Fitted	Antiviral effect of
γ_T	h^{-1}	0.08778	Fitted	Degradation rate
γ_B	h^{-1}	0.03685	Fitted	Degradation rate
γ_I	h^{-1}	0.8782	Fitted	Degradation rate
γ_G	h^{-1}	0.04265	Fitted	Degradation rate
n_{TB}		2.261	Fitted	Hill coefficient for sigmoidal
n_{TI}		1.329	Fitted	Hill coefficient for sigmoidal
n_{TG}		3.971	Fitted	Hill coefficient for sigmoidal
n_{BT}		1.236	Fitted	Hill coefficient for sigmoidal
n_{IT}		4.666	Fitted	Hill coefficient for sigmoidal
n_{IB}		3.282	Fitted	Hill coefficient for sigmoidal
n_{IG}		2.144	Fitted	Hill coefficient for sigmoidal
n_{GT}		4.762	Fitted	Hill coefficient for sigmoidal
n_{GI}		3.795	Fitted	Hill coefficient for sigmoidal
n_{VT}		1.373	Fitted	Hill coefficient for sigmoidal
n_{VB}		2.045	Fitted	Hill coefficient for sigmoidal
n_{VG}		3.346	Fitted	Hill coefficient for sigmoidal
q_{TB}		1.443	Fitted	Maximum effect of sigmoidal
q_{TI}		1.139	Fitted	Maximum effect of sigmoidal
q_{TG}		47.4	Fitted	Maximum effect of sigmoidal
q_{BT}		2.037	Fitted	Maximum effect of sigmoidal
q_{IT}		0.8768	Fitted	Maximum effect of sigmoidal
q_{IB}		0.4818	Fitted	Maximum effect of sigmoidal
q_{IG}		0.8328	Fitted	Maximum effect of sigmoidal
q_{GT}		7.214	Fitted	Maximum effect of sigmoidal
q_{GI}		3.727	Fitted	Maximum effect of sigmoidal
q_{VT}		6.942	Fitted	Maximum effect of sigmoidal
q_{VB}		42.18	Fitted	Maximum effect of sigmoidal
q_{VG}		1.109	Fitted	Maximum effect of sigmoidal
K	$\mathsf{FFU\,mL}^{-1}$	28000000	Fitted	carrying capacity
r	0.1319	h^{-1}	Fitted	replication rate

B

Software and libraries

B.1 Numerical integration of the Ordinary Differential Equations

For numerical integration in the Borreliosis Models, the deSolve package for R was used [197; v. 1.10-8].

The model used in development and testing of the iterative fitting strategy was implemented and solved in C++ using a 5th order Dormand-Prince method. Since datahandling and plotting was performed in R, the Rcpp package [50] was used to provide an interface of the compiled code as an R library.

The models for the cytokine network were implemented in Python using PyDSTool [35], which provides a convenient wrapper around using integrators and models in C.

B.2 Differential evolution algorithm

The Differential Evolution algorithm was applied with the Parameters $CR = 0.5$ and $F = 0.8$ and the DE/local-to-best/1/bin strategy, unless stated otherwise. Population size was chosen as $N_P = D$, where D is the dimensionality of the optimisation problem. Except for the evaluation of new parameter estimation strategy, the algorithm was terminated if it failed to improve the value more than machine precision for more than 200 generations.

For the evaluation of the novel parameter estimation strategy, the DEoptim [142] package was used. In all other cases, an own implementation in Python was used for reasons of flexibility and performance. The code can be made available to anyone upon request to the e-mail address sb@theoretical-biology.de; a class reference can be found in the appendix.

B.3 Figures

All plots were created using either ggplot2 in R [231] or Matplotlib in Python [88].

C

Python source code documentation

Class Reference for the Python source code used in the iterative fitting procedure. Code is available upon request from Sebastian Binder <sb@theoretical-biology.de>.

C.1 ODEModels.py

A module providing classes for integrating ordinary differential equations. It makes use of PyDSTool and provides a high-level wrapper around its functionality as well as convenient functions for handling and plotting of full ODE models and some sanity checks.

class `ODEModels.ODEModel`(*modelname*, *RHS*, *pardomain*, *tdomain*, *aux={}*, *data={}*, *integrator=<class 'PyDSTool.Generator.Dopri_ODEsystem.Dopri_ODEsystem'>*, *external={}*, *tunits='h'*, *yunits=None*)

Base class for all ODE models. This makes use of PyDSTool, which is capable of generating highly efficient C code from a model specification in Python.

`__init__`(*modelname*, *RHS*, *pardomain*, *tdomain*, *aux={}*, *data={}*, *integrator=<class 'PyDSTool.Generator.Dopri_ODEsystem.Dopri_ODEsystem'>*, *external={}*, *tunits='h'*, *yunits=None*)

Constructor

Parameters

- **RHS** (*dict.*) – Right hand sides of the ODE system.
- **modelname** (*str.*) – Model identifier
- **pardomain** (`Pardomain`) – bounds for model parameters and initial conditions
- **tdomain** (*list*) – time interval [t_min, t_max]
- **aux** (*dict.*) – auxilliary functions {"fn_name": ([par1, par2, ..., par_n], "function spec")}
- **data** (*dict.*) – experimental data
- **integrator** (*str.*) – integration routine to use. Defaults to a C implementation of a 8th order Dormand-Prince method. Choose Radau_ODEsystem for stiff systems. The The Vode_ODEsystem type does not depend on externally compiled code and can be used in case of problems with compiling. It's (obviously) less performant, but still a lot faster than Matlab (~factor 30).
- **external** (*dict.*) – external inputs to the model. Dictionary key is the state variable, value is a list [timevector, datavector]
- **tunits** (*str.*) – time measurement unit
- **yunits** (*dict.*) – variables measurement unit {"variable_name":"yunits"}

Returns `ODEModel`

`__weakref__`

list of weak references to the object (if defined)

`_check_pardomain(`*pars*`)`
Ensure that parameters lie within bounds, raise Exception if not.

Parameters **pars** (*dict.*) – model parameters

`_check_pars_present(`*pars*`)`
Check whether all required model parameters and all initial conditions are given. Should only be called /after/ computing automatically calculated parameters.

Parameters **pars** (*dict.*) – model parameters. Initial conditions have to be specified as parameters with naming scheme – state variable name suffixed by "0".

`_get_external(`*inputspec*`)`
Create interpolation functions from a dictionary with data. These interpolation functions are required to use data as input in PyDSTool directly. Caveat: PyDSTool only understands linear interpolation. If you require smooth functions, *don't do this*. For most problems, sufficiently dense sampling of a smooth function to create points usable as inputs here will do no harm, though.

Parameters **inputspec** (*dict.*) – data to use as input. Format: {"state_variable":[[t_0,t_1,...,t_n],[y_0, y_1, ..., y_n]]}

Returns dict. – input specification for DSTool

`_get_plot_grid()`
Get a dictionary with a timegrid where output for model plots should be produced. Produces 10000 evenly distributed timepoints in the interval self.tdomain.

Returns dict. – model output time grid

`_get_subplots()`
Get Matplotlib Figure and subplots arranged in a grid with max. 3 rows for plotting all state variables.

Returns `Figure`,list of `Axes`

`_ics_from_pars(`*pars*`)`
Get a dictionary with initial values from a Parameters instance.

Parameters **pars** (*dict.*) – model parameters

Returns dict. – initial conditions

`_plot_data(`*ax*, *variable*, *error_estimate*`)`
Add data points to a given subplot. If n > 1, add error bars.

Parameters

- **ax** (`Axes`) – subplot with model output
- **variable** (*str.*) – variable name
- **error_estimate** (*str.*) – "SD"|"SE", which error estimate to use for error bars.

`_set_plot_labels(`*ax*, *variable*`)`
Add title, x label and y label to a given subplot.

Parameters

- **ax** (`Axes`) – subplot to label
- **variable** (*str.*) – name of the state variable plotted in ax

`_strip_ics(`*pars*`)`
Get a dictionary without the initial condition specifications from a Parameters instance. Complementary to _ics_from_pars.

Parameters **pars** (*dict.*) – model parameters

Returns dict. – model parameters without initial conditions

`compute`(*pars*)
Compute a trajectory with given model parameters.

Parameters **pars** (*dict.*) – model parameters. Initial conditions have to be specified as parameters with naming scheme – state variable name suffixed by "0".

Returns `Trajectory` – model trajectory

`get_plot`(*pars*, *error_estimate='SD'*, *subplots=False*)
Produce a plot with the model output given model parameters pars. If available, add data points and, if n >1, error bars for data.

Parameters

- **pars** (*dict.*) – model parameters
- **error_estimate** (*str.*) – "SD"|"SE", which error estimate to use for error bars.
- **subplots** (*bool*) – Combine plots for all variables in one figure with multiple subplots.

Returns list of `Figure` objects

`out`(*pars*, *times*)
Return model output at given timepoints

Parameters

- **pars** (*dict.*) – model parameters. Initial conditions have to be specified as parameters with naming scheme – state variable name suffixed by "0".
- **times** (*dict.*) – timepoints at which the model should be evaluated for each state variable: {"state_variable":[t_0, t_1, ..., t_n]}. Different time points may be specified for each variable (useful for instance for calculating residuals with given data...)

Returns dict. – model output, {"state_variable":[array([t_0,t_1,...,t_n]),array([y_0,y_1,...,y_n])]}

`set_autopars`(*pars*)
Automatic calculation of parameters that depend on other parameters. Implement in overriding classes. Calculated parameters are checked against self.pardomain before computation!

Parameters **pars** (*dict.*) – model parameters

Returns dict. updated model parameters

C.2 CytokineModels.py

Model implementation for the cytokine response network and individual models for each single variable. These models are autogenerated at import time from the file "modelspec.yaml" in the source directory which contains specifications of all models including a description string __modelname__, the right-hand sides __RHS__ and the parameter bounds __pardomain__.

class `CytokineModels.CytokineModelBase`(*external*, *RHS=None*, *pardomain=None*)
Base class for the whole model. Holds data and functions to build an ODE integrator in C++ using PyDSTool. Derived classes should contain parameter limits, initial conditions and RHS.

`__init__`(*external*, *RHS=None*, *pardomain=None*)
Constructor

Parameters

- **external** (*dict.*) – external inputs to the model. Dictionary key is the state variable, value is a list [timevector, datavector]
- **RHS** (*dict.*) – Right hand sides of the ODE system. If not set, RHS are assumed to be stored in the class attribute __RHS__, useful for subclassing.
- **pardomain** (`Pardomain`) – bounds for model parameters and initial conditions. If not set, parameter bounds are assumed to be stored in self.__pardomain__, useful for subclassing.

Returns CytokineModelBase

_extract_data(*data*)
Read data from Data instance.

Returns dict. – model data

classmethod _get_pardomain()
Create Pardomain with model parameters from dictionary self.__pardomain__.

Returns Pardomain – model parameters

auxilliary()
Get dictionary with auxilliary functions. Inheriting classes can override this to set other auxilliary functions.

Returns dict. – auxilliary functions, format: {'function_name':[[p1,p2,...,pn],"function_spec"}

longname2var(*longname*)
Convenience function: Translate human readable (long) name to variable name.

Parameters **longname** (*str.*) – long variable description

Returns str. – short variable name

var2longname(*var*)
Convenience function: Translate variable name to human readable (long) name.

Parameters **var** (*str.*) – Short variable name

Returns str. – long variable description

CytokineModels.generate_models()
Generates subclasses of CytokineModelBase with models for all systems specified in modelspec.yaml and one model called CompleteSystem that combines all of these. The idea is that each model specified in modelspec.yaml contains a model for one state variable only. This facilitates the iterative strategy out- lined in Binder, Hernandez-Vargas and Meyer-Hermann (2014).

Note Doing this at import time for convenience reasons. Keep in mind that this creates classes according to an external file (modelspec.yaml)!

C.3 Parameters.py

class Parameters.Parameters
Holds a parameter set. Subclass of NumPy array with some convenience functions.

__array_finalize__(*obj*)
Internally used, see "Subclassing NDArray" in Numpy docs for details.

__eq__(*obj*)
Compare two Parameters objects, return True if all parameters are equal.

Returns bool

__getitem__(*key*)
parameters_instance[i] and parameters_instance["parname"] return the value for the parameter named "parname" or the parameter at index i, respectively.

Parameters **key** (*str. or int.*) – positional or string index for parameter

Returns float – parameter value

__ne__(*obj*)
Inverse of __eq__()

Returns bool

static `__new__`(*input_array*, *parnames*)
Constructor method, called before __init__.

Parameters
- **input_array** (*iterable*) – iterable that can be converted to array, e.g. list or numpy array
- **parnames** (list of `str`) – parameter names

Returns `Parameters`

`__reduce__`()
Internally used, see "Subclassing NDArray" in Numpy docs for details.

`__setstate__`(*state*)
Internally used, see "Subclassing NDArray" in Numpy docs for details.

classmethod `from_dict`(*dic*, *parnames*)
Construct Parameters instance from dictionary.

Parameters
- **dic** (`dict`) – Dictionary with {"parameter_name": parameter_value}
- **parnames** – Iterable with parameter names. Has to be set to put the

parameters in the right order, since dictionaries are unordered. :type parnames: `str`. :returns: `Parameters`

`iteritems`()
Iterate over parameter names and values, similar to `dict.iteritems()`

Returns `listiterator`

`iterkeys`()
Iterate over parameter names, similar to `dict.keys()`

Returns `listiterator`

`itervalues`()
Iterate over parameter values, similar to `dict.values()`

Returns `listiterator`

`to_dict`()
Get a dictionary representation for parameter set.

Returns `dict`

Note This loses the order of the parameters!

class `Parameters.Pardomain`(*lower*, *upper*, *parnames*, *PRNG*, *atbounds='reinitialize'*, *resampler=None*)
Holds and enforces valid parameter ranges. Instances are callable: pardomain_instance(pars) returns a parameter object with enforced constraints (self.lower[i] < pars[i] < self.upper[i]). If one of the parameters exceeds its limit, it is projected into the valid interval according to the "atbounds" argument (see http://elektron.elka.pw.edu.pl/~jarabas/ALHE/krakow1.pdf for some suggestions about handling boundaries); Kenneth Price suggests reinitialization, i.e. choosing a parameter from the valid interval at random according to a uniform distribution.

`__call__`(*pnew*)
Modifies a Parameters instance to enforce bounds.

Parameters **pnew** (`Parameters`) – parameters for which bounds should be enforced

Note Modifies the array in place!

`__getitem__`(*key*)
pardomain_instance[i] and pardomain_instance["parname"] return bounds for the parameter named "parname" or the parameter at index i, respectively.

Parameters **key** (*str. or int.*) – positional or string index for parameter

Returns list of `int`: [lower, upper]

`__init__`(*lower*, *upper*, *parnames*, *PRNG*, *atbounds='reinitialize'*, *resampler=None*)

Returns a Pardomain instance.

Parameters

- **lower** (*list of float.*) – List of lower bound values
- **upper** (*list of float.*) – List of upper bound values
- **parnames** (*list of str.*) – List of parameter names corresponding to lower and upper
- **PRNG** (`random.Random`) – Pseudo-random number generator, has to implement a uniform(lower,upper) method.
- **atbounds** (*str.*) – How to handle parameters outside the defined bounds.

resample	Mutate parameter set until the result lies within bounds. Requires self.resampler to be set to the mutation method to be used!
reinitialize	Choose parameter from a uniform probability distribution in interval `[lower[i], upper[i]]`.

- **resampler** (`func`) – Mutation function to resample the parameter set if atbounds == "resample". No effect otherwise.

Returns `Pardomain`

Note resampling is not yet implemented.

`__str__`()

String representation

Returns `str`.

`__weakref__`

list of weak references to the object (if defined)

`get_random_pars`()

Returns a Parameters instance with randomly chosen parameters (uniform prob.).

Returns `Parameters`, random parameters

`get_violations`(*pnew*)

Convenience function, returns a list "violations" of booleans, where violations[i]==True means that the parameter at index i exceeds one of the bounds.

Returns list of `bool`, parameters out of bounds

`to_dict`()

Get a dictionary representation of the parameter boundaries.

Returns dict., parameter boundaries

Note loses ordering of the parameters!

C.4 datahandling.py

class `datahandling.Data`(*transform=<function <lambda> at 0x7f7532641410>, inv_transform=<function <lambda> at 0x7f7532641410>, scale_time=<function <lambda> at 0x7f7532641410>, tdomain=[-inf, inf]*)

Class for reading, providing convenient access and interpolation of data read from a CSV file. The

CSV has to use TAB as a separator and "" as quotation character (if any). Data are assumed to be in long format, e.g.

Variable	Time	Value
x	0	0
x	1	1
x	2	4
x	3	9
y	0	0
y	1	2
y	2	4
y	3	6
...	...	...

`__init__`(*transform=<function <lambda> at 0x7f7532641410>, inv_transform=<function <lambda> at 0x7f7532641410>, scale_time=<function <lambda> at 0x7f7532641410>, tdomain=[-inf, inf]*)

Constructor

Parameters

- **transform** (`func`) – transformation to apply to the dependent variable when reading in data
- **inv_transform** (`func`) – inverse function for transform
- **scale_time** (`func`) – transformation to apply to the independent variable when reading in data
- **tdomain** (list of `float`) – restrict data to this interval of the *independent* variable

Returns `Data`

`__weakref__`

list of weak references to the object (if defined)

`_compute_summary`(*var*, *timeseries*)

Computes a summary for a variable from a measurement series with replicates allowed. If possible, mean, standard deviation and standard error are calculated for each data point.

Parameters

- **var** (`str`) – Variable name
- **timeseries** (list of `numpy.ndarray`) – measurement series, [independent_vector, dependent_vector]

Returns nested `dict` with summary for each variable (variable name as key), format:

Variable name		
Time	`numpy.ndarray`	Independent variable values
Mean	`numpy.ndarray`	Mean dependent variable values
SD	`numpy.ndarray`	Standard deviations of dependent variable
SE	`numpy.ndarray`	Standard errors of dependent variable
raw	2D `numpy.ndarray`	Single values of dependent variable for each point

`cubic_interpolation`(*var*, *fill_value=1.0*)

Get a cubic spline interpolation function for the data

Parameters

- **var** (`str`) – variable name for which the interpolating function should be retrieved
- **fill_value** (`float`) – which value to use if requested value does not lie within the data bounds

`linear_interpolation`(*var*, *fill_value=1.0*)
Get a linear interpolation function for the data

Parameters
- **var** (`str`) – variable name for which the interpolating function should be retrieved
- **fill_value** (`float`) – which value to use if requested value does not lie within the data bounds

`pchip`(*var*)
Get a piecewise cubic hermite spline, similar to Matlab's *pchip*.

Parameters **var** (`str`) – variable name for which the interpolating function should be retrieved

`quadratic_interpolation`(*var*, *fill_value=1.0*)
Get a quadratic spline interpolation function for the data

Parameters
- **var** (`str`) – variable name for which the interpolating function should be retrieved
- **fill_value** (`float`) – which value to use if requested value does not lie within the data bounds

`read`(*filename*, *idvar*, *independent*, *dependent*)
Read data from CSV file in the specified path (see above for format) and create a summary.

Parameters
- **filename** (`str`) – Path to the data file
- **idvar** (`str`) – Field name containing the identifier for a dependent variable, *Variable* in the above example
- **independent** (`str`) – Field name containing the independent variable, *Time* in the above example
- **dependent** (`str`) – Field name containing the dependent variable, *Value* in the above example

C.5 DEfit.py

Classes for Differential Evolution minimisation of arbitrary objective functions. The Differential Evolution routine as proposed by Storn and Price in their influential paper can be applied to a large variety of different optimization problems that typically involve the minimization of an objective function. It is particularly suitable for numerical optimization problems such as estimating parameters of a dynamic model by fitting to data. The model itself can be treated as a black box.

class `DEfit.DEControl`(*freepars*, *NP=0*, *CR=0.5*, *F=0.8*, *itermax=1000*, *abs_delta=2.2204460492503131e-16*, *rel_delta=2.2204460492503131e-16*, *delta_gen=100*, *strategy='DE/rand/1/bin'*, *seed=1444306994*, *parallel=4*, ***kw*)
Class for storing parameters for Differential Evolution algorithm. The purpose is mainly encapsulation of DE parameters and calculation of some automatically set parameters.

`__init__`(*freepars*, *NP=0*, *CR=0.5*, *F=0.8*, *itermax=1000*, *abs_delta=2.2204460492503131e-16*, *rel_delta=2.2204460492503131e-16*, *delta_gen=100*, *strategy='DE/rand/1/bin'*, *seed=1444306994*, *parallel=4*, ***kw*)
Constructor

Parameters
- **freepars** (*list of str.*) – Names of parameters to fit

- **NP** (*int*) – Number of individuals in population
- **CR** (*float*) – Crossover probability
- **F** (*float*) – Mutation strength
- **itermax** (*int*) – Terminate after a maximum of itermax generations
- **abs_delta** (*float*) – Terminate if no improvement by this absolute value in delta_gen generations
- **rel_delta** (*float*) – Terminate if no improvement by this factor in delta_gen generations
- **delta_gen** (*int*) – Check improvement criteria for termination after delta_gen generations
- **strategy** (*str.*) – Which DE strategy to use Strategy to use for DE optimisation. Currently, 2 strategies are implemented: - "DE/local-to-best/1/bin":
  classical DE strategy, but mutation function changed to

$$v_{i,g} = old_{i,g} + (best_g - old_{i,g}) + x_{r_0,g} + F \cdot (x_{r_1,g} - x_{r_2,g})$$

  – "DE/rand/1/bin": classical DE strategy,

$$v_{i,g} = x_{r_0,g} + F \cdot (x_{r_1,g} - x_{r_2,g})$$

- **parallel** (*int*) – number of threads to use

Returns `DEControl`

class `DEfit.DEFit`(*control*, *cost*, *pardomain*, ***kw*)

Implements the actual DEFit algorithm, provides methods for iterating over generations, an observer method, checking of termination criteria and a fit method returning a DEFitResult object.

`__init__`(*control*, *cost*, *pardomain*, ***kw*)

Constructor

Parameters

- **control** (`DEControl`) – DE algorithm parameters
- **cost** (`ObjectiveFunction`) – Objective function to be minimized
- **pardomain** (`Pardomain`) – Fit parameters within this range

Returns `DEFit`

`_checkimprovement()`

Test whether the best candidate in the current generation is significantly better than the best candidate in the last generation, required improvement can be either absolute (abs_delta) or relative (rel_delta). If an improvement is detected, an internal counter is reset to zero. Otherwise, the counter is incremented.

`_do_generation()`

Combine all steps for creating the next generation:

- Generate a new trial population
- Call observer function to notify the user of our progress
- Check for termination criteria
- Increment generation counter
- Store best candidate solution

`_observe()`

Log progress. Logs the cost function values for the whole generation with priority debug and the current best candidate with priority info. See the `Loggable` class for more information on logging priorities and how to restrict messages to a particular log level.

`_terminate()`
Test whether any of the termination criteria are met, either no improvement over the last delta_gen generations or itermax generations reached. If any termination criteria are met, set the internal state terminated to `True`

`fit()`
Main entry point for user interaction. Calling this function starts the optimization procedure. Repeatedly creates new generations until the self.terminated is set to `True` by `_terminate()`

Returns `DEFitResult` – result of the optimization.

class `DEfit.DEFitResult`(*statevars*, *description*, *DEpars*, *result*, *history*)
Holds the results of a fitting procedure and provides methods for serialization to YAML format.

`__init__`(*statevars*, *description*, *DEpars*, *result*, *history*)
Constructor. This is supposed to be called from `from_fit()`.

Parameters

- **statevars** (*list of str.*) – state variables
- **description** (*str.*) – model name
- **DEpars** (*dict.*) – Differential evolution parameters, contents:

seed	`int`, seed used for the PRNG
Population size	`int`, no. of candidates per generation
CR	`float`, Crossover probability
F	`float`, Mutation weight
Strategy	`str`, DE strategy
Freeparame-ters	list of `str`, which model parameters where fitted
Transform	`str`, which transformation was used when calculating the residuals
Parameter bounds	`dict`, fit was performed within these parameter ranges
Bound handling	`str`, how parameters were projected back into the allowed range if they exceeded the bounds
Terminatin delta_abs	`float`, minimum improvement until algorithm terminates, absolute value
Terminatin delta_rel	`float`, minimum improvement until algorithm terminates, relative value
Termination generations	`int`, after how many generations termination criteria were checked
Maximum iteration	`int`, terminated after this many generations regardless of improvement

- **result** (*dict.*) – Optimization result

cost	`float`, best cost function value
Parameters	`dict`, best parameter set

- **history** (*dict.*) – Progress over algorithm generations

Generations needed	How many generations were required to reach termination criteria
Lowest costs	The cost function values of the best candidates in each generation, ordered
Best parameters	The best parameter set in each generation, ordered

Returns `DEFitResult`

`__str__()`
Pretty-print a string representation of the result.

Returns str.

`__weakref__`
list of weak references to the object (if defined)

classmethod `from_fit`(*fitinstance*)
Create a results object from instance of `DEFit`.

Parameters **fitinstance** (`DEFit`) – `DEFit` instance after running the fitting procedure

Returns `DEFitResult`

classmethod `from_yaml`(*filename*)
Get a results object saved in YAML format.

Parameters **filename** (*str.*) – path to YAML file

Returns `DEFitResult`

`to_yaml`(*filename*)
Dump a results object to a YAML file.

Parameters **filename** (*str.*) – full path and filename to YAML file

class `DEfit.ModelCost`(*model*, *transform=False*, *scale=False*, *prunelog=False*, *weights=False*, ***kw*)
Cost function to use for optimisation of an ODE model. Provides calculation of residuals (diff. model output vs data) and transformation/scale functions.

`__call__`(*pars*)
Return cost function value for evaluation of the model with given parameters.

Parameters **pars** (`Parameters`) – model parameters

Returns float – model cost

`__init__`(*model*, *transform=False*, *scale=False*, *prunelog=False*, *weights=False*, ***kw*)
Constructor

Parameters

- **model** (`ODEModel`) – model, has to provide observed data for state variables.
- **transform** (*str.*) – Right hand side of a transformation function to be applied to simulation results and data before calculating costs. - log10: base 10 logarithm - log2: base 2 logarithm - log1p: 1 + base e logarithm - identity: identity
- **scalebyerr** – If not bool(scalebyerr)==False, scale data and simulation results by the measurement error of each variable in each point. Accepts "SD" for standard deviation and "SE" for standard error of the mean.
- **scalebyvar** – Boolean; scale simulation results and data by the value of each variable in each point.
- **scalebymax** – Boolean; scale simulation results and data by the maximum value that the variable reaches in the *data*
- **prunelog** – Boolean; replace zeroes in simulation results and data by a small value. Workaround to use log transformations with data and simulation results containing zero.

Returns `ModelCost`

`residuals`(*pars*, *varname*, *longname*)
Calculate residuals $y_i - \hat{y}_i$

Parameters **pars** (`Parameters`) – model parameters

Returns `numpy.ndarray` – residuals

class DEfit.ObjectiveFunction(*logfile=<open file '<stderr>', mode 'w' at 0x7f7545b831e0>*, *minloglevel=50*, ***kw*)

Base class for objective functions to be minimized. Derived classes have to implement __call__.

__call__(*pars*)

Subclasses of ObjectiveFunction are supposed to implement a __call__ method returning the value of the objective function as a scalar, given a Parameters instance pars.

Parameters **pars** (Parameters) – parameter vector for objective function

Returns float – model cost value

class DEfit.Population(*control*, *pardomain*, *cost*, ***kw*)

Holds a population of Parameters instance candidates and provides methods to select, mutate and recombine them.

__init__(*control*, *pardomain*, *cost*, ***kw*)

Constructor

Parameters

- **control** (DEControl) – parameters for DE algorithm
- **pardomain** (Pardomain) – parameter bounds
- **cost** (ModelCost) – cost function

Returns Population

__weakref__

list of weak references to the object (if defined)

breed()

Calculate the next generation. Makes a copy of the parent generation and iterates over all candidates in this generation. For each individual, a mutant candidate is generated (self.mutate), recombined with the parent candidate (self.crossover) and selected.

crossover(*parent*, *offspring*)

Crossover between parent and offspring. Currently only implements the classical DE crossover strategy:

1. An index pos for a parameter vector is taken at random
2. for each position index i, a uniform random number rnd between 0 and 1 is generated.
3. if rnd < control.CR or if i==pos, the parameter is taken from the offspring (mutated candidate); otherwise, the parent value (candidate in previous generation) is used.

Parameters

- **parent** (Parameters) – candidate from parent generation
- **offspring** (Parameters) – mutated candidate for next generation

Returns Parameters – new candidate

get_best()

Get the best candidate solution in the current generation.

Returns Parameters – best candidate

mutate(*i*)

Mutate an individual according to DEcontrol parameters. See DEControl for a description of the different mutation strategies.

Parameters **i** (*int*) – position of the mutated candidate in the population.

Returns Parameters – mutated candidate

select(*newpop*)

Selection function, returns the next generation of candidates. It currently only implements the "best" strategy: a mutant is only taken for the next generation if it yields a smaller cost

function value than that of its parent; otherwise, the parent is used. Other strategies typically involve taking the parent generation and all generated mutants, sorting them according to their cost and selecting by e.g. taking the best control.NP individuals or performing some kind of fitness proportionate selection. This can be easily implemented here.

Parameters **newpop** – list of candidates (Parameters instances) to test

against the current generation. :type newpop: `Parameters` list :returns: `Parameters` list – next generation

`select_parents`(*i*, *n=3*)

Return a given number of parents for the candidate at position i in the generation.

Parameters

- **i** (*int*) – position of the individual in the new population
- **n** (*int*) – number of parents to select

Returns list of n `Parameters`

C.6 Logging.py

This module provides methods for logging to files or streams. The main reason for using this is that the standard `Logging` module, which provides similar functionality much more elegantly, is that `Logging` does not work easily together with `multiprocessing` which is used extensively in my fitting routines. This is not a bug in `Logging`, but rather a result of `multiprocessing` using `pickle` to serialize data for parallelization and the fragility of this serialization process. More specifically, the problem is that file `threading.Lock` instances are not serializable. Here, I do not lock files manually. Using `threading.Lock` is not the best approach when using multiprocessing, anyway, since it makes file writes thread safe, but not process safe. `multiprocessing.Lock` could be used instead, but I have not implemented this yet and its impact on performance remains to be tested. This module is best used by subclassing `Loggable`.

note This is *not* thread safe, so expect garbled Logfiles when using this together with `multiprocessing`

class `Logging.Loggable`(*logfile=<open file '<stderr>', mode 'w' at 0x7f7545b831e0>*, *minloglevel=50*, ***kw*)

Provide logging functionality.

`__init__`(*logfile=<open file '<stderr>', mode 'w' at 0x7f7545b831e0>*, *minloglevel=50*, ***kw*)

Constructor

Parameters

- **logfile** (Open stream or `str`) – Where to log
- **minloglevel** (`int`) – minimum level for log messages
  - 50: log all messages (debug, info, warning, error, exception)
  - 40: log info, warning, error, exception
  - 30: log warning, error, exception
  - 20: log error, exception
  - 10: log exception

Returns `Loggable`

`__weakref__`

list of weak references to the object (if defined)

`debug`(*msg*)

Log a message with level 50 (DEBUG).

Parameters **msg** (`str`) – message to log

`error`(*msg*)
Log a message with level 20 (ERROR).

Parameters **msg** (`str`) – message to log

`exception`(*msg*)
Log a message with level 10 (EXCEPTION).

Parameters **msg** (`str`) – message to log

`format`(*msg*, *loglevel*, *textwidth=130*)
Pretty-print log messages with a prefix.

Parameters

- **msg** (`str`) – message to log
- **loglevel** (`int`) – log level of the message (10|20|30|40|50)
- **textwidth** (`int`) – maximum length of a line in the logfile

Returns `str` – formatted message

`info`(*msg*)
Log a message with level 40 (INFO).

Parameters **msg** (`str`) – message to log

`warning`(*msg*)
Log a message with level 30 (WARNING).

Parameters **msg** (`str`) – message to log

`write`(*msg*, *loglevel*)
Write a message to the log file if the minimum log level is reached.

Parameters

- **msg** (`str`) – message to be logged
- **loglevel** (`int`) – log level of the message